Biomineralization in domestic pig molars

Pro gradu –tutkielma

Susanna Sova

HELSINGIN YLIOPISTO
GEOTIETEIDEN JA MAANTIETEEN LAITOS
Biogeotieteen osasto

20.10.2015

HELSINGIN YLIOPISTO – HELSINGFORS UNIVERSITET – UNIVERSITY OF HELSINKI

Tiedekunta/Osasto – Fakultet/Sektion – Faculty/Section	Laitos – Institution – Department	
Matemaattis-luonnontieteellinen tiedekunta	Geotieteiden ja maantieteen laitos	
Tekijä – Författare – Author		
Satu Susanna Sova		
Työn nimi – Arbetets titel – Title		
Biomineralization in domestic pig molars		
Oppiaine – Läroämne – Subject		
Geologia		
Työn laji – Arbetets art – Level	Aika – Datum – Month and year	Sivumäärä – Sidoantal – Number of pages
Pro gradu -tutkielma	10/2015	82

Tiivistelmä – Referat – Abstract

Biomineraalit ovat olleet tärkeässä osassa eliöiden monimuotoisuuden evoluutiossa. Biomineraalit mahdollistavat eliöille mm. ionien varastoinnin, hyökkäys- ja suojautumiskeinoja, ravinnon hienontamisen, sekä liikkumisen. Hampaiden kiille on kovin ja pisimmälle mineralisoitunut osa nisäkkään kehossa. Vaikka hampaan kehitys tunnetaan paremmin kuin monen muun elimen, kiilteen kehityksen tuntemus on vielä puutteellista. Kiilteen kehitys on biologisesti hidas prosessi: Esimerkiksi ihmisen ensimmäinen poskihammas alkaa mineralisoitua syntymän aikaan ja hammas puhkeaa suuhun noin kuuden vuoden iässä, jonka jälkeen mineralisaatio vielä jatkuu kuukausien ajan. Mineralisaation aikaiset häiriöt tai myöhemmät kiillevauriot jäävät pysyviksi, sillä kiille ei uusiudu enää hampaan puhkeamisen jälkeen.

Tämän työn tarkoitus on kuvata sian poskihampaiden mineralisaatio, eli maturaatio mineralogian ja fysiikan menetelmin. Sika on kasvispainotteinen sekasyöjä, jolla on ihmisen kaltaiset, pyöreänystermäiset poskihampaat. Vaikka sian hampaat ovat kookkaat, ne kehittyvät suhteellisen nopeasti, mikä tekee niistä työn tarkoitukseen sopivan tutkimuskohteen.

Yksi menetelmällisistä tavoitteista oli tutkia ominaisuuksiltaan tunnettujen mineraalien käyttöä mikrotomografia-kuvien suhteelliseen kalibrointiin. Kalibroituja mikrotomografiakuvia verrattiin perinteisemmillä mineraali- ja hammastutkimusmenetelmillä (esim. ohuthieillä ja kovuustesteillä) saatuihin tuloksiin. Tulokset osoittavat että mikrotomografia on hyvä lähtökohta biomineraalien tutkimiseen, mutta se ei korvaa perinteisempiä, destruktiivisia menetelmiä. Kuvien suhteellinen kalibrointi mineraalirakeiden avulla osoittautui toimivaksi menetelmäksi, mutta auttoi myös erottamaan ongelmat kuvannuksessa paremmin kuin vain itse hammasnäytteet.

Avainsanat – Nyckelord – Keywords

hampaat, sus scrofa domesticus, biomineralisaatio, kiille, hampaan maturaatio, 3D-kuv

Säilytyspaikka – Förvaringställe – Where deposited

Geotieteiden ja maantieteen laitos, Kumpulan tiedekirjasto

Muita tietoja – Övriga uppgifter – Additional information

HELSINGIN YLIOPISTO – HELSINGFORS UNIVERSITET – UNIVERSITY OF HELSINKI

Tiedekunta/Osasto – Fakultet/Sektion – Faculty/Section	Laitos – Institution – Department	
Faculty of Science	Department of Geosciences and Geography	
Tekijä – Författare – Author		
Satu Susanna Sova		
Työn nimi – Arbetets titel – Title		
Biomineralization in domestic pig molars		
Oppiaine – Läroämne – Subject		
Geology		
Työn laji – Arbetets art – Level	Aika – Datum – Month and year	Sivumäärä – Sidoantal – Number of pages
Master of Science Thesis	10/2015	82

Tiivistelmä – Referat – Abstract

The evolution of biominerals, including teeth, has been an important step in the evolutionary diversification of organisms. For an organism, biominerals allow various advantages, such as ion storage, protection, food capture and processing, and locomotion. In mammals, tooth enamel is the hardest and most mineralized part of the body. Although tooth development is better known than that of many other organs, the maturation of enamel is still not completely understood. Enamel formation is a slow process biologically. In humans, the mineralization of the enamel in the first permanent molars starts at the time of birth, and the process continues even after the eruption of the teeth at the age of six years. Any disturbances during the enamel formation or other damage later in life will become permanent, as enamel does not reform.

The aim of this work is to document the maturation of domestic pig molars, and use mineralogical and physics research methods to study enamel growth. The domestic pig (Sus scrofa domesticus) is a plant-dominated herbivore with large, bunodont molars. The relatively fast development of pig teeth together with their large size makes pig teeth a suitable model for comparisons of different methods.

One of the methodological interests was to test if mineral grains can be used in computational microtomography for relative calibration of the absorption models. Three minerals (fluorapatite, quartz and siderite) were chosen by their physical and chemical features. The calibrated absorption models were compared with the results of more traditional methods, such as thin sections and hardness tests. X-ray diffraction and scanning electron microscopy were also used for structural studies. The results show that the microtomography is a valuable starting point for the traditional destructive methods used in the study of biomineralization, but does not substitute for the other methods. The mineral calibration was an efficient method for the microtomography-absorption models. Additionally, the calibration minerals allowed detection of microtomography artifacts better than using teeth only.

Avainsanat – Nyckelord – Keywords

Teeth, biomineralization, tooth maturation, Sus scrofa, 3D-imaging, microtomography

Säilytyspaikka – Förvaringställe – Where deposited

Department of Geosciences and geography, Kumpula Science Library

Muita tietoja – Övriga uppgifter – Additional information

1. INTRODUCTION

Biomineralization refers to the process by which organisms form inorganic, crystalline substances (Lowenstam & Weiner 1989). The biomineralization is a time-consuming and complicated process that is regulated by interactions between genes, nutrition, and environment. Any disturbances in the biomineralization process can have serious effects and in extreme cases be lethal to the organism. Some biomineral-containing structures, such as the shells of bivalves keep a record of the entire lifetime of an organism, whereas others, such as teeth, record only a certain period of life. There are also mineralized tissues, such as bones that remodel throughout life, but all biominerals store information at least from their formation period. Biomineralization is a widespread phenomenon in the biosphere, and it has changed the dynamics of life history many times by offering armor, arms and other evolutionary advantages to living organisms. The evolution of biominerals has also constituted the basis for a rich record of life history in the form of fossils.

The structural study of hard parts in living organisms started in the first half of the nineteenth century. In 1844, James Scott Bowerbank published a paper "*On the structure of shells of molluscan and cochyferous animals*" where he showed that mollusk shells are far from being simple aggregates of unorganized mineral particles, and his conclusion was that mineralized structures of living animals are not themselves cellular (Cuif et al. 2011). The increasing quality of optical microscopes, the introduction of X-ray diffraction in 1930s, and scanning electron microscope in 1950s provided a notable improvement to the study of biominerals. One discovery that contributed to a major renewal in biomineral research resulted from the development of thermodynamics. In 1947, H. C. Urey, a chemist, realized that by measuring oxygen-isotope ratios of calcium carbonate in belemnite fossils, it is possible to obtain information about the climate change and environmental conditions at the time when that organism lived. For the first time, numerical values with unprecedented precision were provided for an environmental parameter of the past. This application led to the expansion of the use of biominerals, in addition of the fossil morphology, as proxies for understanding ancient environments.

Current biomineralization research is a multidisciplinary field that spans both the inorganic and the organic world. It combines evolutionary and developmental biology, mineralogy and paleontology, but also many other fields such as dentistry, and material research. Consequently, researchers from different disciplines have different perspectives, methods and vocabulary. In the case of teeth, and especially in the case of tooth enamel, the long history of research has made the nomenclature of the field complex and sometimes even misleading.

In the enamel research, the last decades have deepened our knowledge on the three-dimensional microstructure and mechanical properties of enamel (e.g. Boyde & Fortelius 1986, von Koenigswald et al.1987, Boyde 1989, Ferguson et al. 2005, Tafforeau et al. 2012), the chemistry of enamel (e.g. Robinson et al. 1995a and b, Austin et al. 2013) and gene networks in tooth development (e.g. Bite-it database). Although the development of teeth is better known than that of many other organs, the maturation of enamel is still not completely understood. Lately, environmental influences have become an important question in the study of biomineralization, for example, in the study of enamel defects of animals in polluted areas (e.g. Kierdorf et al. 1993, 1996, 2000, 2012), and of humans in urban regions (e.g. Willmott et al. 2008, Fagrell et al. 2010, Farah and Swain 2010).

The aim of this work is to study biomineralization in pig molars using modern mineralogical and physics research methods. The domestic pig (*Sus scrofa domestica*) has relatively large teeth that develop comparatively fast, which makes them a practical model to study biomineralization. Compared to the mouse, the standard species used in developmental research, the pig dentition is more similar to human dentition in size, shape and tooth number.

Thin sections that are the traditional method to observe the internal structure of minerals and teeth, give more precise information than x-ray computed tomography (microCT), but only in two-dimension and from a smaller area or one plane. In this study, I examine whether microCT provides useful and comparable information about the process of biomineralization. The microCT is not a destructive method, and it allows the imaging of three-dimensional morphology of samples. I also test if the microCT-absorption models could be calibrated to the same gray scale with three grains of known minerals.

Together with microCT and, more precise but destructive methods, I examine whether the spatiotemporal details of biomineralization processes can be distinguished on pig molars. The Vickers hardness tester measures the absolute hardness of test points on a polished surface, which can be correlated with the previously determined electron density models on the tooth structure. The X-ray diffraction analyses (XRD) allow obtaining information about the size and orientation of crystals in the samples, and scanning electron microscopy (SEM) is used to observe the enamel rod size and orientation. Unlike in the previous studies on in pig enamel properties (e.g. Karlström 1931, Kirkham et al. 1988, Wang et al. 2014), here I have compared all the molars with a focus on maturation of enamel and dentin.

2. FROM A LIVING CELL TO CRYSTALLINE SUBSTANCE

Minerals are crystalline elements or chemical compounds that have been formed by different geological processes (Nickel 1995). Biominerals are produced by biological organisms, but otherwise their crystal structure, chemical composition and physical properties are the same as with their counterparts in the lithosphere. Although there are almost 5000 known minerals, only 33 different crystalline substances are formed by biological processes (Table 1). All biogenic minerals are also known to be produced by geological processes, meaning that the living organisms have not found a way to produce any crystalline substances that would not also be crystallized inorganically (Lowenstam & Weiner 1989). Biomineral-producing species are found from all kingdoms of life (Prokaryota, Protoctista, Plantae, Fungi and Animalia).

Table 1. Known crystalline substances that are formed by biological processes. There are 33 different biominerals from all the mineral classes except from the class of Silicates (Lowenstam & Weiner 1989, Nickel-Strunz 2001).

Mineral class	Mineral	Chemical formula
01 Elements	Sulfur	S_8
02 Sulfides	Pyrite	FeS_2
	Sphalerite	(Zn,Fe)S
	Wurtzite	(Zn,Fe)S
	Galena	PbS
	Greigite	$Fe^{2+}Fe^{3+}{}_2S_4$
	Mackinawite	(Fe,Ni)S0.9
03 Halogenides	Fluorite	CaF_2
	Hieratite	K_2SiF_6
04 Oxides and Hydroxides	Magnetite	$Fe^{2+}Fe^{3+}{}_2O_4$
	Goethite	$Fe^{3+}O(OH)$
	Lepidocrocite	FeO(OH)
	Ferrihydrite	$Fe^{3+}{}_2O_3•0.5(H_2O)$
	Todorokite	$(Na,Ca,K)_2(Mn^{4+},Mn^{3+})_6O_{12}•3\text{-}4.5(H_2O)$
	Birnessite	$(Na,Ca,K)x(Mn^{4+},Mn^{3+})_2O_4•1.5(H_2O)$
	Opal	$SiO_2•n(H_2O)$
05 Carbonates and Nitrates	Calcite	$CaCO_3$
	Aragonite	$CaCO_3$
	Vaterite	$CaCO_3$
	Monohydrocalcite	$CaCO_3•(H_2O)$
	Hydrocerussite	$Pb_3(CO_3)_2(OH)_2$
07 Sulphates	Gypsum	$CaSO_4•2(H_2O)$
	Celestite	$SrSO_4$
	Barite	$BaSO_4$
	Jarosite	$KFe^{3+}{}_3(SO_4)_2(OH)_6$
08 Phosphates	Hydroxylapatite	$Ca_5(PO_4)_3(OH)$
	Fluorapatite	$Ca_5(PO_4,CO_3)_3F$
	Whitlockite	$Ca_9(Mg,Fe^{2+})(PO_4)_6(PO_3OH)$
	Struvite	$(NH_4)MgPO_4•6(H_2O)$
	Brushite	$CaHPO_4•2(H_2O)$
	Vivianite	$Fe^{2+}{}_3(PO4)_2•8(H_2O)$
10 Organic compounds	Earlandite	$Ca_3(C_6H_5O_7)•4(H_2O)$
	Whewellite	$Ca(C_2O_4)•(H_2O)$
	Glushinskite	$Mg(C_2O_4)•2(H_2O)$

The three most common biomineral groups are calcium carbonates, opal and phosphates. Calcium carbonates are the most abundant biominerals, and they form the largest individual crystals of biominerals (Cuif et al. 2011). The largest biologically formed calcium carbonate crystals can reach a size of several hundred micrometers, whereas the crystal size of the other biominerals is on the nanometer scale. Several carbonate biominerals are known (Table 1), but only calcite and aragonite are common.

Calcite is thermodynamically the more stable of these two, and for that reason, the frequency of aragonitic fossils decreases dramatically towards older deposits. Calcium carbonates ($CaCO_3$) are produced predominantly by marine organisms, such as mollusks, corals, and sponges.

After calcium carbonates, opal is the most abundant biomineral (Lowenstam & Weiner 1989). Opal is a hydrated amorphous form of silica ($SiO_2 \bullet n(H_2O)$) (IMA 2014/09) and lacks a systematically arranged crystal structure. It is regarded as a mineral species for historical reasons, and is one of the few amorphous substances that is accepted among the minerals by International Mineralogical Association (IMA). Unlike crystalline biominerals, opal is formed within the cell (Cuif et al. 2011). In biogenic opal, the silica tetrahedra are bound together by water and organic matter and, even if the crystal structure is lacking, these organisms have highly controlled overall morphology. Diatoms (algae), radiolarian (protozoa) and sponges are the main producers of biogenic opal.

The third most important biomineral is apatite $Ca_5(PO_4)_3$(OH, F, Cl (Fig. 1) (Lowenstam & Weiner 1989). Apatite is a general term for three chemical end-members: hydroxylapatite, fluorapatite and chlorapatite. Fluorapatite is the most common of these in the lithosphere, but hydroxylapatite is the most common in biominerals. Chlorapatite is not a known biomineral.

Apatite crystal structure is very receptive to incorporate foreign ions, such as barium(2+), carbonate(2-) and magnesium(2+) (Lowenstam & Weiner 1989, Austin et al. 2013). In addition, bioapatite crystals are very small and, for example in teeth, the composition of apatite is not constant in different parts of a tooth (Robinson et al. 1995a, Smith 2013), which makes the mineralogical identification of biogenic apatites often complicated. Bioapatite is mostly known from teeth and skeletons of vertebrates but it also occurs in some invertebrate structures. From a geological perspective, phosphate minerals are not quantitatively important formations (Cuif et al. 2011). Besides apatite, there are four other known phosphate biominerals (Table 1).

In addition to the dominant biomineral groups; calcium carbonates, opal and apatite, there are rare oxide, sulfide, sulfate and hydroxide biominerals (Table 1) that are present

in many taxa, but their quantities are low (Lowenstam & Weiner 1989). Additionally, Lowenstam & Weiner (1989) included other amorphous "organic minerals" and amorphous substances to biominerals, but they are not accepted as minerals by the IMA.

Biominerals are heavier than other biogenic substances, and this property creates some restrictions to the living organisms themselves. However, the advantages that biominerals offer to organisms are diverse including toxic waste deposition, ion storage, structural support, protection, magnetic orienteering, and food processing. Most of the biominerals also contain hydroxyl groups and/or bound water molecules. Biominerals can be re-dissolved with minimal energy expense for reuse, even if the principal function of biomineral is to provide structural stability. For example, if the food of a nursing mother is deficient of calcium and phosphorus, some of these components will be extracted from her skeleton.

Some organisms are able to produce several biominerals; for example, birds have a phosphate-based skeleton, they lay calcareous eggs, and migratory birds have a ferromagnetic-mineral-containing organ that detects magnetic fields (Lowenstam & Weiner 1989, Kirschvink & Gould 1981). The biomineralization process is sensitive to environmental parameters (Lowenstam & Weiner 1989, Cuif et al. 2011). For example, temperature has an influence whether a coral skeleton is composed of calcite or aragonite, and among mammals, very high fluorine concentration in drinking water can negatively affect the tooth and bone composition, and in worse case the whole skeletal structure.

2.1 Evolution of biominerals

The fossil record and our knowledge of the evolution of life depend on biominerals, as mineralized substances are much more likely preserved in sediments than soft tissues. However, the earliest known biological formations are not biominerals but stromatolites that date back to 3500 Ma (million years ago). Stromatolites are formed by benthic microorganisms that trap sediment particles from water suspension and bind them together in layers with a biofilm (Riding & Awramik 2000). At the peak of the summer season, evaporation promotes salinity and saturation of calcium carbonate of the sediment interstitial water to a state of hypersalinity and hypersaturation. These conditions result in an extremely slow sedimentation and accumulation rate that allows stromatolite formation by a series of precipitation events within the bacterial mat, producing submillimeter-scale laminae. There are different bacteria that produce stromatolites but the common feature in all these occurrences is the extremely slow accumulation rate (Riding 2007). As these microorganisms do not form the crystals themselves, stromatolites are not true biominerals, even if the formations are biogenic. Stromatolites were very abundant and diverse in early history of the life and they reached their peak abundance at approximately 1250 Ma. Stromatolites are still being formed in a few bays of western Australia and the Bahamas, where water is very saline and warm.

The oldest fossils that show evidence of true biomineralization are manganese deposits that were formed by bacteria at the Proterozoic eon, at approximately 1600 Ma (Lowenstam & Weiner 1989). At 1000 Ma, cyanobacteria show first traces of carbonate biomineralization and heavily encrusted species appear to the fossil record approximately 580 Ma. The first mineralized eukaryotic algae appeared during the Late Proterozoic eon, at approximately 750 Ma, but the large composite mineralized skeletons occurred at approximately 570 Ma. At the boundary of the Cambrian period, at approximately 540 Ma, a massive increase in the diversity of carbonate mineralizing organisms occurred among metazoans. This initiated the Phanerozoic eon, the eon of visible life, which is predominantly documented through biomineral remains. By the end of the Cambrian period, all kingdoms of life had species that incorporated biominerals into their structure and all known biominerals had appeared to the geological record (Lowenstam & Weiner 1989) (Fig. 1).

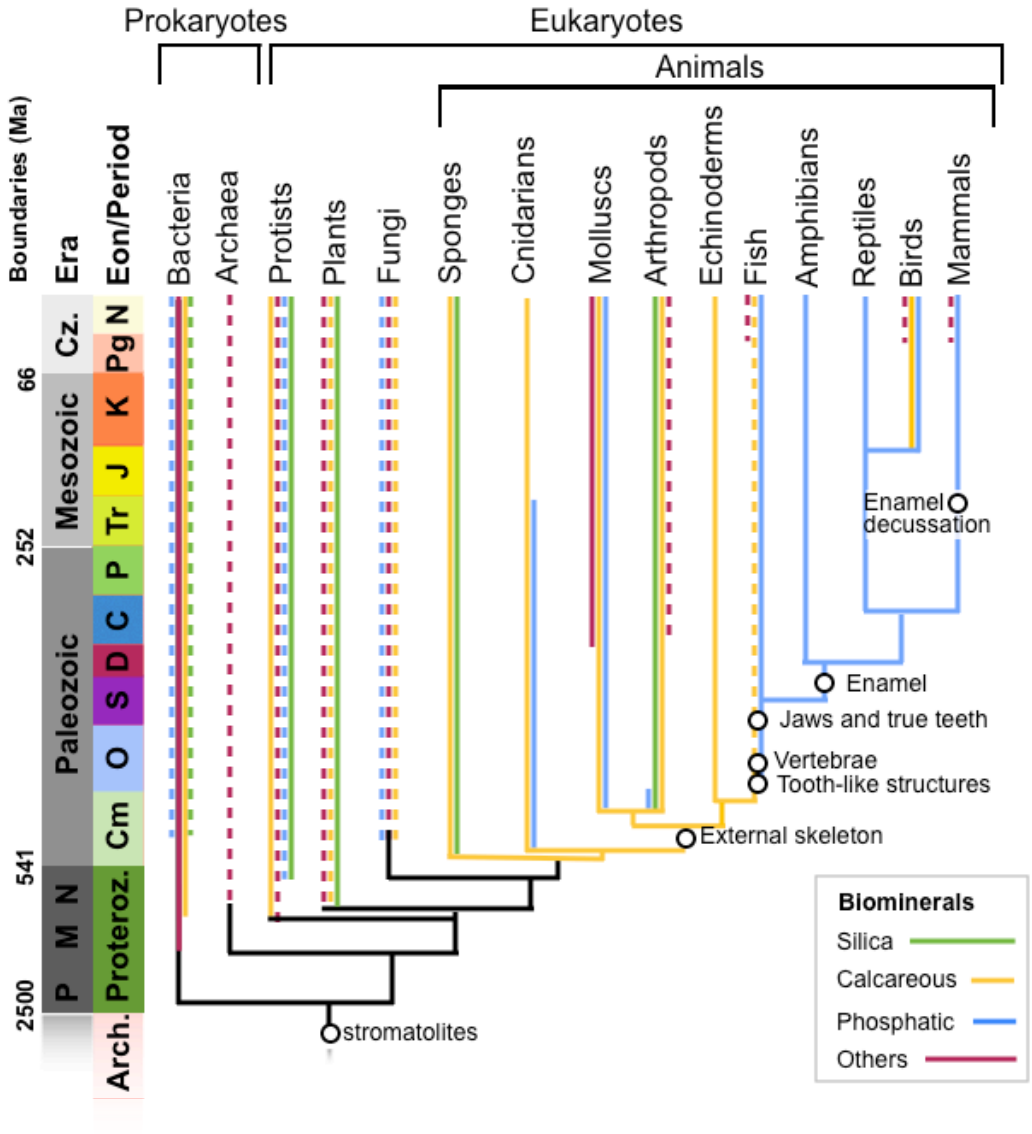

Fig 1. The evolution of biominerals. The colored lines indicate the distribution of biominerals in the fossil record. The dashed lines indicate uncertainty in the timing of appearance of a particular biomineralization process. “Others” include oxides, sulfates, sulfides and hydroxides. The nodes do not necessarily represent the appearance of the crown groups listed on the top (Lowenstam & Weiner 1989, Haaramo 2015)

At the end of the Cambrian period, organisms producing calcium carbonate biominerals were dominant and the abundance of these species increased exponentially (Lowenstam & Weiner 1989). Biogenic calcium carbonate accumulation has been abundant on the ocean floors from the late Cretaceous to the present. Such accumulation has greatly affected the chemistry of the oceans and indirectly also the chemistry of the atmosphere, as the organisms are using carbon that is sequestrated from the atmosphere to the oceans (Pilson 2013). On continental environments, biocarbonates have never played a major role, with the exception of some local fresh water bodies.

Biological silicification appears by the end of the Proterozoic eon (Lowenstam & Weiner 1989). Until the Jurassic period, radiolarians were the major silica-utilizing phylum, but during the past 50 million years diatoms have become more important. Diatoms, radiolarians and silicoflagellates are the main contributors of the biogenic silica cycle of oceans in global scale through time (Pilson 2013).

The fossil record of phosphate biominerals starts during the late Precambrian. Early in the evolution of the biomineralization, there were several phyla producing phosphate minerals, but they either became extinct or evolved carbonate skeletons (Lowenstam & Weiner 1989). The concentration of seawater phosphate was relatively high at the end of the Precambrian, and progressively lowered during the Cambrian period, which may have affected the dynamics of biomineralization. Since the mid-Ordovician, approximately 470 Ma, the vertebrates have been the most prominent group of phosphatic biomineralizers. Various fish groups evolved and radiated during the late Ordovician and Silurian, and the bony fishes evolved at the end of the Silurian period, at approximately 420 Ma (Ungar 2010).

The first amphibians began to occupy niches on land at the end of the Devonian, at approximately 360 Ma (Ungar 2010). In water, the mineralized plates and scales served as protection from predators, and the cartilaginous endoskeleton acted as a support for locomotion. Once animals colonized the land, a mineralized endoskeleton become more important in providing support. The first fully terrestrial vertebrates, reptiles, evolved on land at the end of the Carboniferous, approximately 320 Ma. One of the evolutionary steps that made living possible on land was a mineralized eggshell that protects the embryo from dehydration in dry conditions (Ungar 2010). The first known mammalian fossils date back to the Late Triassic, approximately 225 Ma (Ungar 2010), and the earliest known birds date back to the Middle Jurassic, approximately 160 Ma (Godefroit et al. 2013). The evolution of flight brought again new challenges for the skeleton, as both strength and lightness were important.

2.2 Evolution of dental tissues

As teeth are the most common evidence of life history left for paleontologists, the evolution of teeth has been better studied than that of any other organ. The first tooth-like structures have been found from conodonts (Fig. 2) that existed from the late Cambrian to the end of the Triassic period. Conodonts were small, jawless eel-like creatures that have been considered as the earliest skeletonizing vertebrates (Jones et al. 2012). Conodonts had food processing apparatus in their oral cavity that consisted of 15–19 elements that were 0.2 to 2 mm long. The conodont feeding elements resemble later teeth in many ways; they have apatite caps on top of a dentin-like basis and wearing facets on their surfaces show evidence of complex occlusion and chewing (Smith & Sanson 2000, Goudemann et al. 2011).

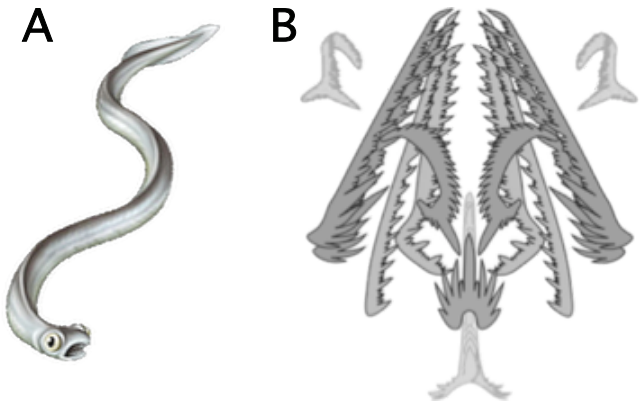

Fig 2. A) Reconstruction of a conodont. The conodonts are an extinct group of eel-like vertebrates. B) The conodont feeding elements. Each animal had 15–19 elements that formed a bilaterally symmetrical array in its oral cavity. These feeding elements were 0.2 to 2 mm long and they had an apatite cap on a dentin-like base. Edited from Goudemand et al. 2011.

Besides from the conodont feeding elements, dentin has also been found from the dermal armor of early jawless fish (Smith and Sanson 2000). The armor plates are composed of dentin and bone, and in some fish species, the plates were covered by a highly mineralized cap of enameloid (Kawasaki and Weiss 2006). Dentinous tissues rapidly diversified during the Ordovician and Lower Silurian periods. In different types of dentins, there are different levels of order in structure and different degree of mineralization, but the fundamental properties of dentin, such as sensory function, continuous growth and reparative ability, have preserved through evolution of dentin (Smith and Sanson 2000).

Dermal denticles of shark and scales of many fossil fish are covered by an enameloid cap. Enameloid is a general name for different hypermineralized apatite caps that do not have any particular structure, and it can be also found from teeth of modern fish. Whereas tetrapod enamel is formed only by ectodermal cells, both ectodermal and mesodermal cells form enameloid. The organic matter in enameloid is mainly composed of collagen fibers that are also present in dentin and bone, but not in true enamel (Line & Novaes 2005). Unlike enamel, fish enameloid has naturally high fluorine content, and shark enameloid is composed of fluorapatite instead of hydroxylapatite (Cuif et al. 2011, Enax et al. 2012). The fluorine has an ability to promote precipitation and growth of apatite crystals (Suga et al. 1983).

Early fossil actinopterygians (ray-finned bony fish), and living bichirs and gars have more enamel-like structure, so-called ganoine on their dermal skeleton (Qu et al. 2015). New genetic evidence strengthens the hypothesis that ganoine is homologous with enamel because many of the enamel–specific genes are found in a recently sequenced genome of the spotted gar. However, *amelogenin*, a key gene required for the formation of enamel, has not been found in gar but it is present in lobe-finned fish *Latimeria.* The enamel of lobe-finned fish, amphibians and most reptiles has a simple structure with closely packed hydroxylapatite crystals that are roughly parallel to each other and perpendicular to the enamel surface (Fig. 3) (Line & Novaes 2005).

Jawed vertebrates evolved over 450 million years ago, during the Silurian period (Ungar 2010). Lower vertebrates, such as fish, amphibians and reptiles, generally have one-cusped teeth (Line & Novaes 2005). Early synapsids (mammal-like reptiles) had relatively simple dentition that erupted early and were replaced continuously (Kawasaki and Weiss 2006). When tooth shape started to become more complex and the occlusion more precise, the number of teeth reduced. Sharks can replace their teeth 200 times in their lifetime, reptiles can replace them about 45 times and most mammals only once (Ungar 2010). Mammalian and some reptilian (crocodilians) teeth have roots that develop after the crown formation.

The ongoing diversification of mammals was intensified by the availability of new food sources and the Cretaceous–Paleogene extinction (Line & Novaes 2005, Wilson et al. 2012). This diversification was accompanied by an increasing body size that resulted in

species that had bigger teeth and more robust masticatory muscles. Concurrently with the increasing size, there was a shift in feeding habits from insectivorous to carnivorous and herbivorous diets. These changes in feeding habits increased the stresses imposed on teeth by the impact of mastication, which increased tooth abrasion and the risk of enamel fracture.

Mammalian enamel is characterized by enamel rods (also called enamel prisms) that suppress crack propagation in tooth enamel (Fortelius 1985, von Koenigswald et al. 1987, Lucas 2004). The enamel rods are bundles of apatite crystals that extend from the enamel-dentin junction (EDJ) to the enamel surface (Line & Novaes 2005), and their development is associated with the differentiation of herbivores and carnivores from insectivores (von Koenigswald et al. 1987). During the early Paleocene, a simple radial enamel, in which the enamel rods follow a straight course from EDJ to tooth surface (Fig. 3 A), gave rise to an arrangement where these horizontal rod layers were inclining alternately towards left and right (Fig. 3 B, C). In the early Paleocene, enamel rod decussation in mammalian enamel was limited to the central part of the enamel (Fig. 3 B), and the angle of the rod decussation was small (Line & Novaes 2005). The angle enlarged gradually in such way that in mammalian species of the late Paleocene, the angle of decussating layers reached nearly 90 degrees, and the decussation extended throughout the tooth enamel (Fig. 3 C). Rod decussation is present in the enamel of most modern placental mammals except insectivores (von Koenigswald et al. 1987).

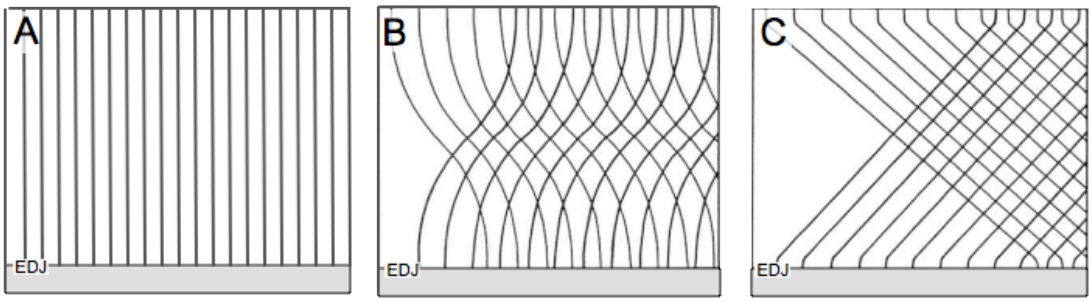

Fig 3. Schematic picture of different enamel rod courses from EDJ to enamel surface. A) Parallel enamel rods. B) Enamel that has decussating enamel rods only in central part and the decussation angle is low. C) Enamel with strong enamel rod decussation trough entire enamel thickness. EDJ = enamel-dentin junction. Edited from Koenigswald et al. 1987.

The orientation of decussating rod layers has changed during evolution. Primitively, layers were horizontal (Fig. 4 A) and slightly undulating (von Koenigswald et al. 2011). In many taxa, the horizontal orientation was modified to vertical, wave-like, and an

arch-shaped configurations that follow the tooth morphology (Fig. 4 B-F) (von Koenigswald et al. 2011). The thickness of the decussating layers can vary from one to more than 30 rods (von Koenigswald 1987, Koenigswald et al. 2011) and the transition of the rod layers may be abrupt or gradual (Fortelius 1985, Korvenkontio 1934). The orientation and patterning of rod layers may differ among the tooth families, and the course of enamel rods can differ even in different parts of a single tooth or, in different depths of the tooth enamel. Enamel rod decussation has evolved independently in various placental lineages (Fortelius 1985, von Koenigswald et al. 2011) and its pattern may be used to infer phylogenetic relationships and to identify higher taxa (Line & Novaes 2005). Different configurations of decussating enamel layers are mainly related to phylogenetic lineages, but is also related to dietary specification (Ziscovici et al. 2014, Line & Novaes 2005).

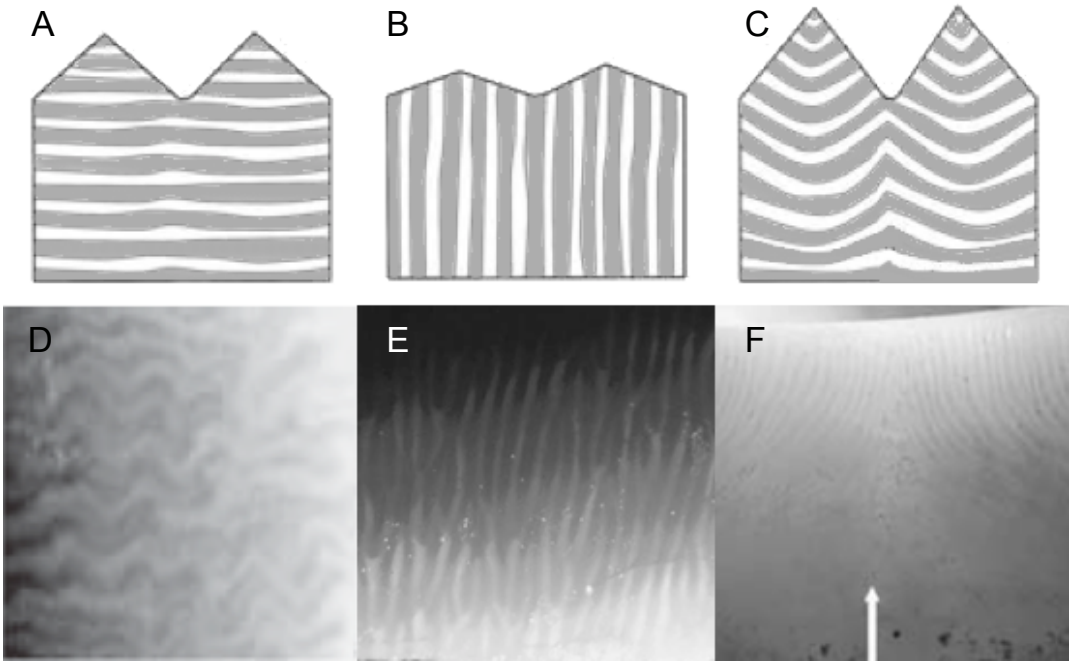

Fig 4 A-C) Schematic examples of different orientations of decussating enamel rod layers. A) Horizontally decussating enamel rod layer orientation is the most common phenomena in placental mammals. B) Vertical layer orientation is known among rhinoceros. C) Curved configuration that slightly follows tooth morphology. D-F) Photos of different enamel decussation patterns. As the orientation of alternate layers is towards left and right, the light reflects differently form every second layer (this phenomena is called Hunter-Schreger bands). D) Horizontally zigzagging enamel rod layers in enamel of spotted hyena *(Crocuta crocuta)* premolar. E) Vertical configuration of enamel rod layers *(Floridaceras whitei)* Detail: shearing plate of upper premolar. F) Arc-shaped configuration *(Tapirus sinensis)* Detail: interface (arrow) in the transverse lophs of a lower molar. Edited from Koenigswald 2011, Tseng 2012.

The evolution of enamel can be divided into three stages; the appearance of enamel-specific proteins that allowed the formation of a true enamel, the development of Tomes' processes that allowed the formation of enamel rods, and the morphological changes of Tomes' processes that caused the enamel rod decussation, which strengthened enamel and made it more resistant to tensional forces (Line & Novaes 2005). These events improved the biomechanical properties of enamel and allowed the adaptation to a crushing-grinding mode of chewing, which led to the diversification and evolution of mammals.

Most vertebrates do not chew, and food is mainly processed chemically in the gut. One-cusped reptilian teeth are suited for catching or holding prey for ingestion (Fig. 5), but the teeth of mammals can also be specialized for shearing, slicing, crushing, chewing, sieving or defense. Besides varying in size, mammalian teeth can be single- or multicusped, and the cusps of a single tooth can be large or small, round or sharp, and equal or variable in size and shape (Jernvall 1995).

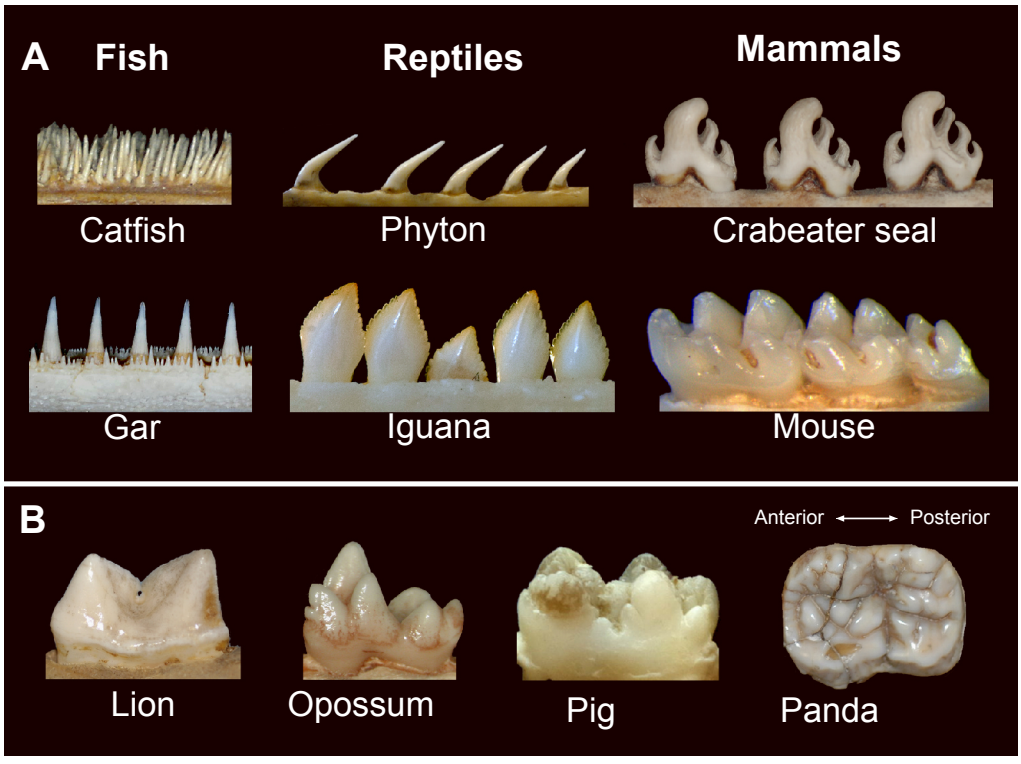

Fig 5 A) Buccal view of post-canines of different vertebrates: Fish and reptile teeth are generally numerous and simple, whereas mammals have often fewer teeth but they are more complex in shape. B) Isolated post-canines of different mammals: Carnivore molars are generally simple with sharp edges, whereas herbivore molars are rounder and more complex. M1 of lion that is a carnivore. M3 of opossum and M1 of pig, both are omnivores. M2 of panda that is a herbivore with very complex molars. Teeth are shown from lateral views, except panda molar that is shown from occlusal view. Teeth are not in scale. Edited from Jernvall & Thesleff 2012.

2.3 Structure of mammalian teeth

The tooth consists of a crown and one or more roots. (Fig. 6). The tooth neck separates the crown and the roots, and is right beneath the gum line. The tooth crown can have one or more cusps, and is generally covered by an enamel layer. The distribution and thickness of the enamel layer can vary among teeth and species. The roots are covered by cementum and periodontal ligaments that attach the tooth to the jawbone. Many herbivores also have cementum on the tooth crown and some mammals have ever-growing teeth and lack closed roots.

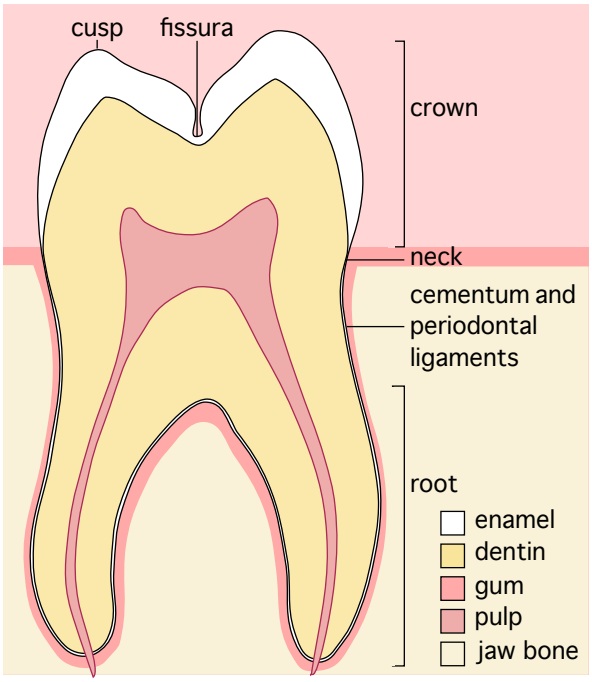

Fig 6. Schematic representation of tooth structure, frontal section. The visible part of the tooth is called crown and often covered by enamel. Tooth crown can have one or more cusps that can be similar, or differ in size and shape. Dentin, which is harder than bone but softer than enamel, forms the bulk of the tooth. In mammals the tooth is attached to the jaw with cementum and periodontal ligaments that surround the roots of the tooth. Nerves and blood vessels travel from the jaw into the pulp. Ever growing teeth do not have closed roots. Edited from Ash & Nelson 2009.

Most reptilian and fish teeth look relatively similar regardless of which part of the jaws they are situated in, whereas mammals typically have a heterodont dentition; teeth have different shape and they are specialized to different purposes along the jaw. Mammalian teeth are classified to different tooth families according to their relative location on the jaw. Four tooth families are usually recognized: incisors that are plate-like or one-cusped, one cusped canines, and variable forms of premolars and molars (Jernvall 1995). Premolars and molars are together called post-canines and in many cases they are more difficult to tell apart from each other (Lucas 2004). The number of teeth differs among species, and entire tooth families may be absent, like canines and premolars in murine rodents. A dental formula denotes the number of teeth in each

tooth family on one side of the jaw, and is told in the following order: Incisors (I), canines (C), premolars (P) and molars (M). Upper jaw (maxilla) and lower jaw (mandible) can have different number of teeth, and therefore they are described separately in the dental formula, upper teeth followed by lower teeth (I/I, C/C, P/P, M/M).

2.4 Dental diversity in mammals

Mammalian teeth are specialized for different processing of food depending on the animal's diet (Ungar 2010, Lucas 2004). Whereas in most vertebrates the occlusion of upper and lower teeth is not well developed, mammals typically have a very precise occlusion. The number of cusps per tooth varies among mammals: toothed whales have single-cusped teeth and warthogs can have over 20 cusps in one tooth (Jernvall 1995). The carnivore postcanine dentition is usually simpler and more adapted for shearing; tooth cusps form bladelike structures that enable the cutting of skin and flesh. The herbivore postcanine dentition is the most diverse of all vertebrate teeth and in general, herbivores have complex, multicusped postcanines that work like a mortar and pestle. Tooth cusps can be joined together by crests resulting in complicated cusp patterns.

Because plants are fibrous and often poor in nutrition, the occlusal surfaces of herbivore postcanines become modified by wear. Among herbivores the secondary shape of teeth is often functionally more important than the primary shape (Fig. 7) (Fortelius 1985). Many herbivores also have taller (hypsodont) teeth that allow a greater capacity to wear. Several aspects of the overall tooth shape, such as the general complexity of crown topography, correlate more with the diet of the species than the phylogeny (Evans et al. 2007). Therefore, whereas some details of tooth shape are important in determining the phylogenic affiliation of fossils, many other aspects of tooth shape are useful in inferring the diet of extinct species, and even environmental variables, such as rainfall (Fortelius et al. 2002). Hence, teeth are useful in paleontology in multiple ways.

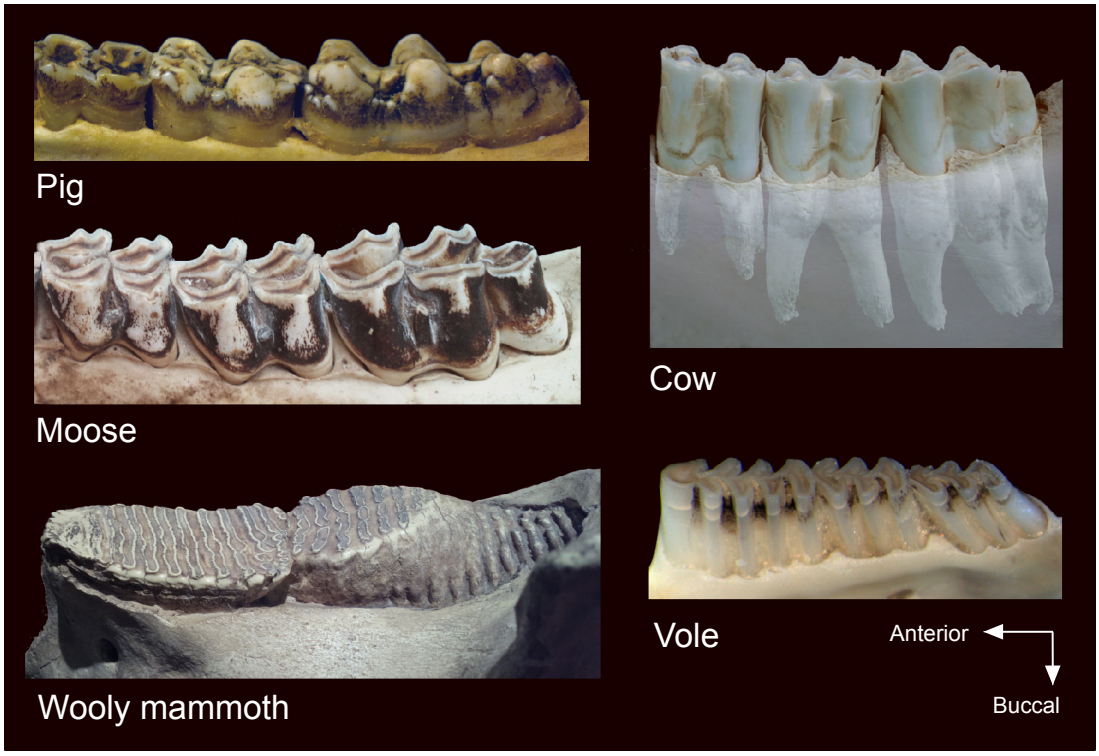

Fig 7. Secondary shapes of mammalian molars from buccal view: The pig is a foraging omnivore, eating mostly tubers, bulbs and seeds. In pig and cow teeth, the M1 (left) is the first to expose the secondary morphology, as it is the first molar to erupt. The cow and moose are herbivores. The vole is a plant-dominated omnivore. The wooly mammoth was a herbivore with a horizontal tooth replacement. Teeth are not to scale. Edited from Jernvall & Thesleff 2012.

Most mammals are diphyodont, i.e. they have two distinct tooth generations: deciduous teeth and permanent teeth (Ungar 2010). The deciduous teeth are often fewer and smaller with thinner enamel and bigger dentin tubules, and they develop faster than the permanent teeth (Ash & Nelson 2009). The timing of tooth eruptions varies greatly among species. Mammals usually have permanent teeth forming below the deciduous teeth and pushing them out as they erupt. This is called a vertical replacement of teeth. There are some taxa, for example elephantiformes and rock-wallabies, that have a horizontal replacement where the new teeth erupt from the back of the mouth and push the anterior teeth forward until they fall out. In elephants, post-canine tooth replacement is limited to six teeth, and after the last tooth is worn out, starvation and death follows. However, the post-canines in rock-wallabies have open-ended replacement.

Humans are also heterodont and diphyodont (Ungar 2010). Humans have 20 deciduous teeth and 32 permanent teeth (Fig. 8). The development of the deciduous teeth takes 2–3 years and the permanent molars 6–8 years (Table 2) (Ash & Nelson 2009). The deciduous premolars are typically molariform, thus young individuals are also able to

masticate food with their deciduous teeth. The human dental formula for the permanent teeth is I 2/2, C 1/1, P 2/2, M 3/3, which means that most people have two incisors (I), one canine (C), two premolars (P), and three molars (M) on each side of upper jaw and lower jaw.

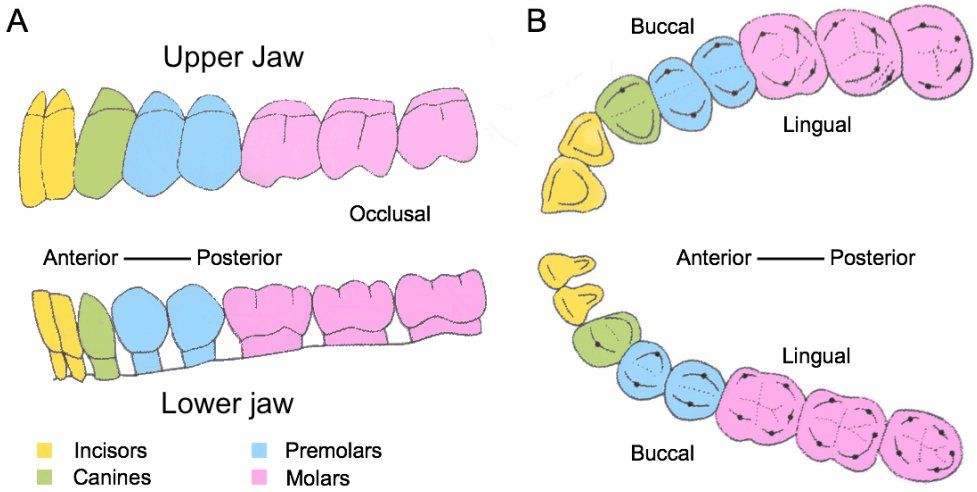

Fig 8. Human has 32 teeth in the permanent dentition. The deciduous dentition does not have molars and the premolars have more molar-like morphology. A) Buccal view of human dentition: upper and lower half-jaws of permanent teeth. B) Occlusal view of human dentition: upper and lower half-jaws of permanent teeth. Edited from Ungar 2010.

Humans have blade-like incisors for biting. Canines are single cusped and pointed. Premolars and molars have low and rounded (bunodont) cusps that are suited for crushing and grinding. The postcanine dentition of humans is typical of a primate with an omnivorous diet.

Table 2. The tooth development of human molars. Human has all teeth erupted by age of 21 years. Observations are based on radiographic pictures. (Ash & Nelson 2009).

Molar human	**M1**	**M2**	**M3**
Visible mineralization	at birth	2.5–3 yr	8–10 yr
Crown complete	2.5–3 yr	7–8 yr	12–16 yr
Eruption starts	6–7 yr	11–12 yr	17–21 yr

In this work, the word *buccal* is used for the side of the lips and cheeks, *lingual* for the tongue side, *anterior* for further away from the body axis, and *posterior* for the backbone side (Fig. 8). The surfaces that are used for mastication are called *occlusal* surfaces. The nomenclature for tooth enamel is mainly following the Glossary of Enamel Microstructure by W. v. Koenigswald (1999) and Berkovitz et al. (2002).

2.5 Tooth development

Tooth development includes two different processes: tooth patterning and maturation. Tooth patterning determines tooth size and number, and cusp size, shape and number (Jernvall & Jung 2000). Tooth maturation includes mineralization of dentin and enamel, and is generally a slower process than the tooth patterning.

Tooth development starts by the interaction between two ectodermal tissues: epithelium and mesenchyme. Epithelium and mesenchyme together form all the ectodermal appendages, such as teeth, hair and glands (Gilbert 2006). In teeth, the enamel is formed from epithelium, whereas dentin and the jawbone are formed from mesenchyme (Gilbert 2013). In the human embryo, the first signs of tooth development can be seen during the 5th or 6th embryonic week. First, the tooth-forming region, the dental lamina, appears in the dental epithelium (Fig. 9). Next appear the dental placodes that give arise to tooth families. Tooth buds of individual deciduous teeth appear in the placodes, and then invaginate into the dental mesenchyme (Fig. 10). The germs of the permanent teeth appear later on the lingual side of the deciduous teeth. The M1 develops from the extension of the placode, whereas the other molars bud from the posterior end of the preceding molar.

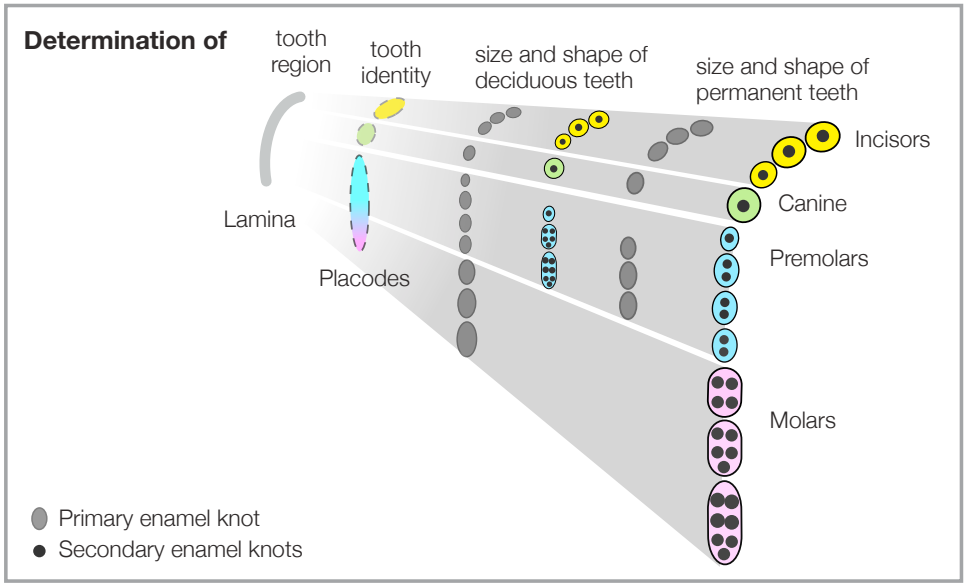

Fig 9. Schematic representation of dentition formation in mammals, occlusal view. Dental lamina determines the tooth region in the jaw after which the dental placodes determine the tooth families. The appearance of the enamel knots determines the tooth size and cusp number. Developmentally the first premolar and the molars belong to first generation of teeth, but they are considered to be part of the permanent dentition because they are not replaced. Edited from Jernvall & Jung 2000.

During the following cap stage (Fig. 10), an area of non-dividing epithelial cells, enamel knot, forms in the tip of the tooth bud, and the cap-like formation marks the future crown base. The cap stage is followed by a bell stage during which the epithelium continues to grow and fold, and species-specific cusp patterns begin to appear. In a single-cusped tooth, a primary enamel knot that appeared already in the cap stage, gives rise to the tip of the crown. In multicusped mammalian teeth, the cell division stops again in secondary enamel knots that form at the places of future cusps (Jernvall & Thesleff 2012). After the appearance of the secondary enamel knots, the cells underneath the folding epithelium differentiate into odontoblasts that start to secret dentin matrix. Once the first layer of dentin (mantle dentin) is secreted, ameloblasts that differentiated from epithelium start to secrete enamel matrix. The secretion continues as the ameloblasts move away from the enamel-dentin junction (EDJ), leaving behind a protein matrix in which immature mineral crystals are embedded (Robinson et al. 1995b). Tooth cusp formation is thought to be regulated by a patterning cascade progressing from one secondary enamel knot to another (Jernvall 2000, Jernvall & Thesleff 2012). This cascade begins from the tallest cusp, proceeds towards the shorter cusps, and ends at the shortest cusp. The same developmental cascade of cusps and other characters of crown tend to follow the evolutionary steps of tooth morphology (Harjunmaa et al. 2014, Luo 2014). The shape of individual tooth cusps, apart from enamel thickness, is a result of relative growth differences between the inner enamel epithelium and the underlying mesenchyme (Jernvall & Jung 2000).

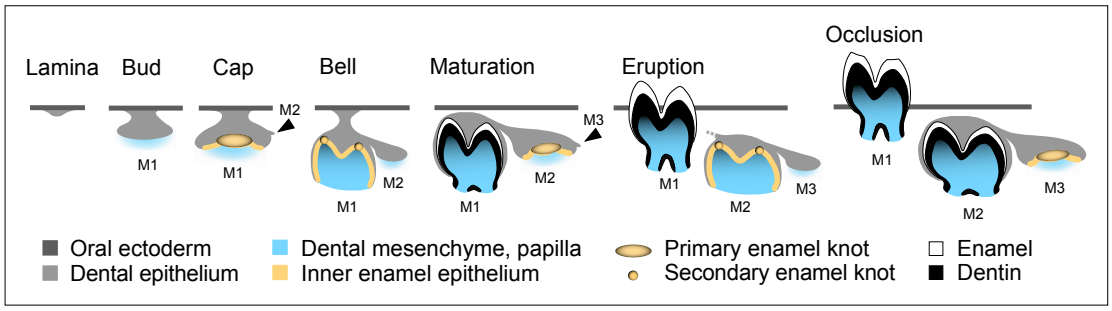

Fig 10. Sequential formation of mammalian molars, lateral view. Individual molars develop from an extension of the dental placode. The process goes through several stages that determine the tooth morphology before the mineralization, and tooth eruption. Once the tooth is erupted, its morphology can change only by wear or damage. Edited from Jernvall & Thesleff 2012.

When the enamel matrix secretion process starts, the ameloblasts acquire a columnar morphology and their basal secretory appendages, Tomes' processes (Robinson et al. 1995b). The enamel matrix has the structural features of mature enamel, but includes

about 15% of mineral material, 65% of water, and 20% of proteins (Berkovitz et al. 2002). Ninety percent of the proteins are amelogenins, and the rest are a mixture of other proteins, such as tuftelins and ameloblastins (Berkovitz et al. 2002). Crystals of hydroxylapatite start to grow almost immediately within the newly secreted matrix. At this stage, the crystals are more variable in size and shape than in matured enamel. The shape and angle of the Tomes' processes are thought to control the initial orientation of the matrix proteins and ultimately the orientation of the apatite crystals and the enamel rods (Mathur & Polly 2000). Apatite crystals orient roughly perpendicularly to the secretory surface (Boyde 1989, Fortelius 1988).

At the end of the bell stage, the tooth crown is fully formed (Fig. 10). The matrix secretion is followed by enamel maturation; the nuclei of apatite crystals continue to grow in length and thickness, the proteins are broken down and removed from the matrix together with most of the water. Roots start to grow after the completion of the crown, and continue their growth during the tooth eruption (Jernvall & Thesleff 2012). The cementum that finally attaches the tooth to the jaw together with the periodontal ligaments, is secreted by cementoblasts.

Even though the matrix formation by ameloblasts and odontoblasts is a cyclic process, the periodicity is not completely regular. Pigmented parallel growth layers, enamel striae (of Retzius), are often seen in thin sections of tooth enamel. They represent hypomineralization and are thought to be caused by metabolic disturbances during the mineralization (Berkovitz et al. 2002). The enamel formed before birth do not have pronounced enamel striae, but birth causes a line, called neonatal line that is the most prominent of all the incremental lines. Weaning, fever, and other traumatic events in individual's life can also cause distinct enamel striae (Schwartz et al 2006, Eli et al. 1989). In humans and pigs, the M1 is the only permanent tooth where the neonatal line can be found, and it is not present in unborn fetuses (Schour & Hoffman 1939). Daily increments can be detected as cross-striations in between the enamel striae (Berkovitz et al. 2002). The terminations of the enamel striae create circumferentially travelling ridges and grooves, perikymata, on the surface of the tooth crown (Fig. 11).

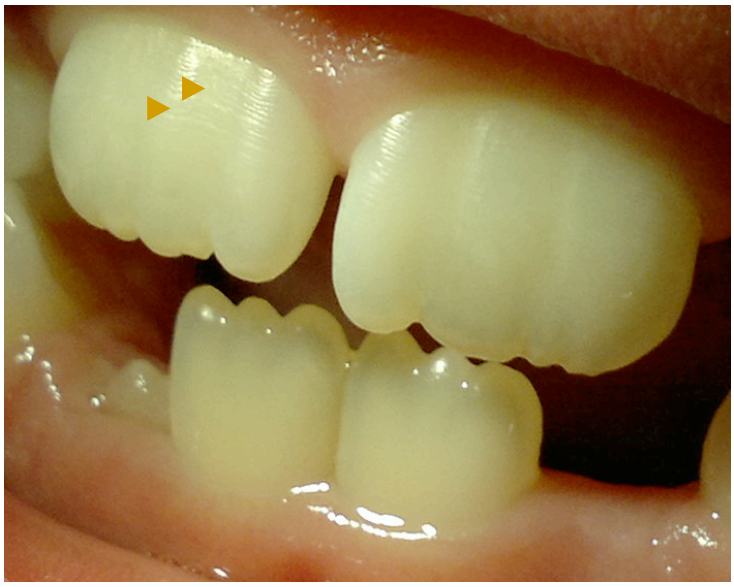

Fig 11. The outlines of the enamel striae appear as a horizontal lineage on the surface of the tooth crown (arrows). This feature is called perikymata. Here are incisors of an 8-year-old boy, which are not fully erupted.

Over one hundred genes are known to be expressed during the different stages of the enamel formation (Bite-it 2015). These genes are involved in matrix formation, the breakdown and removal of proteins, and mineralization. Over twenty of these genes are essential in a way that absence of these genes causes distinct defects in the tooth enamel of laboratory mice (Bei 2009). Several hundreds of genes are known to be involved in the whole process of tooth formation.

The ameloblasts die prior to tooth eruption and therefore, the tooth enamel does not regenerate once the enamel formation is completed (Cuif et al. 2011). Any damage during enamel formation or later on will be permanent, and therefore, tooth enamel has been used to investigate the life history of an individual. The enamel maturation process still continues in the oral cavity, for example approximately for more six months in humans.

Fully matured human enamel is 92% apatite mineral; the rest is mostly water and less than 1% is organic matter (Fig. 12). Enamel has the same constitution as dentin and bone, but the enamel goes through a longer maturation (Lucas 2004). Tooth enamel is the hardest and most resistant substance that a mammal can produce, but it is also brittle and dependent on the underlying dentin for support (Lucas 2004, Von Koenigswald et al. 2011). Enamel is a selectively permeable substance, allowing water and certain ions to pass through via osmosis. The susceptibility of the mineral component apatite for dissolution in acidic environments is the basis for tooth decay (caries).

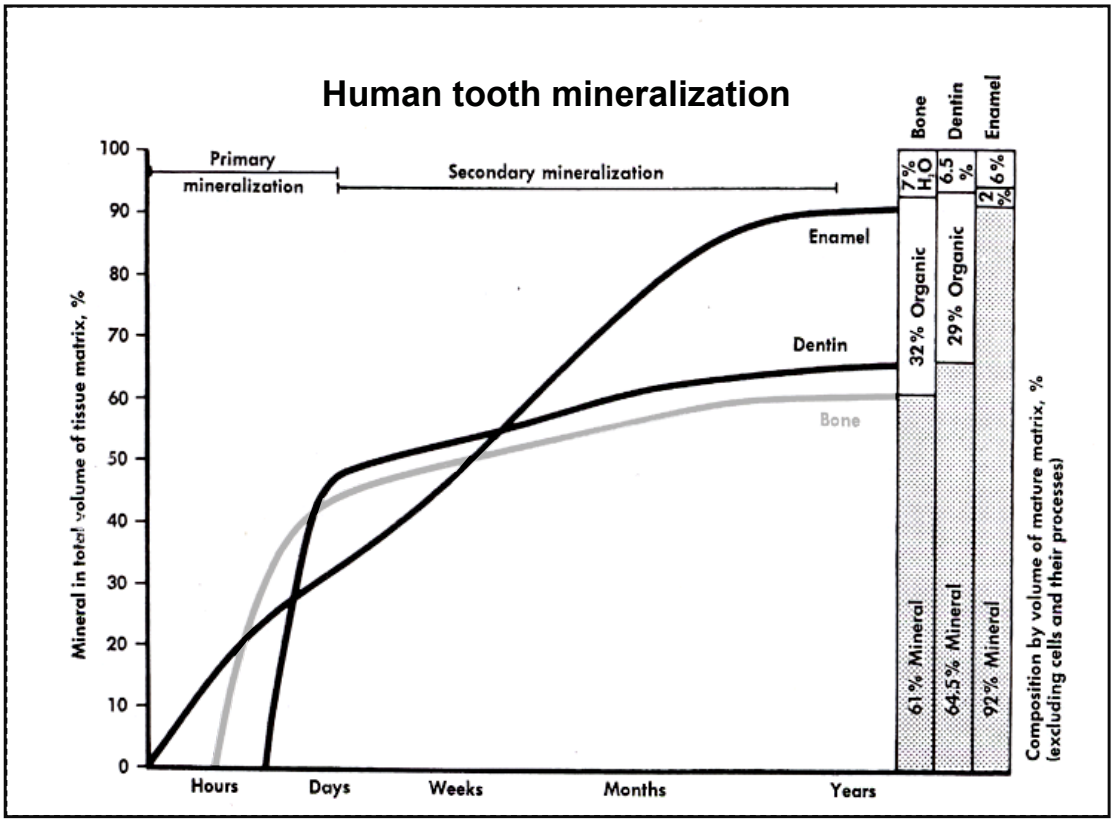

Fig. 12. Schematic representation of the maturation of human enamel, dentin and bone. In the beginning, the mineralization of dentin is faster than that of enamel, but slows down after the primary mineralization. Enamel mineralization continues more constantly and for a longer period than the mineralization of dentin or bone, but the latter ones keep their renewal capability through life (edited from Sicher 1966).

Compared to the enamel mineralization, the dentin mineralization is faster in the beginning, but slows down after the primary mineralization (Fig. 12). Mature dentin consists approximately 65% of hydroxylapatite, 29% organic matter, and the rest is water (Sicher 1966). This composition makes dentin hard but elastic. The dentin contains microscopic channels, so called tubules that travel on a gentle s-shape pattern through the entire thickness of dentin, and some species also have tubules in enamel (Sahni & Lester 1988). Fluid filled tubules are thin close to the EDJ and unite to become larger channels towards the direction of the pulp. As a result, the dentin is semi-permeable, and can convey the sensation of pain and promote tooth decay (Berkovitz et al 2002). Unlike the enamel, the dentin has renewable capability because odontoblasts remain viable after the tooth eruption. In response to excessive wear, caries or irritants, reparative secondary dentin is laid down at an accelerated rate.

The cementum that covers the roots and attaches the tooth to the jaw has a mineral content of 65% in its mature stage (Berkovitz et al. 2002). Cementum is capable of

repairing itself to some extent, and it is more similar to dentin than to enamel. In human teeth, cementum most often overlaps the enamel in the enamel-cementum junction (ECJ), but there is variation: either a sharp line where the enamel and cementum meet but do not overlap, or a gap between enamel and cementum, are also possible (Fig. 13).

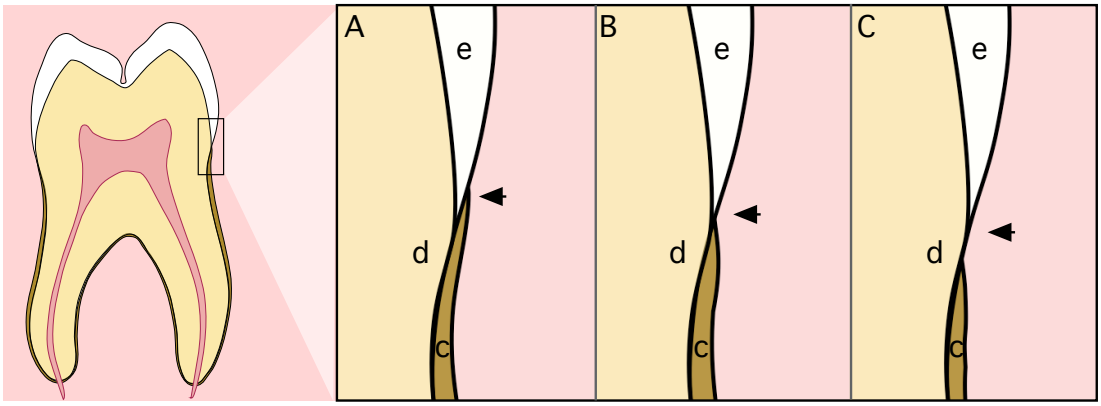

Fig. 13. Three patterns of the ECJ (arrows). A) The cementum overlaps the enamel for a short distance. B) The cementum and the enamel meet but do not overlap. C) The cementum and the enamel do not meet and the dentin is exposed between them. E = Enamel, D = Dentin, C = Cementum (edited from Berkovitz et al. 2002).

2.6 Enamel structure

The internal structure of enamel is determined by the enamel rods, and the arrangement of these rods. The enamel rods travel from EDJ to the enamel surface, with their path dependent on enamel complexity (Fig. 14). Each rod consists of several million of tightly packed apatite crystals that are approximately parallel to the course of enamel rod. The thickness of enamel rods is usually around 5–6 µm in diameter and up to 2.5 mm in length (Berkovitz et al. 2002). In between the enamel rods is interrod enamel that has similar composition but its crystal orientation deviates by 40–60° from that of the enamel rods (Berkovitz et al 2002).

In the molars of most modern placental mammals that have molar width larger than 4 mm, the enamel rods are decussating (von Koenigswald et al. 1987). When a polished tooth or tooth section is exposed to polarized light, the light causes an optical effect called Hunter-Schreger-bands (HSB) on the decussating enamel rod layers; alternating brighter and darker bands reflect the arrangement of the rods layers (Fig. 14 a) (von Koenigswald 2011 and reference therein). In enamel of most mammals, the layer

thickness is from 6 to 15 parallel rods; larger mammals tending to have thicker layers, but in rodent incisors the decussating rod layers can be one rod thick (Fig. 14 d). The arrangement of the enamel rods differs among species (Fig. 14 b-f).

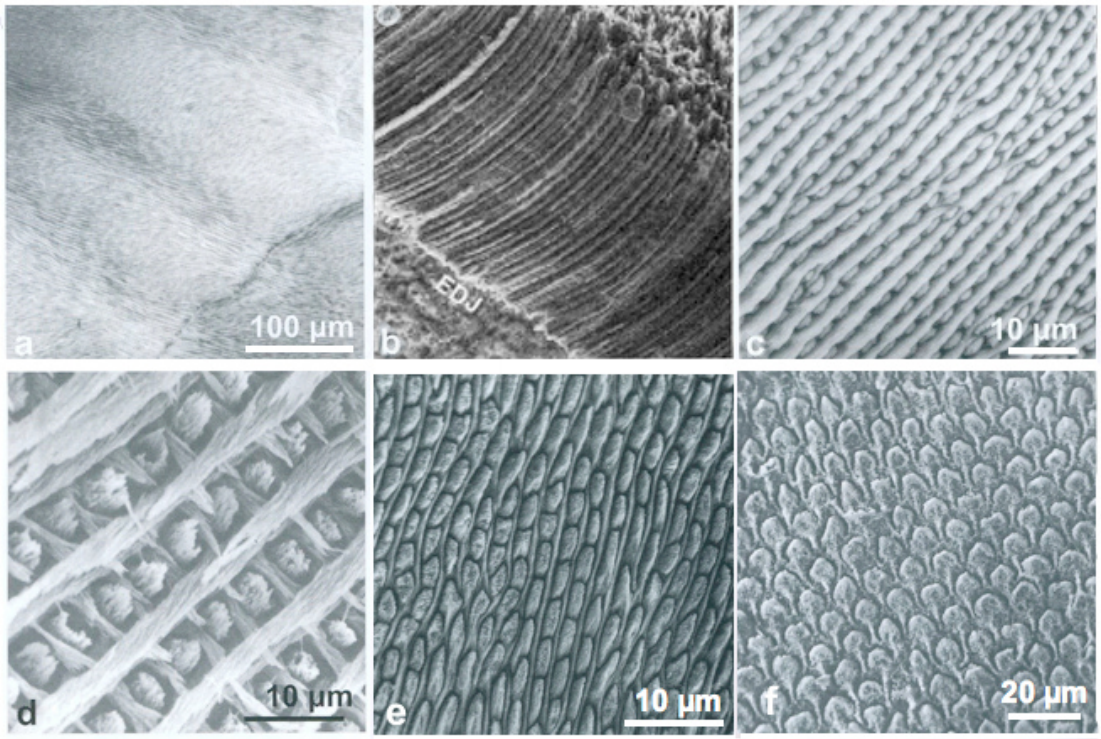

Fig. 14. Arrangements of enamel rods in different resolution and species. a) Hunter-Schreger bands are an optic phenomenon caused by decussating enamel layers (deer enamel). b) Parallel enamel rods in early Paleocene condylarth *Conacodon* (no scale in the original figure). c) Enamel rod arrangement in horse incisor d) Enamel structure of jerboa (rodent). e) Enamel structure of pig. f) Enamel structure of human, so-called keyhole pattern (edited from Cuif et al. 2011, Koenigswald et al. 1987, Boyde 1989).

Usually the rods do not decussate in the outer layer of enamel, and the apatite crystals are approximately parallel to each other. In the region of the cusp where enamel is exposed to the greatest stress, the enamel rods interweave to form a more complex arrangement; this is called gnarled enamel (Lucas 2004, Nanci 2014, Berkovitz et al 2002).

2.7 Domestic pig dentition

Pigs and hogs are artiodactyls that are endemic to Africa and Eurasia, but they have been introduced to almost everywhere where humans live (Ungar 2010). Most suids live in forest, woodland or savannah habitats, and they are plant-dominated omnivores. *Sus scrofa domesticus* (domestic pig) was domesticated from *Sus scrofa*, wild boar, presumably in 13 000–12 700 BC. Pig eats tubers, bulbs, nuts, seeds, insect larvae, carrion, and also small vertebrates, when able to catch one (Hillson 2005). In contrast to humans, pigs have larger incisors in the lower jaw than in the upper jaw. The canines are relatively bigger than ours (Fig. 15), and pigs have extreme sexual dimorphism in the canines: male canines are ever-growing, large and curvy with enamel only on two sides of teeth, and female canines are smaller, with a complete enamel hood and roots. Domestic pig molars are round-cusped bunodont teeth that have four taller cusps with several subsidiary cusplets. Molars have thick enamel that wears down quite rapidly to expose the dentin. The dental formula of pig is I 3/3, C 1/1, P 4/4, M 3/3.

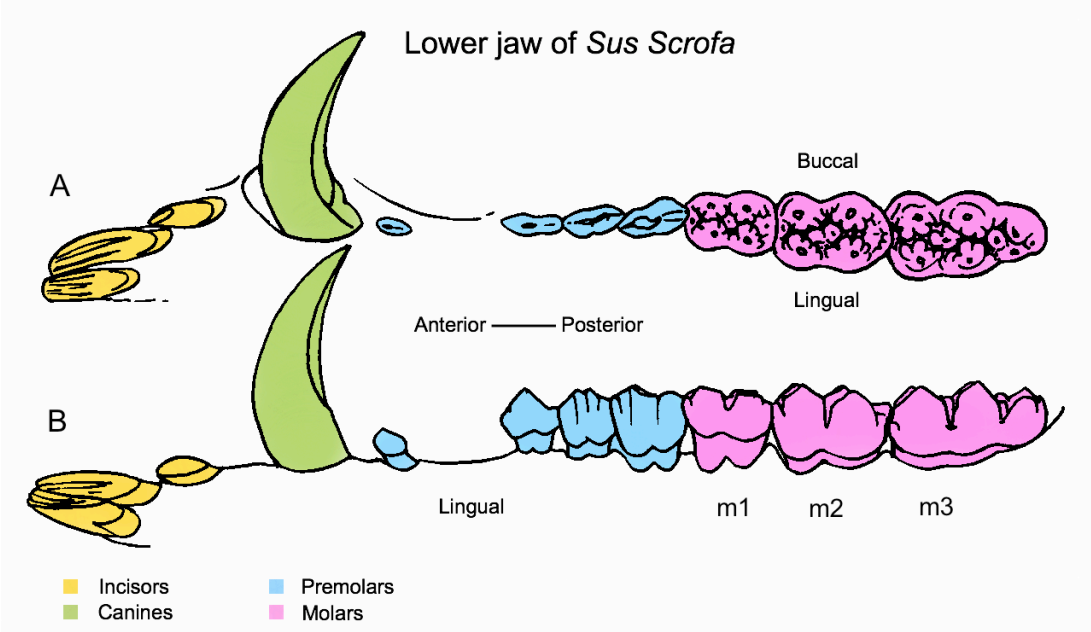

Fig 15. Pig (*Sus Scrofa*) has 44 teeth in the permanent dentition. The pig is an omnivore like human, and has large, bunodont teeth with thick enamel and deep fissures. A) Occlusal view of a half mandible B) Lingual view of a half mandible. Edited from Hillson 2005.

Compared to human teeth, pig teeth develop considerably faster, although they are larger than human teeth (Table 3). The mature enamel of the domestic pig is softer than human enamel (Karlström 1931) and its mineral content is only 60% by volume at the time of eruption (Kirkham et al. 1988). The M1s of the domestic pig start to mineralize

approximately three weeks before birth and erupt at age of four months. The life span of a domestic pig is 7–8 years (Karlström 1931).

Table 3. Tooth development of domestic pig following Tonge & McCance 1973, McCance et al. 1961. The pig has all teeth erupted by age of 16 months. Observations based on radiographic pictures and histology. ED = embryonic days, domestic pig gestation takes approximately 115 days.

Molar pig	**M1**	**M2**	**M3**
Visible mineralization	93 ED	4 months	8 months
Crown complete	2-3 months	7 months	12 months
Eruption starts	4 months	9 months	16 months

Pig molars have more complex morphology than human molars and there is also more variation in molar size and shape, especially in the posterior part of M3. Where human molars compose of a trigonid and a talonid with two cusps in each, pig molars have smaller cusplets that surround the main four cusps and a distal expansion of talonid M3 (Fig. 16). A more precise molar terminology is described in Fig. 16.

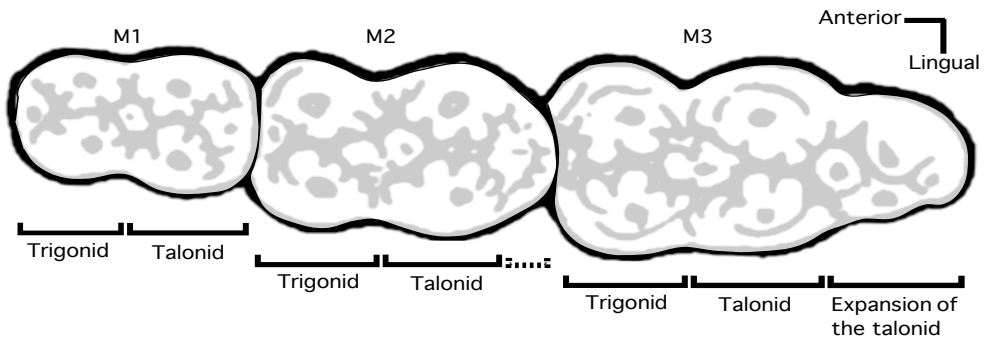

Fig 16. In pig molars, the four main cusps are surrounded with smaller cusplets. The anterior part of a molar is called the trigonid and the posterior part is called the talonid. The M3 has a well-developed posterior expansion of the talonid. Many measurements in this work are done from the lingual cusps. The linguo-trigonid cusp is called the metaconid and the linguo-talonid cusp is called the entoconid. Edited from Thenius 1989.

3. MATERIALS AND METHODS

Three half mandibles of domestic pigs (*Sus scrofa domestica*) were supplied by HK Ruokatalo food manufactory. Pigs A (right side of lower jaw), B and C (left sides of lower jaws) were approximately 6 months old and they weighed approximately 200 kg. Only the first molars (M1) were erupted, second (M2) and third molars (M3) were still inside the jawbone (Fig. 17). All pigs had the M1 in occlusion and Pig A and C had visible wear facets on the cusps (Table 4). The crowns of M2s were fully formed and the resorption of alveolar bone had already started in Pigs A and C. The root formation had not started yet any in M2s. The M3s were still much smaller than other molars, and in Pig B, the M3 was still attached to the M2.

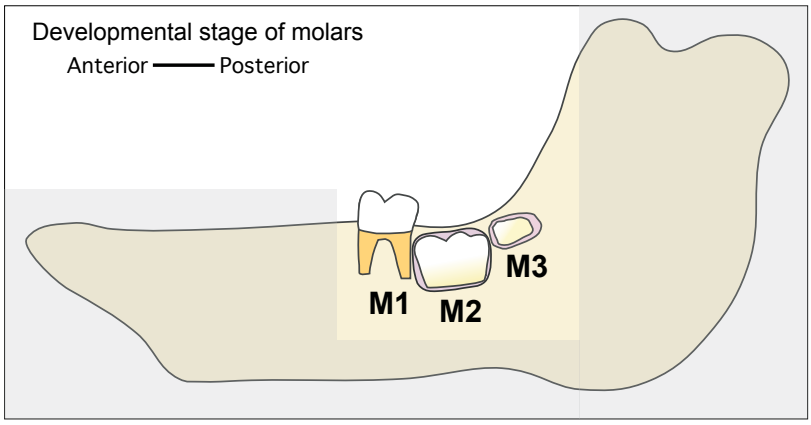

Fig 17. The develop-mental stage of the tooth samples. The M1 was erupted and in occlusion in all the pigs. The crown of the M2 was fully formed and the alveolar bone had started to resorb above the tooth in Pigs A and C. The M3 were still comparably small to their final size. The relative develop-menttal stage of other teeth is not drawn.

Museum specimens (FMNH-2047, N105, 5924) from the Finnish Museum of Natural History were used for the comparative measurements of the final size of the molars.

Table 4. The stages of development of the studied molars. Pig A molars are lower right, Pig B and C molars are lower left. M2s and M3s were still inside the jawbones in their crypta.

Pig	M1	M2	M3
A (W-R3)	Erupted, facets	Crown complete, no roots	Late bell stage
B (W-L1)	Erupted	Crown complete, no roots	Bell stage, still attached to M2
C (W-L2)	Erupted, facets	Crown complete, no roots	Late bell stage

The roots of the M1s were cut, as they were not needed in this study. To get the developing M2s and M3s from their crypta, the jawbones were opened with a bone saw, a chisel and a hammer. The teeth were taken out within their dental sacs and all tooth samples were stored in 70% ethanol at 4 °C. All the molars were scanned using microscopic x-ray computed tomography (microCT) and the other studies were done

from destructive preparations of Pig B molars. With microCT, it is possible to obtain three-dimensional absorption models of the samples without destroying them.

The destructive methods include Vickers hardness measurements, X-ray diffraction (XRF), polarized light microscopy and scanning electron microscopy (SEM). Vickers hardness tester gives mechanical comparison points to the microCT electron density models of the degree of mineralization in the teeth. Using petrographic thin sections, it is possible to precisely document the microscopic structure of the tooth cross sections. Using x-ray diffraction methods (XRD), it is possible to get information about crystal structure (phase identification), crystal orientation and the degree of mineralization in the samples. Scanning electron microscope (SEM) permits the observation of the enamel and dentin structure. All imaging and analysis were done at the University of Helsinki.

3.1 Computational x-ray microtomography (microCT)

The tomographic measurements were performed at the Laboratory of Micro-tomography at the Department of Physics. The imaging set-up is a custom-built microtomography system, which is manufactured by phoenix-x-ray System and Service GmbH (General electric), Germany (Kallonen 2011). The X-ray source is a fixed-target transmission type x-ray tube with a tungsten filament cathode and a tungsten transmission anode, target that is fused onto a 400 μm thick beryllium window.

The following parameters were used in the study: source voltage of 120 kV, source current of 170 μA, image voxel size of 10/13/24 μm down-sampled digitally to 44 μm, 5 mm Al-filter, projection images were taken over rotation step of (360°/1200 rotation), exposure time 500/750 ms, and frame averaging of 8. Tomography reconstructions were done using the program Datos /X by phoenix-x-ray System and Service GmbH (General electric).

3.1.1 The relative calibration of the microCT absorption models and imaging

Nine mineral grains were selected from the collections of the Division of Geology (Fig. 18) to test how different minerals with (relatively well) known density values absorb x-rays during the microCT scanning. Three of them (fluorapatite, quartz and siderite) were chosen as standards for the relative calibration of the microCT absorption intensities in the tooth measurements (Table 5). As there was no sample of hydroxylapatite in the collections, fluorapatite was chosen from the apatite group. Each tooth was scanned with the three mineral standards that were used for image calibration.

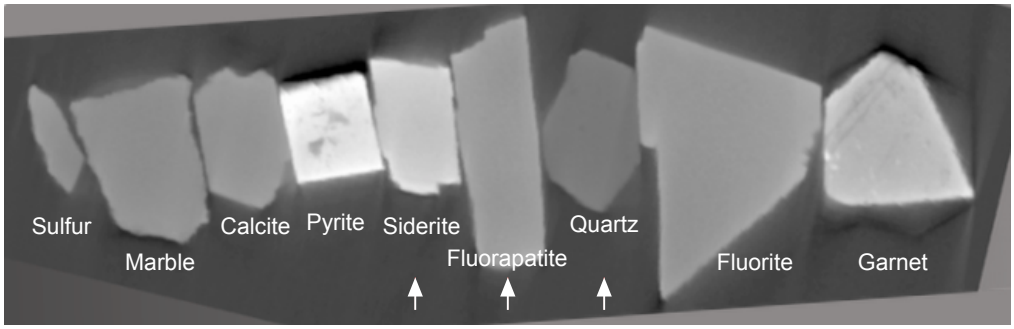

Fig. 18. After a test scan of nine mineral samples, siderite, fluorapatite and quartz (arrows) were selected to be used as standards to calibrate the gray scale electron density range of the microCT measurements during the tooth measurements.

The reconstructions of the teeth were segmented with public domain Java image processing and analysis program Fiji (ImageJ). Gray scales of absorption models were calibrated with the three minerals: The gray values of the mineral grains in the absorption models were measured from 1000x1000 µm squares of a homogenous area in center of each mineral grain (Fig. 19).

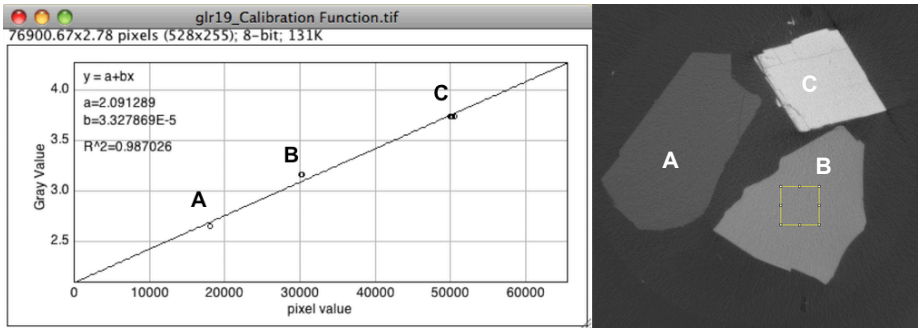

Fig. 19. The RED calibration function of the mineral grains for one reconstruction. The gray values were measured from 1000x 1000 µm squares in the core of each mineral grain. This was repeated five times for each grain in different spots in each absorption model. A = quartz, B = fluorapatite, C = siderite.

The measurements were repeated five times using different areas, and then the known electron densities (Table 5) were given the mean of the measured gray values of the corresponding areas to equalize the relative electron density values (RED) of each tooth model.

Table 5. The electron densities of hydroxylapatite and minerals that were used to calibrate the microCT reconstructions. The enamel is 96% of hydroxyl apatite, which has slightly lower electron density than fluorapatite. The RED of dentin near to electron density of quartz (Mineralogy database 2014)

Mineral	Chemical formula	Electron density
Hydroxylapatite	Ca5(PO4)3(OH)	3.15 gm/cc
Fluorapatite	Ca5(PO4)3F	3.17 gm/cc
Quartz	SiO2	2.65 gm/cc
Siderite	Fe++CO3	3.74 gm/cc

Comparison of the calibration lines of the reconstructions show small differences and there is less dispersion in the lower electron density values than in the higher values (Fig. 20).

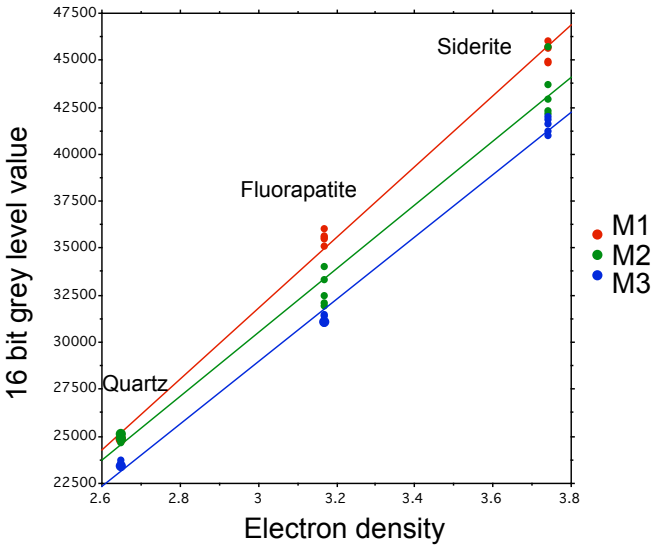

Fig. 20. Comparison of the electron density lines of minerals with corresponding microCT-obtained absorption measurements. Molars (M1, M2, M3) were scanned with calibration minerals individually. Although scans show differences, the relationship between known electron densities and absorption measurements remains linear. Individual points denote the repeated measurements of the mineral grains.

3.1.2 Measurements from microCT -images

The electron density measurements were taken of each sample from the lingual cusps of the trigonid (the metaconid) and the talonid (the entoconid). A line was drawn from the cusp tip to the tip of the pulp cavity (Fig. 21 A). A second measurement was a segmental line in the enamel adjacent to the EDJ, from the cusp tip to the tooth neck (Fig. 21 B). In the M3 of Pig B, the EDJ was not recognizable yet and the measurement was done in the middle of the visible area.

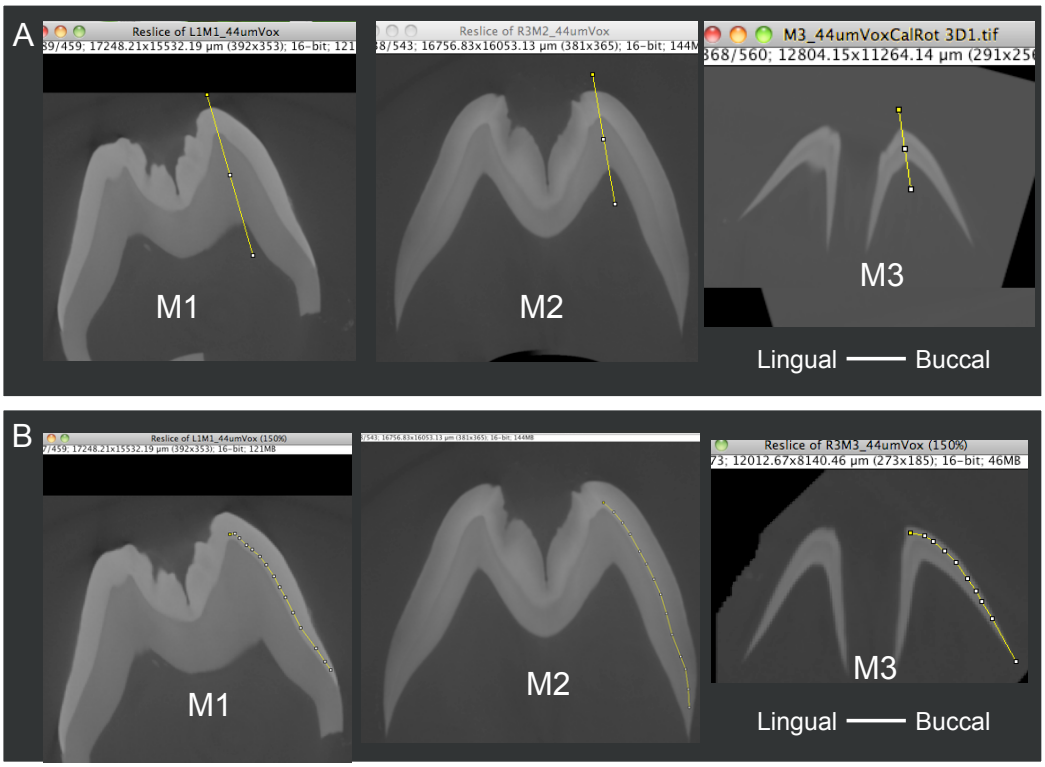

Fig 21. Two different electron density measurements (yellow lines) were made from the buccal cusps of trigonid and talonid of each molar. First, a crosscut of enamel and the dentin at the cusp tip (A), and the second measurement line follows the buccal side of the enamel from the cusp tip to the tooth neck (B).

The distances between the cusps were also measured from the microCT images. One measurement was made between the cusps of the trigonid and the talonid of the lingual and the buccal side (Fig. 22 A), and another measurement was made between the buccal and the lingual cusps of the trigonid and the talonid (Fig. 22 B). These measurements were compared with the corresponding measurements from the museum specimens (FMNH-2074, N105, 5924) from the Finnish Museum of Natural History.

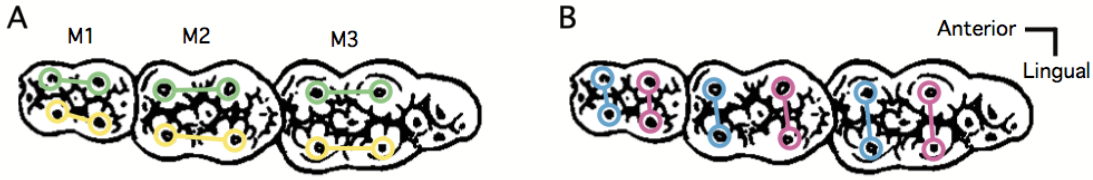

Fig. 22. Two types of cusp distances were measured from the microCT images. A) Distance between the buccal cusps of the trigonid and the talonid (green lines), and the lingual cusps of the trigonid and the talonid (yellow lines). B) Distance between the buccal and lingual cusp of trigonid (blue lines), and between the buccal and lingual cusp of the talonid (pink lines). Comparative measurements of fully formed teeth are based on photos from the museum specimens.

3.2 Hardness measurements

Hardness test samples were prepared from the molars of Pig C. One cross-section sample per molar was mounted to hard epoxy and the observed surface was polished on transverse plain of the trigonid cusp (Fig. 23). The hardness measurements were done with Leitz Miniload Micro Hardness Tester for Vickers hardness at the Division of Geology. During the Vickers hardness measurements, a pyramidal diamond indenter was let to penetrate on the sample surface for 20 seconds with a weight of 490,3 mN, and the diameter of the indentations was measured. The larger the indentation is, the deeper the diamond pyramid has penetrated into the material, and the softer the material is. The measures were repeated from the enamel and the dentin of all the molars.

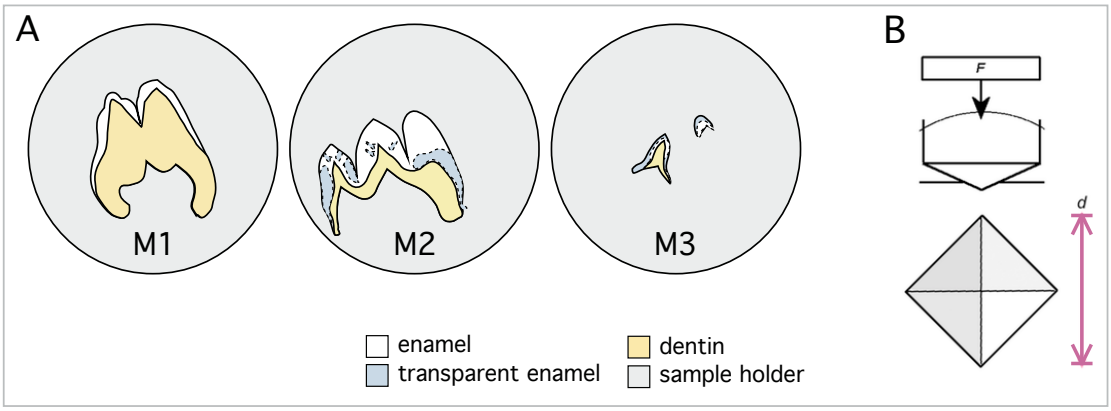

Fig. 23. A) Hardness samples were mounted to hard epoxy. B) The Vickers diamond point was let to penetrate on the sample surface for 20 sec with 490,3 mN weight, and the diameter of the indentations was measured in μm. Vickers hardness measurements were done on the molars of the Pig C.

3.3 X-ray diffraction analyses (XRD)

X-ray diffraction method (XRD) is used to identify and determine the crystal structure of solid materials. Here it was used to observe the degree of the mineralization, and the orientation of crystals from polished sections of teeth and powder samples. The X-ray diffraction measurements of enamel, dentin and jawbone were carried out with Philips Xpert PW3020 X-ray powder diffractometer at the Division of Geology.

The 2-theta angular range of 5°–75° was measured with 8 s steps, and step size of 0.05° for the hydroxylapatite phase identification from the powder samples of enamel, dentin and jawbone. The 2-theta angular range of 24°–42° was measured with 8 steps and step size of 0.05° for crystal orientation analyses of enamel in the tooth sections. The x-ray

diffraction patterns of the samples were compared with a peak list of hydroxylapatite from ICDD (International Centre for Diffraction Data) PDF-4 Minerals 2014 Powder Diffraction File.

All samples were measured on glass slides. Powder samples of enamel, dentin and jawbone were ground in an agate mortar in acetone suspension and spread on a glass in acetone suspension to form a thin homogenous layer. In addition, slightly polished thin sections of different orientations of teeth were measured to observe the dominant orientation of apatite crystal in enamel. Most of the thin sections were cut along tooth axis and along enamel rods, but one tangential sample of M1 perpendicular to enamel rod orientation was also studied. The X-ray diffraction measurements from the thin sections were made before the final polishing and glass cover.

3.4 Polarized light microscopy

Cross-sections of teeth were prepared for microscopic examinations. One thin section from each molar of the Pig C was prepared in the thin section laboratory of the Division of Geology. The preparation method was the same that is used for petrographic thin sections and the final thickness of the thin sections is approximately 30 μm. The teeth were covered with epoxy before cutting and polishing to avoid the fractioning. Imaging was done with Leica dFc450c microscope, at the Division of Geology.

3.5 Scanning electron microscope imaging (SEM)

A Scanning electron microscope (SEM) was used to observe the enamel and dentin of the M2 of Pig C. The M2 imaging was done at the Electron Microscopy unit of the Institute of Biotechnology at Viikki campus. Prior to imaging, the fractured surface of the M2 was treated with 30% phosphoric acid for 30 seconds, rinsed with deionized water and coated with gold by vapor deposition. In addition, XRD powder preparation of M1 enamel was imaged using SEM at the Division of Geology.

4. RESULTS

Below I will report the results separately for each of the three pigs studied.

4.1 Tooth size and relative electron density (RED)

4.1.1 Pig A molars

The M1 crown dimensions are 18.2 mm in length, 10.6 mm in width, and the crown height is 9.9 mm from the metaconid tip to the ECJ in the tooth neck (Fig 24, M1). The RED of the enamel is approximately 3 gm/cc, corresponding closely to the electron density of fluorapatite (3.17 gm/cc, Table 5) and indicating a highly mineralized state. The RED of the dentin is approximately 2.7 gm/cc and the EDJ is sharp from the cusps to the tooth neck. Enamel is worn down at the trigonid cusp tips and the dentin is exposed. Cementum has approximately the same electron density as the dentin.

The M2 crown dimensions are 22.5 mm in length, 13.7 mm in width, and the crown height is 13.6 mm (Fig 24, M2). The crown morphology of the M2 is already fully formed but the root development has not started yet (determined from the fresh specimens). The gradient of enamel maturation extends to two directions; from inside to out and from top to down. Specifically, the electron density is higher closer to the EDJ than close the tooth surface and in the main cusps than in the lower cusplets and tooth neck. In the tooth neck region, the electron density of enamel is lower than the electron density of the dentin. The RED of the dentin is approximately 2.7 gm/cc. The EDJ is sharp at the main cusps of the trigonid and the talonid, but not distinct at the smaller cusps, tooth neck, and cusp valley region. The enamel on the metaconid tip was slightly damaged during the jaw opening process.

The dimensions of the visible part of M3 are 18.0 mm in length, 10.6 mm in width, and the crown height is 6.0 mm (Fig 24, M3). In the M3, the mineralization has started in the trigonid, talonid and at the expansion of the talonid. Compared to a fully formed M3, all the cusps are still very close to each other with no mineralized ridge between them. The RED of the enamel and the dentin are equal, decreasing slightly to the direction of the EDJ. The REDs of the EDJ are approximately 2.6 gm/cc. The EDJ can be distinguished as a darker zone in the absorption models.

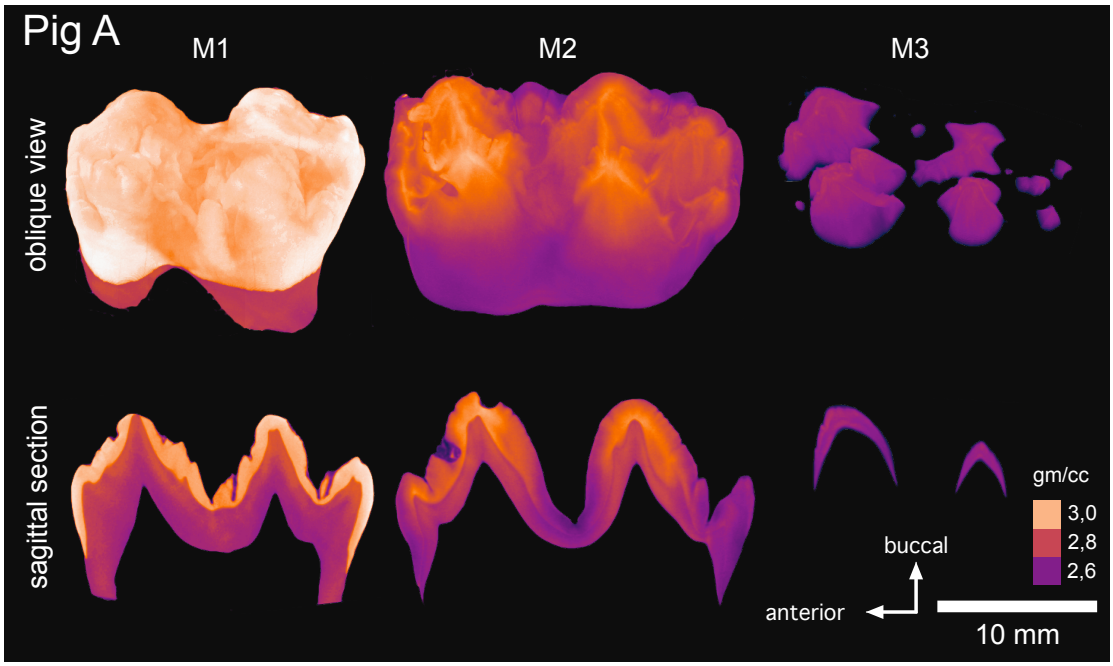

Fig. 24. Absorption models of Pig A molars: the M1 is fully erupted and in the trigonid cusps are worn to expose the dentin. The crown formation of M2 is complete but root formation has not started yet. The development of M3 is in early bell stage: Biomineralization has started in the main cusps of trigonid, talonid and the extension of talonid, but the cusps are not connected and the crown base formation has not started yet.

By comparing the molars with each other, the progression of mineralization is visible in the enamel, but the dentin has more constant values throughout the thickness (Fig. 28). The RED of the M2 enamel is comparable to the values of the M1 at the EDJ, but the values decrease towards the tooth surface. The enamel of M2 is thicker than in the M1, but the dentin is thinner in the M2 and thins down to the direction of the neck. The dentin has approximately the same electron density in M1 and M2, and in both teeth, the values are slightly decreasing in the direction of the pulp. In M3, the electron density of enamel and dentin stays clearly below the two other molars. The trigonids and the talonids do not have detectable RED difference in any molar (Fig. 28).

4.1.2 Pig B molars

The M1 crown dimensions are 19.0 mm in length, 12.0 mm in width, and the crown height is 11.1 mm from the metaconid cusp tip to the ECJ (Fig 25, M1). The RED of the enamel in the fully erupted M1 is close to 3 gm/cc. The relative electron density of the dentin is approximately 2.7 gm/cc, and the EDJ is sharp from cusps to the tooth neck. The tooth has reached occlusion but shows only light wear.

The M2 crown dimensions are 23.4 mm in length, 14.0 mm in width, and the crown height is 11.0 mm (Fig 25, M2). The crown of the M2 is nearly formed but the root development has not started yet. The electron density of the enamel is still lower than that of the dentin and, consequently, the shape of the EDJ is dimly visible through the enamel. The RED of the enamel is approximately 2.65 gm/cc at the EDJ, but decreases to the direction of the tooth surface. The RED of the dentin is slightly lower than that in the M1. In the smaller cusps and in the tooth neck region, the electron density difference between the enamel and the dentin disappears.

The M3 crown dimensions are 6.6 mm in length, 6.0 mm in width, and the crown height is 2.6 mm (Fig 25, M3). In the M3 the mineralization has started at tips of the trigonid and the talonid cusps but the cusps are still close to each other with no mineralized ridge between them. The expansion of the talonid cannot be seen from the absorption model. The RED of trigonid part is close 2.7 gm/cc in the cusp tip region, but the RED of talonid cusp tips stay under 2.5 gm/cc.

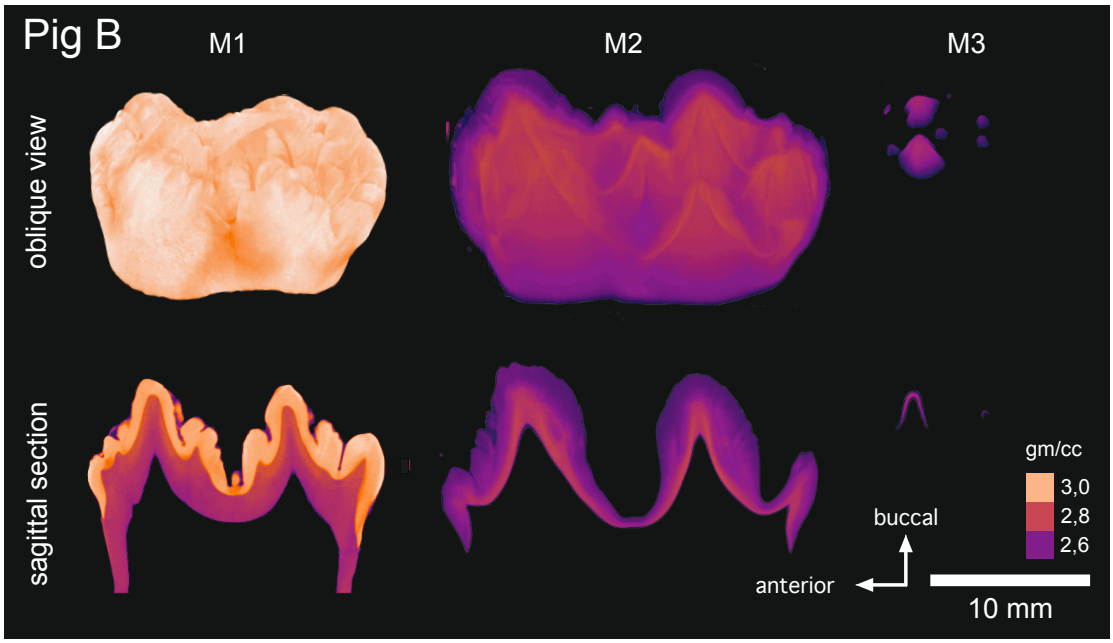

Fig. 25. Absorption models of Pig B molars: the M1 is fully erupted and the trigonid cusps are slightly worn. The crown formation of the M2 is complete but root formation has not started yet. In the M2, the enamel has lower electron density than the dentin. The development of the M3 is in early bell stage: Biomineralization has started in the main cusps of trigonid and talonid but not in the extension of talonid.

When comparing these molars to each other, the different stages of development are well visible. The electron density of the M1 enamel is clearly higher than that of the M2, even if the RED of dentin in both teeth are almost on same level. The electron density of the M2 enamel is lower at the surface but increases towards the EDJ, but remains below the level of M1 or dentin. As in the M2, the dentin mineralization is still ahead the enamel mineralization, and the shape of EDJ is visible in the absorption model. The dentin is thinner in M2 than in the M1, and thins down to direction of neck. The M3 is still very small; the enamel and the dentin are not possible to distinguish. The electron density of M3 in Pig B stays below other molars in the enamel and the dentin, and reaches the highest values at the EDJ of the trigonid. The electron densities of the trigonids and the talonids do not have detectable differences, except in M3, where the trigonid has higher electron density than the talonid (Fig. 28, Pig B).

The absorption model of the M2 indicates the difference in the shapes of the EDJ and the enamel surface. The cuspal morphology EDJ is sharper than the rounder (bunodont) morphology of enamel surface. A comparable difference in shapes can be observed in the M1, when the fully mineralized enamel is digitally removed exposing the EDJ (Fig. 26).

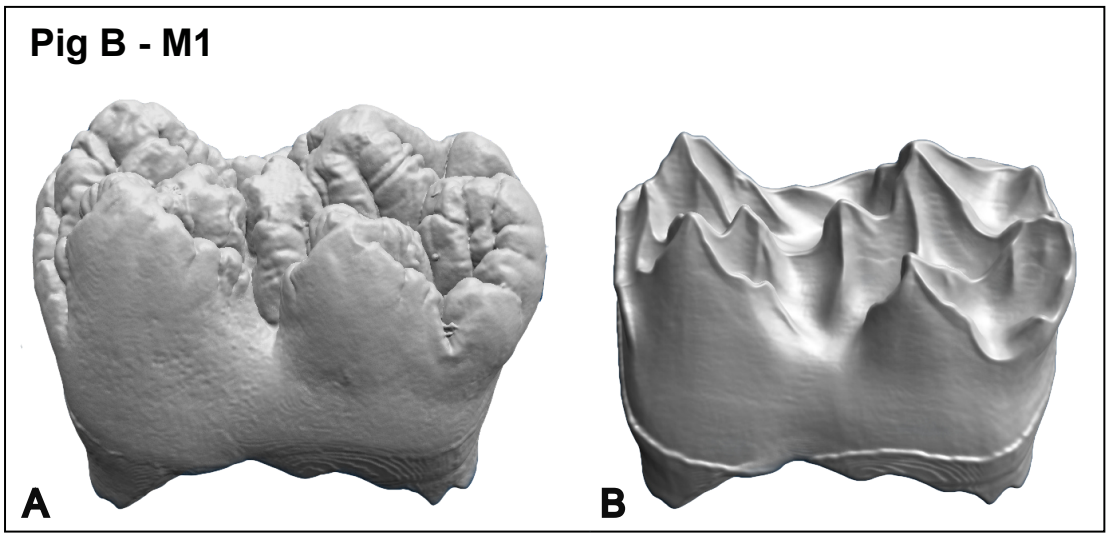

Fig. 26. The M1 of Pig B. a) Enamel surface b) EDJ made visible by removing the enamel using the in Fiji volume viewer. The edge at the tooth neck is the border of the cementum.

4.1.3 Pig C molars

The M1 crown dimensions are 18.0 mm in length, 11.1 mm in width, and the crown height is 9.9 mm from the metaconid cusp tip to the ECJ (Fig 27, M1). The fully erupted M1 is close to 3.0 gm/cc, but the enamel seems still not to be fully mineralized in between the cusps (Fig. 27, M1). The thin parts of the enamel at the tooth neck show the highest electron density. The RED of the dentin is 2.7 gm/cc. The EDJ is sharp from the cusps to the tooth neck. The enamel is worn down at the trigonid cusps and thinned the talonid cusp tips.

The M2 crown dimensions are 22.2 mm in length, 13.3 mm in width, and crown height is 9.9 mm (Fig 27, M2). The crown of M2 is fully formed but root development has not started yet. In the M2, the electron density is above 2.9 gm/cc at the cusp area, but falls constantly to the direction of tooth neck, being below 2.6 gm/cc in neck region. The electron density of enamel and dentin are equal in the tooth neck area. The RED of dentin is equal to the M1 (2.7 gm/cc). The dentin is slightly ticker than in the M1 and thins down to direction of roots. EDJ is also sharp on the main cusps and cusplet tips, but less distinct in the tooth neck area.

The M3 crown dimensions are 17.3 mm in length, 10.2 mm in width, and crown height is 5.6 mm (Fig 27, M3). In the M3 the mineralization has started in all main cusps, the cusps are still near to each other without mineralized ridge between the cusps. The tips

of smaller cusps and future extension of talonid can be seen as small spots. The REDs of enamel and dentin are comparable to each other. The RED of enamel seems similar to M2 cuspal enamel (approximately 2.9 gm/cc).

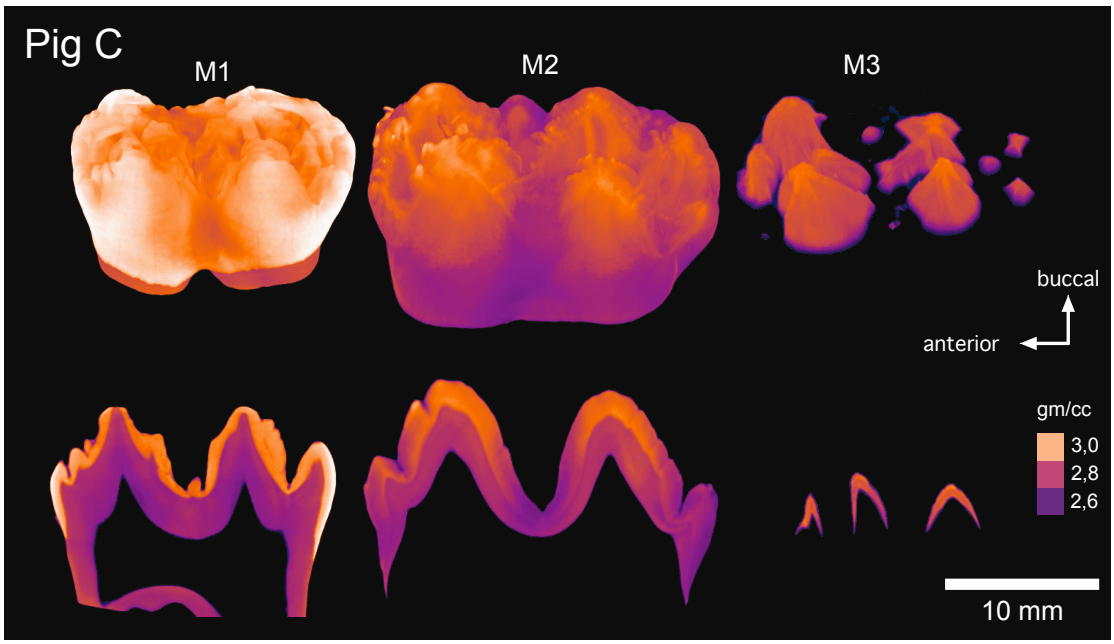

Fig. 27. Absorption models of Pig C molars: the M1 is fully erupted and the cusps are worn. The crown formation of M2 is complete but root formation has not started yet. The development of M3 is in early bell stage: Biomineralization has started in the main cusps of trigonid, talonid and the extension of talonid, but the cusps are not connected and the crown base formation has not started yet. The enamel of M3 has relatively high electron density compared to the M3s of the other pigs.

In the teeth of Pig C, there are no big differences between the electron densities of the trigonids and the talonids. When comparing the molars to each other, the electron density of the M2 enamel is lower at the surface, but reaches the same level as the M1 close to the EDJ (Fig. 28). The dentin is generally thicker in the M1 than in the M2 but their RED is equal. The electron density of dentin of M3 is clearly above to any other molar in the pigs studied (Fig. 28), and this was determined to be an artifact (see discussion). The electron density of M3 is the lowest at the EDJ and highest values are in the enamel.

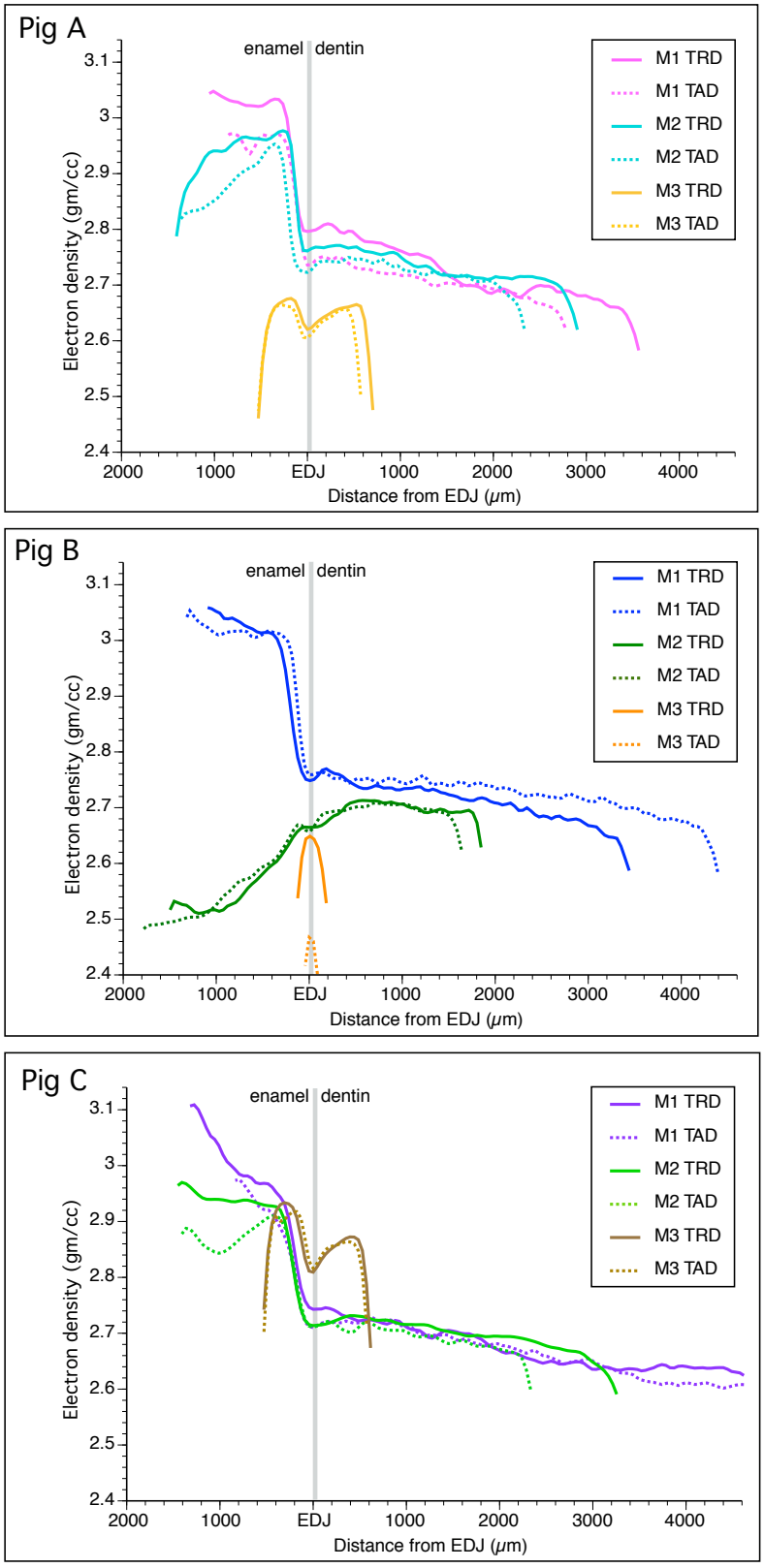

Fig. 28. Comparison of the RED-values of enamel and dentin through the cross-sections at the lingual cusp tips of the pig individuals. In Pig A, there is no big difference between the M1 and M2 REDs, except at the enamel surface. The RED of the M3 is constantly less than that of the other teeth and the lowest RED is at the EDJ. In the Pig B, the RED of the enamel in the M2 is still well below the values of M1, but the dentin of M2 of Pig B is already almost on the same level than the dentin of the M1. The RED of M3 in Pig B is the highest at the EDJ of the trigonid, and the talonid part has lower values than the trigonid. In Pig C M1 and M2 resemble the results of Pig A but M3 has higher values, even if the shape of RED-curve looks similar. The RED of M3 dentin differ from the values of the other teeth. TRD=trigonid, TAD=talonid.

4.1.4 Comparison of the tooth maturation stages among the pig individuals

The differences in the electron density and the enamel thickness are small in the M1s (Fig. 31). In all the M1s, the RED of the enamel stays quite constant, approximately 3.0 gm/cc from the cusps to neck (Fig. 29).

The enamel maturation of the M2 is more advanced in Pigs A and C compared to Pig B, but all the M2 crowns are morphologically at the same stage of development. The REDs of enamel are equal in the pigs A and C: approximately 2.9 gm/cc on cusp area but fall to 2.6 gm/cc at the neck region (Fig. 29). The dentin formation is also further in Pig A and C compared to Pig B, but differences of RED of dentin are small (Fig. 28). In M2 of the Pig B, the valleys between the cusps are broader and the enamel is thinner in that area (Fig. 25). Its REDs stays above 2.6 gm/cc and does not considerably change from the cusp tips to the tooth neck.

The RED profiles of the M3s differ more from each other than the profiles of the M1s and M2s (Fig. 29). In Pig C, the enamel of the M3 appears to be further in a stage of the mineralization, but in Pig A there is one more visible cusplet tip in the central part of the talonid. The enamel of Pigs A and C have similar thicknesses and the electron density curves, but the RED of Pig C seem to be 0.2 gm/cc higher than that of the pig A. Pig C has REDs comparable to the M1 and the M2; 2.9 gm/cc in the cusp tips, where Pig A and Pig B trigonid have values of 2.65 gm/cc in the cusp tips that decrease towards the direction of the tooth neck. Pig B talonid does not reach RED of 2.5 gm/cc (Fig. 29). In M3 of Pigs A and B, the electron density of enamel in the trigonid starts from the same level in cusp tip, but decreases faster in the pig B, and the enamel thickness is under half of that of Pig A. The M3 (as also the M2) of the pig B is at the youngest stage of maturation as the expansion of the talonid is still yet not visible (Fig. 28).

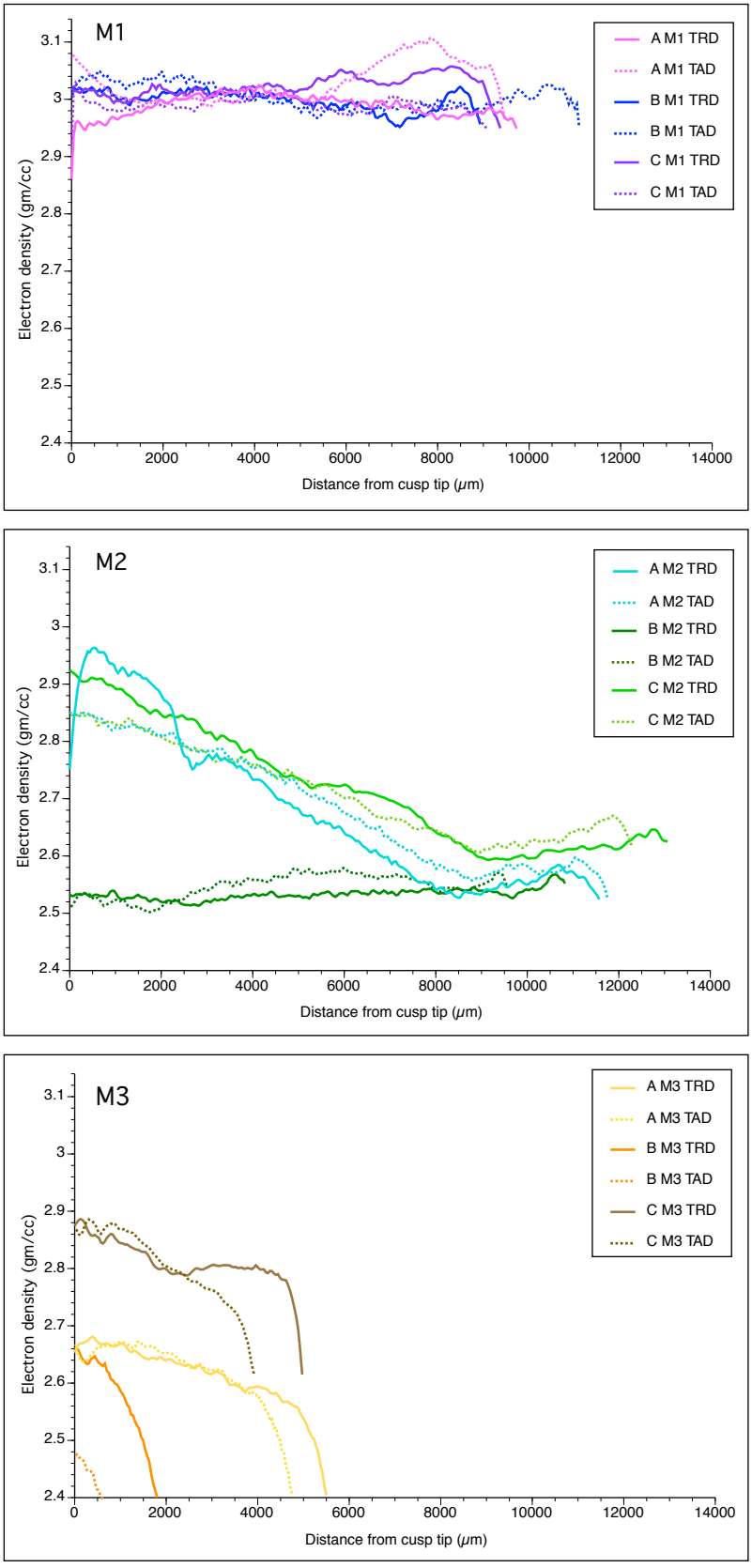

Fig. 29. Comparison of the RED-values of enamel among molars of Pigs A, B and C. The measurement line follows the EDJ on the buccal side of the enamel from the cusp tip to the tooth neck In the M1s, there is no considerable difference in electron density of, but the pig B has slightly thicker enamel in the talonid part. In the M2s, the RED-slope of Pigs A and C are comparably similar, but the enamel of Pig B has almost constant RED from the cusp to the neck. The M3s have the most variation in the electron density, and in the matrix thickness. TRD=trigonid, TAD=talonid.

The advancement of the tooth maturation is also possible to observe from horizontal sections, shown at three virtual sections of the M2s in Figure 30. When comparing the M2-samples of Pigs A and B, the differences in the REDs and the thickness of the dentin are visible. The enamel thickness seems to be quite similar in both teeth near the cusp tips, but in Pig B the enamel thins down faster towards the neck area. In the M2 of Pig A, the bidirectional process of enamel maturation is clearer in a horizontal section. In the cusp tips of Pig A, the enamel has higher REDs than dentin and the highest values are next to the EDJ. Towards the tooth neck, the RED of enamel decreases; first to be at the same level with dentin and eventually below the values of the dentin in the section III (Fig. 30). The enamel of Pig B has a lower RED of enamel than dentin in all three horizontal sections.

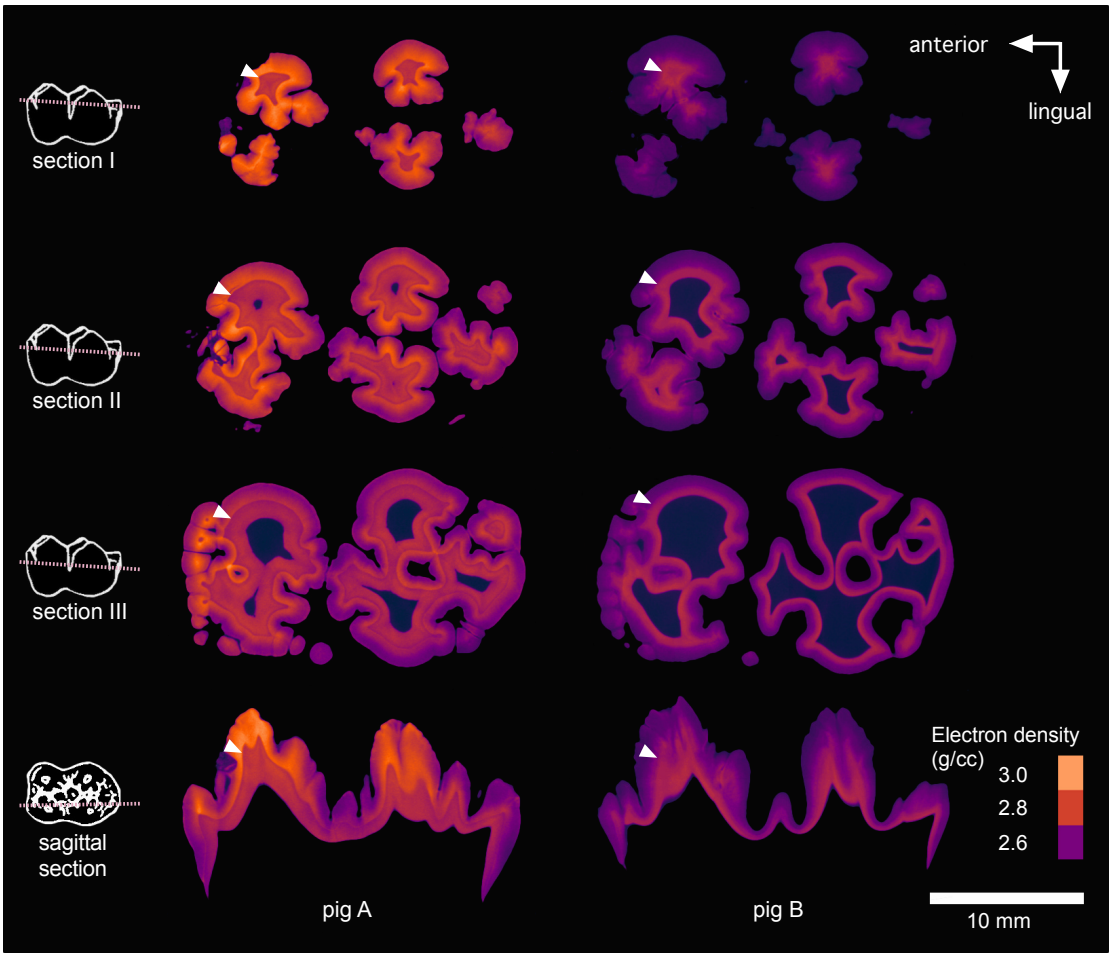

Fig. 30. Comparison of the M2 maturation in Pigs A and B. Pig A, section I: The maturation is more advanced in the dentin than in the enamel in the cusp tips. Section II: the REDs of enamel and dentin are equal, except close to EDJ where enamel has higher values and in the extension of the talonid, where dentin has higher REDs. Section III: The enamel has higher REDs in EDJ than dentin, but lower values in at the enamel surface, especially in the talonid. Pig B has thoroughly lower REDs for the enamel than for the dentin, and the pulp cavity (blue) is still larger than in the M2 of Pig A. White arrows are showing the EDJ.

In all the pigs, the M2 is larger than the M1, and in Pig B has the largest M2 of all the specimens, despite the fact that it is still not as mineralized as in the other individuals (Fig. 31).

The distances between cusp tips of the M1s are comparable between the pigs and museum samples (Fig. 31 A). The M1s have wider talonids than the trigonids except in Pig A where they are equal in width (Fig. 31 B). Compared to the museum specimens with erupted molars, the crowns of the M2s seem to be fully formed.

A clear difference in the tooth size is detected in the developing M3s, which are roughly half the size of the fully formed M3s (Fig. 31). In the museum specimens, the distance between buccal cusps is greater than that of lingual cusps (Fig. 31 A). In the developing teeth, this difference is not yet clear, particularly in Pig B, where the M3 is the smallest. In contrast, lateral separation of M3 trigonid cusps is roughly 2 mm wider than the lateral separation of M3 talonid cusps, a difference that appears to be retained in fully formed teeth (Fig. 31 B). Again, this difference is the smallest in Pig B with the least developed M3.

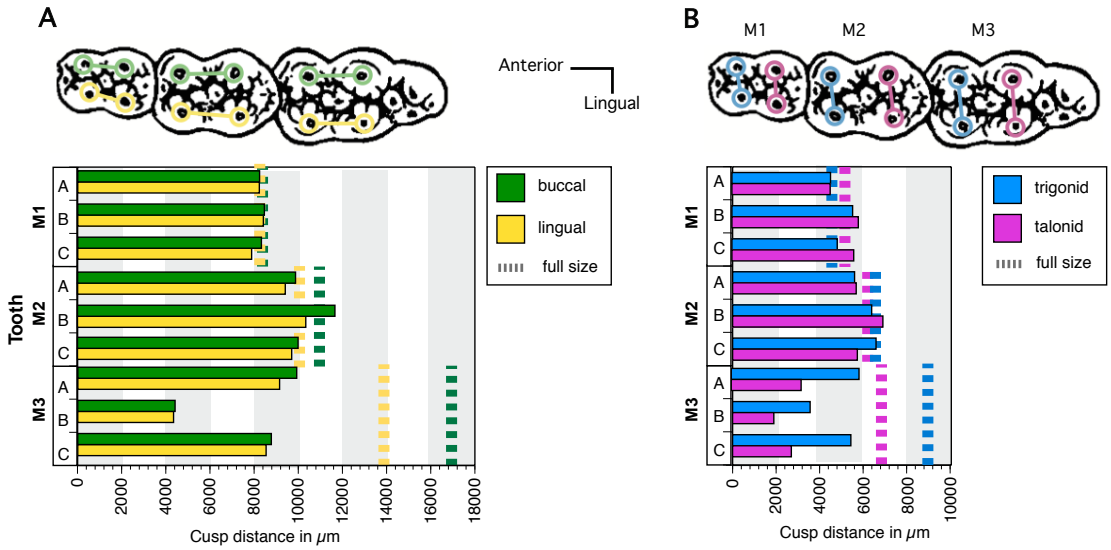

Fig. 31. Trigonid and talonid cusp distances of the molars. Dashed lines: comparative measurement results of fully formed molars from the museum specimens (*n* = 4) A) The distance between the trigonid and the talonid cusps. B) The distance between the lingual and the buccal cusps.

4.2 Hardness measurements

The hardness of enamel and dentin were measured with a Vickers hardness tester for molars of Pig C. The diameter of the indentation was measured in micrometers (µm). The softer the tissue was, the deeper the diamond peak penetrated, and the larger the indentation became.

In the enamel of M1, the Vickers measurements ranged from 26 to 52 µm, largest values were obtained close to EDJ and in neonatal line (Fig. 32). This indicates that the neonatal line and the first layers of enamel are softer than the surrounding enamel. There are no differences in the values in the tooth neck and the cups region otherwise.

In M2, the enamel hardness measurement results range from 67 (close to EDJ) to 86 µm (close the tooth surface). There are no clear differences between the tooth neck and the cusps in the same thickness.

In the M3, the Vickers measurement results of the enamel range from 137 to 147 µm, which indicate that the forming enamel of M3 is softer than the dentin. The Vickers measurements of dentin ranged from 58 to 67 µm for all the teeth, with the exception of one M3 measurement (92 µm) that was very close the tooth outline.

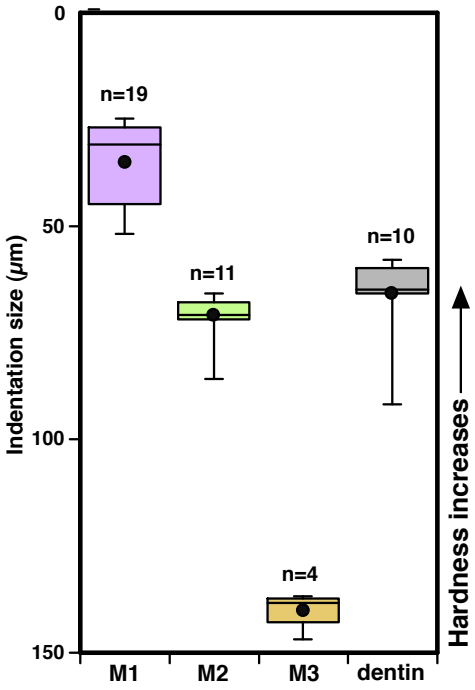

Fig. 32. Graphic presentation of the hardness measurement results of Pig C. The softer the material is, the deeper the diamond pyramid has penetrated it, and thereby caused a larger indentation. The Vickers measurement results of the enamel (M1, M2, M3) indicate that the enamel of the M1 is the hardest and the enamel of M3 is the softest. The hardness values of the dentin are similar among the three molars examined, and the results are combined In this graph. The boxes enclose 50% of the observations; the median and the mean are indicated with a horizontal bar and a black dot, respectively, and the whiskers denote the whole range of the individual measurements.

The Vickers measurements of Pig C indicate that the enamel of the M1 is the hardest and the enamel of the M3 is the softest. The dentin hardness is relatively constant among all the teeth. In the M1, the enamel is harder than the dentin, whereas in the M2, the mean value for the dentin is slightly harder than the enamel and, in the M3, the enamel is substantially softer than the dentin (Fig. 32).

4.3 Thin sections

4.3.1 M1, Pig C

In the thin section of M1, the enamel has a brownish hue (Fig. 33 A). The enamel is the thickest in the tooth cusp region and thins down to the tooth neck. One clear incremental line is visible in the enamel of M1, and the enamel has a different appearance on the different sides of the line (Fig. 33 B). The enamel is paler and more homogenous between the line and the EDJ than between the line and the tooth surface. This accentuated incremental line matches with timing and the description of neonatal line in the literature (Eli et al. 1989). The HSB can also be distinguished in the enamel near the tooth neck (Fig. 33 C). At the tooth neck, the cementum overlaps the enamel for a very short distance. Using the highest magnification of the optical microscope, even individual enamel rods can be distinguished in some areas of tooth enamel (Fig. 33 D). Approximately 15 rods can be counted per HSB in the plane of this particular section.

The enamel and the dentin are separated by a sharp EDJ (Fig. 33 B). The dentin has a gray shade caused by dentin tubules that are weakly seen in the combined photomicrograph. The dentin has different incremental zones rather than distinct lines, and those zones are larger than the incremental lines in enamel.

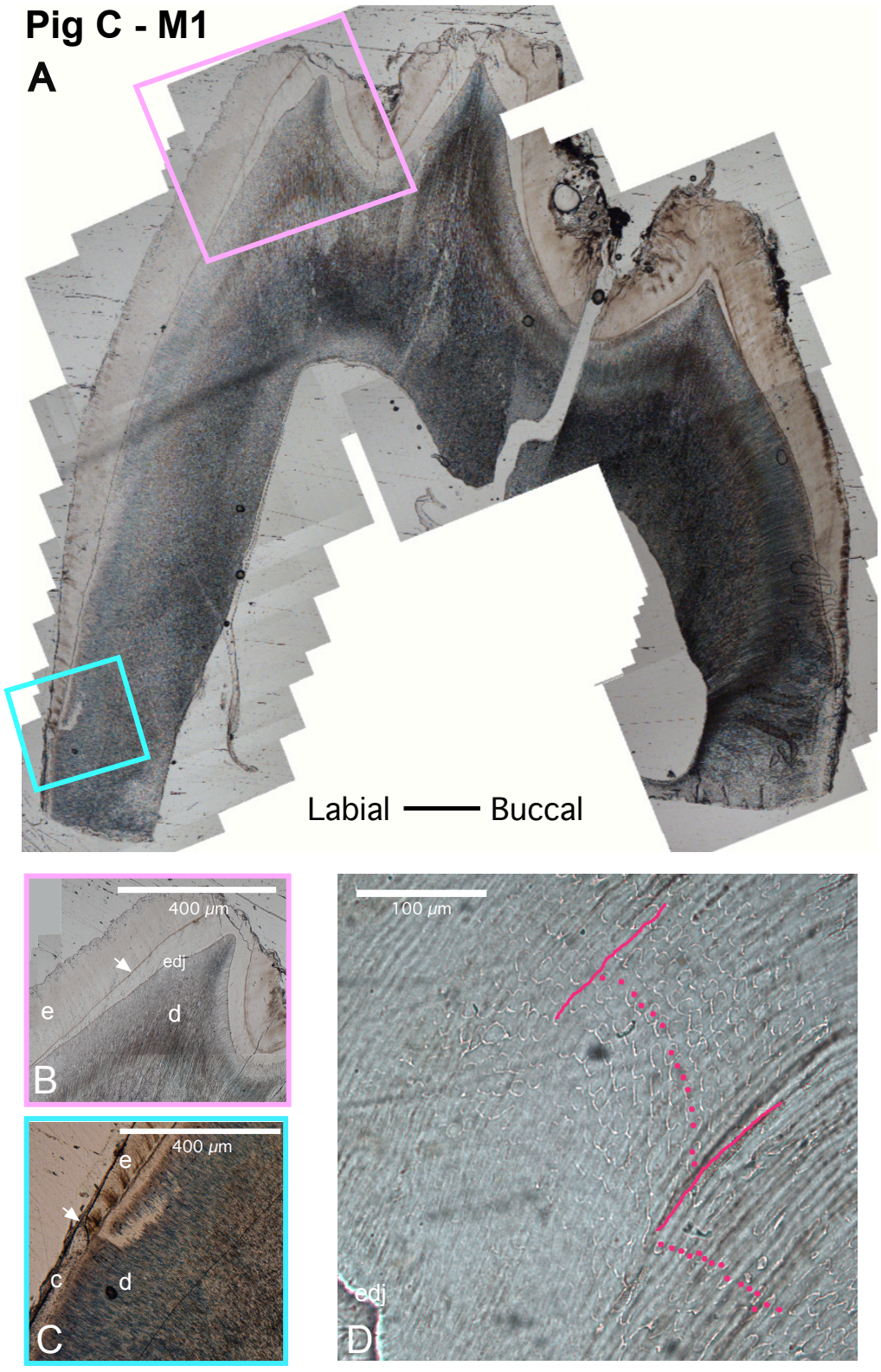

Fig. 33. A) Combined photomicrograph of a thin section of M1 of Pig C under plane polarized light (PPL). B) Neonatal line (arrow) in enamel with a slight hue difference on different sides of it. The label e in the figure denotes the enamel, d is dentin, and edj stands for enamel-dentin junction. C) The enamel-cementum junction (arrow) separates the enamel (e) above it with HSB and cementum (c) below. D) Decussating enamel rods (red dots) in HSB. The red line indicates the boundary of the decussating rod layers.

The course of the enamel rods differs in different regions of the tooth: on the sides of the tooth, the enamel rod course is straight with a slight tilt upwards, and it turns perpendicular to the enamel surface in the last quarter before the surface (Fig 34 A). Under the cusp tips, where the mechanical stress of a tooth is the greatest, the enamel rods undulate, forming so called gnarled enamel (Fig 34 B).

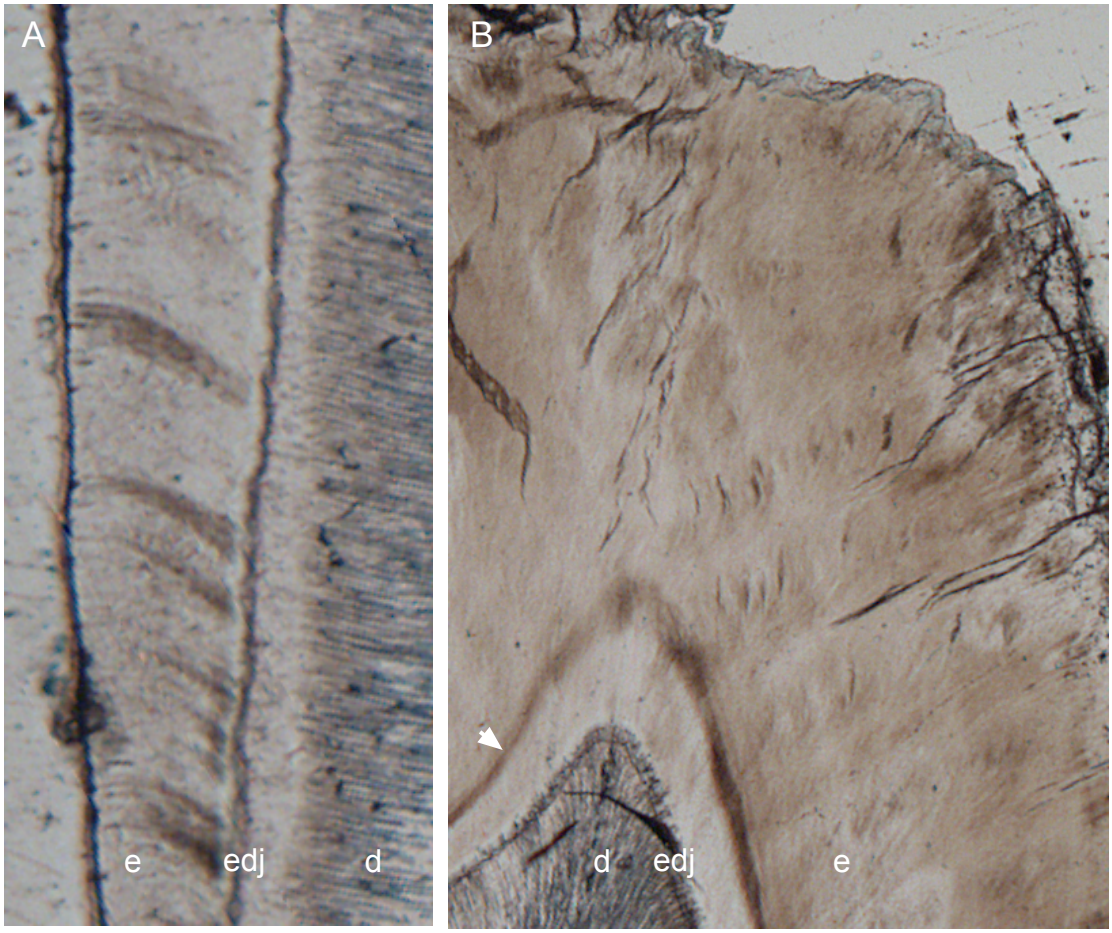

Fig 34. A) Photomicrographs of enamel in thin section (PPL) of M1 of Pig C. On the sides of the tooth, the enamel rod course is inclined upwards from the EDJ. The rod course is almost straight until it curves slightly to be perpendicular to the enamel surface. B) The enamel rods are undulating in the cusp region to form gnarled enamel. The hue in the enamel is paler under the neonatal line (arrow). The label e in the figure denotes the enamel, d is dentin, and edj stands for enamel-dentin junction.

The orientation of apatite crystals in the enamel can be observed using cross-polarized light (XPL). The cross-polarized light illuminates the apatite crystals that differ in orientation from the vibration orientation of light, whereas the crystals that coincide with the vibration orientation of light appear dark. This emphasizes the differences of crystal orientation and, for example, the HSB become more distinct. (Fig. 35). Using crossed polarizing filters, the optical extinction of the crystals is offset a few degrees from the course of the enamel rods, indicating that the orientation of the apatite crystals

does not precisely coincide with the course of the rods. The dentin has no decussation of structure and the crystal orientation generally follows the tooth growth and morphology.

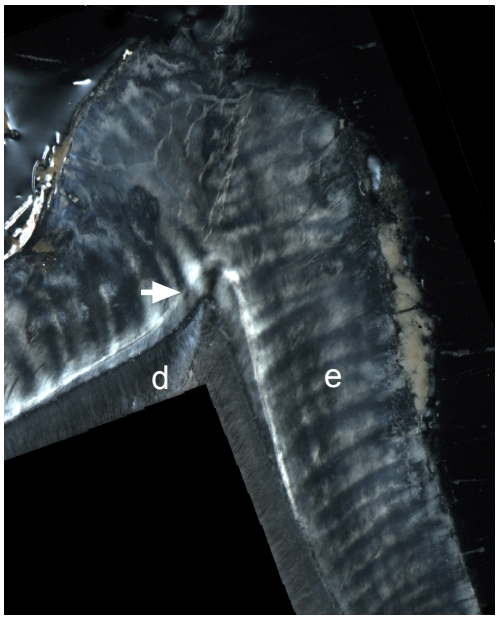

Fig. 35. Combined photomicrograph of thin section of M1 of Pig C (XPL). In enamel (e), the HSB are well visible under cross-polarized light. When the vibration direction of the light coincides more or less with the long axis of the enamel rods, the rods appear dark as the crystals appear optically extinct. Whereas the enamel rods appear illuminated when the vibration direction of light differs from the long axis of enamel rods. In this image, the neonatal line (arrow) is seen as a white line around the cusp. There is no decussation in dentin (d), which therefore appears more homogenous under XPL. The black area in the lower left of the image represents non-photographed part in the combined photomap.

The use of the accessory gypsum plate emphasizes some characters of the enamel, dentin and cementum, and it makes possible to observe the optic sign of the length of the apatite crystals (Fig. 36 A). Apatite is a uniaxial mineral and has negative optic sign. Therefore its interference color is blue when the c-axis is parallel to the first order retardation (gypsum) plate of the microscope. In areas where the crystal orientation is not coherent or the c-axis is parallel to the vibration direction of light, the enamel appears pink. Apatite crystals in teeth are very small, in human enamel about 70 nm thick and the crystal size in dentin is half of that, therefore there is room for several crystals on the thickness of one thin section, which also affects the interference colors. In the enamel in Fig. 36 B, the different crystal orientations of the neighboring HSB can be seen as alternating bluish and pink regions, and this phenomenon is emphasized along the neonatal line. The enamel rod decussation ends before the enamel surface, and the crystal orientation is coherent in outer layers of enamel (36 C). The first layer of dentin, the mantle dentin, also has a coherent crystal orientation, parallel to the outer enamel crystal orientation and perpendicular to the EDJ (Fig. 36 C). Above the mantle dentin, the dentin tubules curve to the direction of the pulp. The crystal orientation follows that course, which is seen in color change.

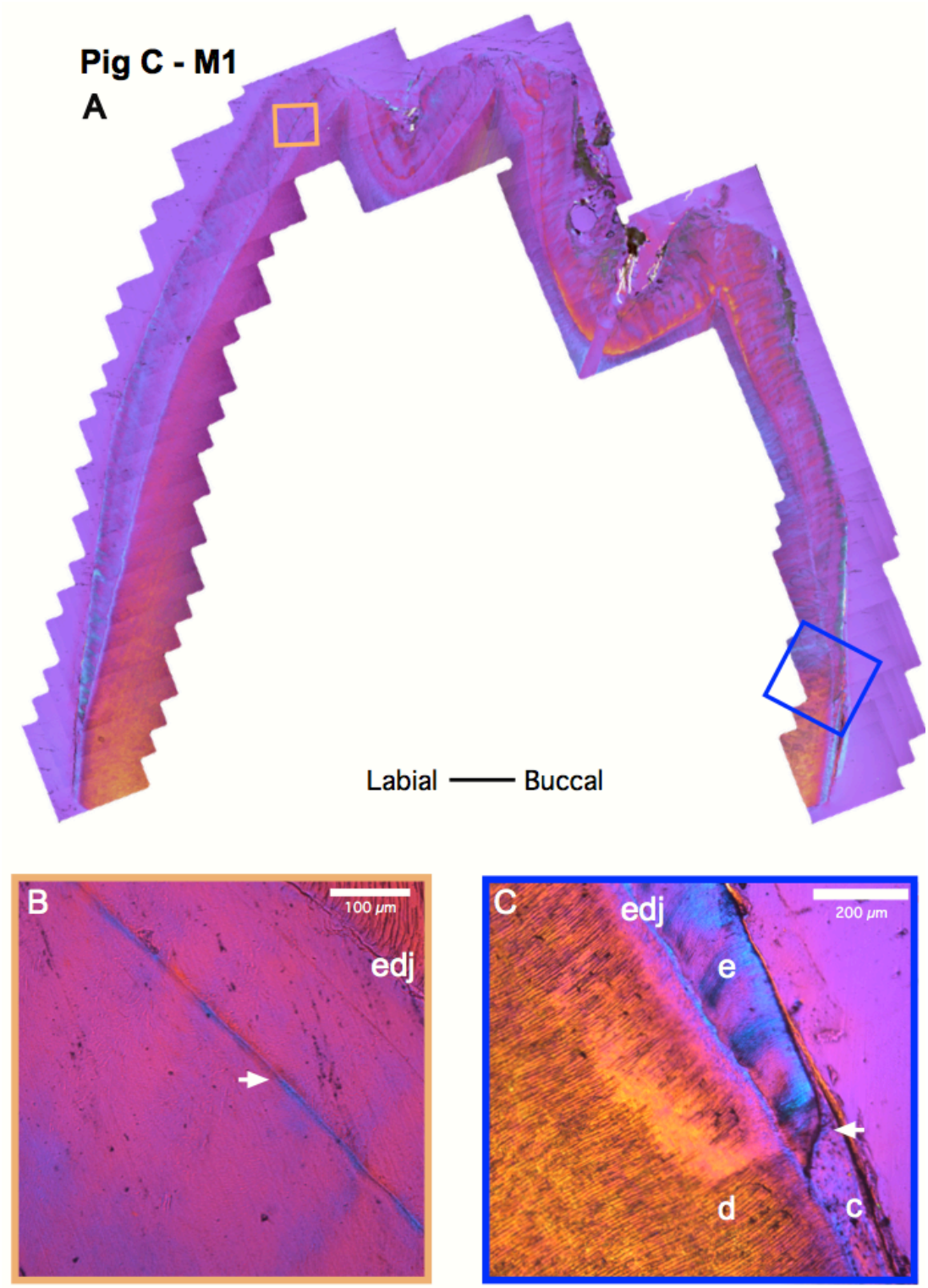

Fig 36. A) Combined photomicrographs of a thin section of M1 of Pig C under cross-polarized light and using gypsum accessory plate. Apatite is a uniaxial mineral and has negative optic sign. Therefore its interference color is blue when the c-axis is parallel to the first order retardation (gypsum) plate of the microscope. The areas where the crystal orientation is not coherent or the c-axis is parallel to the vibration direction of light, the enamel appears pink. B) The neonatal line (arrow) is optically more coherent than the surrounding enamel why its interference colors are stronger. C) The HSB are seen as blue and pink stripes in the enamel (e). The HSB do not continue to the enamel surface where the apatite crystals turn into a uniform orientation showing a blue interference color. The mantle dentin is seen as blue line in the EDJ, from where the interference color of dentin changes to pink and yellow by following the crystal orientation. The dentin (d) has a striped appearance caused by the dentin tubules. The ECJ (arrow) and cementum (c) are visible in the lower-right corner.

4.3.2 M2, Pig C

In the M2 of Pig C, the very first secreted enamel layers in the cusp tips are transparent. The enamel rod decussation becomes visible where the pigmented layers start (Fig. 37 A). At the tooth neck, where the enamel still had lower electron density, it is again transparent. Two thick incremental lines stand out in the enamel, but several thin incremental lines are also visible (Fig. 37 B). The thickness of the enamel and the dentin is the greatest in the tooth cusp region and both thin down towards the tooth neck. The EDJ is clearly visible.

The first layers of the enamel are less pigmented than the following layers (Fig. 37 B). The incremental lines are thinner near the EDJ. Contrary to the neonatal line in M1, the two incremental lines with greater pigment intensity do not have optical extinction but stay opaque also when thin section is rotated and with accessory gypsum plate (Fig. 37 C).

The gentle S-shape lineation of the tubules forms a radial pattern through the dentin, but transforms to a dotted pattern under the cusp tips and near the tooth neck because of the different cut of tubules. The tooth structure is more complex in the cusp region, and there the tubule formation is more complex. The dentin is dominantly gray in thin sections.

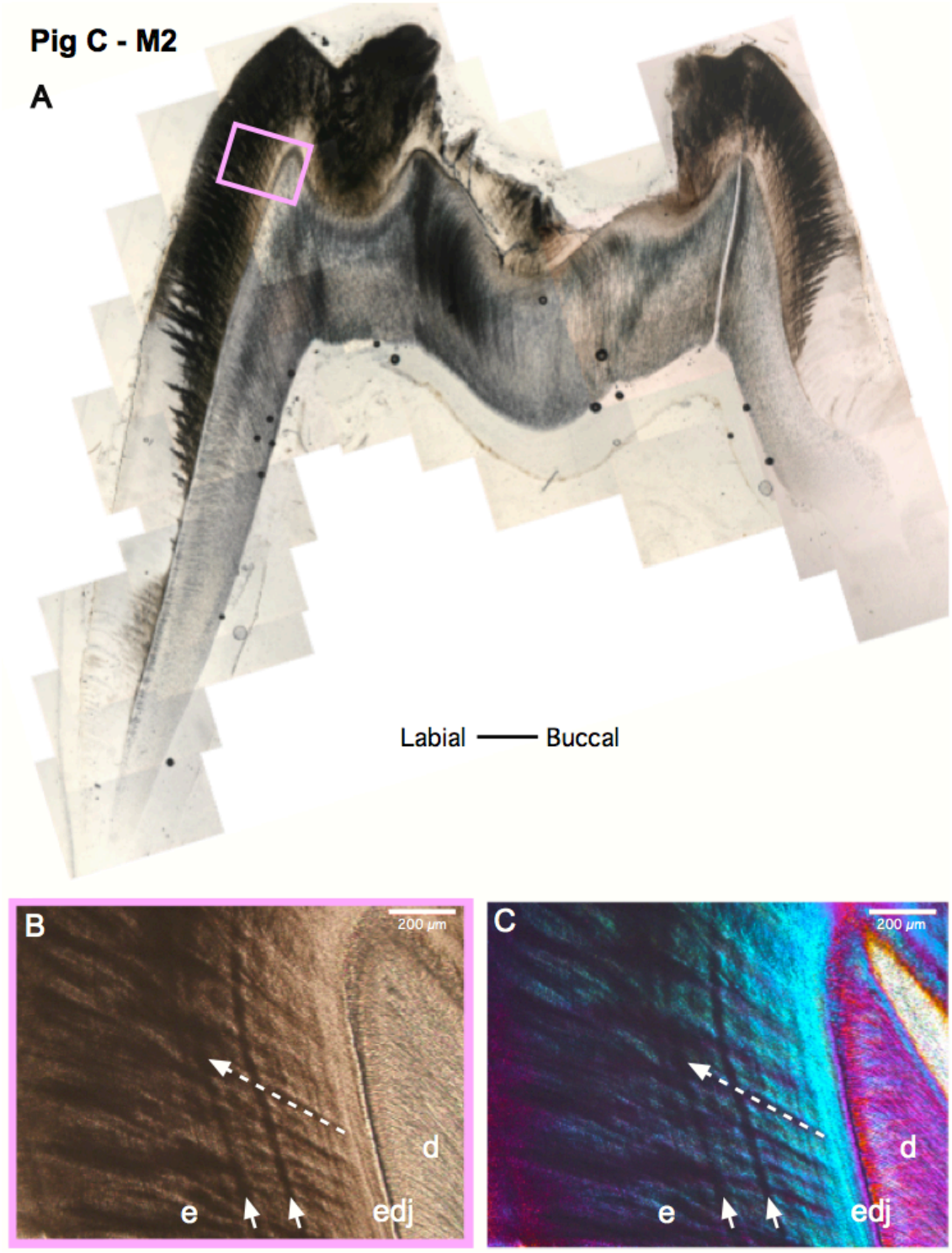

Fig 37. A) Combined photomicrographs of a thin section of Pig C M2. B) Detail of the incremental lines in enamel (e) with two accentuated lines (arrows) under PPL. The enamel rods travel in 45° angle compared the incremental lines (dashed line). Dentin (d) is visible in on the right side of the EDJ (edj). C) The same area under XPL and using a gypsum plate. Enamel is less pigmented near the EDJ. Due to their high pigment content, the two accentuated lines (arrows) remain opaque even when the table is rotated. This is distinct from the optically active neonatal line (cf. Fig. 36 C). In dentin, the crystal orientation is reversed on different sides of the cusp, as shown by the yellow and pink interference colors at the right side of the image.

4.3.3 M3, Pig C

The bell-stage M3 has a gelatinous consistency. Only the cusp tip areas have started to mineralize and both the enamel and the dentin are still thin (Fig. 38 A). The enamel of the M3 is pigmented similarly to the M2, but there is no visible difference between the inner and outer layers of the enamel. The enamel has an undulating appearance on the occlusal region of the cusps (gnarled enamel) whereas on the sides of the tooth the enamel rods are travelling straight (Fig. 38 B, C). The accessory gypsum plate highlights the HSB pattern. In the thin section, despite the thinness, the dentin of the M3 appears similar than in the other molars.

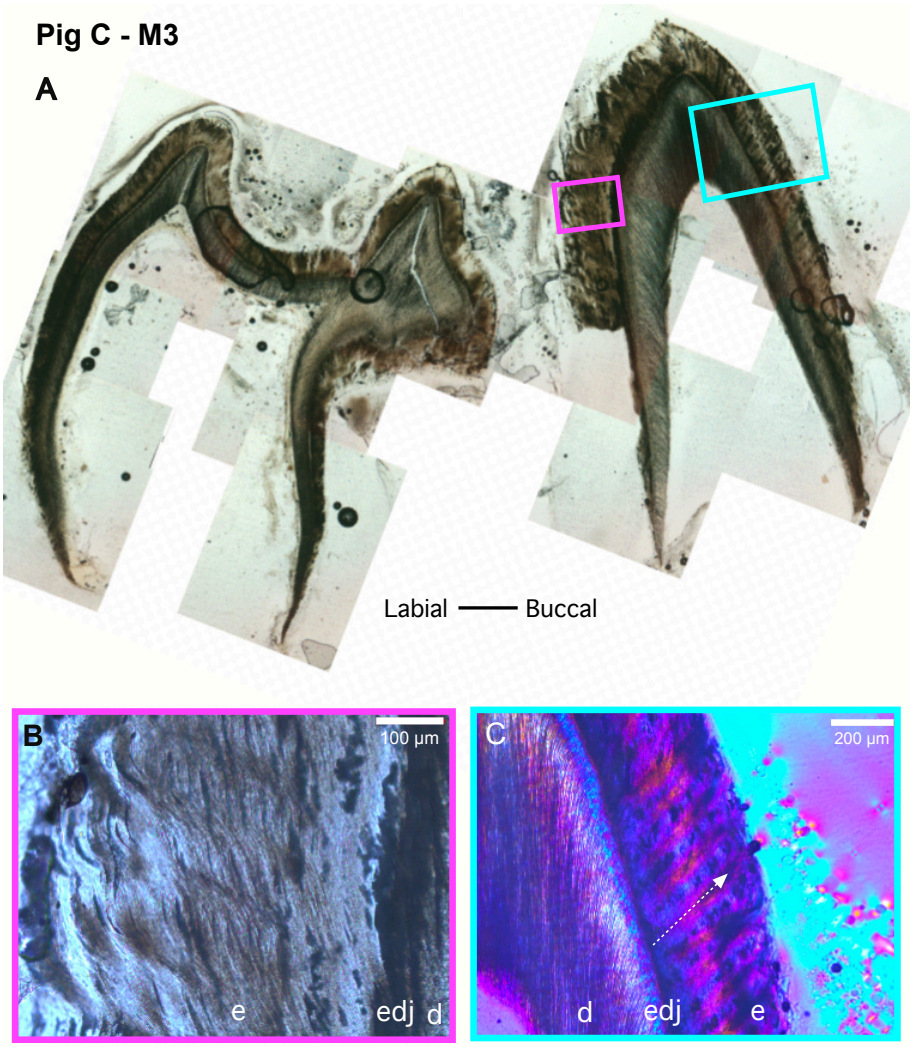

Fig 38. A) Combined photomicrographs of a thin section of Pig C M3 under PPL where the cusp area has started to mineralize. Dentin is thinner than in the other molars, but other ways it appears the same. B) Detail of gnarled enamel under PPL. C) Cusp side under XPL and using a gypsum plate. Decussating enamel rods are travelling upwards (arrow) from the EDJ. Dentin (d) is on the left and the mantle dentin is seen as a blue line above the EDJ. NOTE: the enamel rod underneath the arrow is declined compared to the course of the other rods, which is not generally the case. The label e in the figure denotes enamel, d is dentin, and the edj stands for the enamel-dentin junction.

4.4 X-ray diffraction analyses

During an X-ray diffraction measurement, the sample is irradiated using coherent monochromatic X-ray beam. The beam reflects from the crystallographic planes of the sample material that are parallel to the sample stage (Fig 39 A). The crystal structure either enhances or suppresses the reflection as explained by the Bragg's Law:

$$n\lambda = 2d\sin\theta\,,$$

where

n is the order of reflection

λ is the wavelength of the monochromatic radiation

d is the spacing between the crystallographic planes

θ is the angle of reflection

The reflection of different d-spacings can be found by scanning the θ and 2θ angles of the diffractometer (Fig 39 A). The positions of the diffraction peaks in the diffractogram depend on the available d-spacing between the crystallographic planes in the sample mineral or minerals (Fig. 39 B). The widths of the peaks provide an indication of the average size of the crystals. The intensity of the peak depends on how frequently the particular crystallographic orientation coincides with the sample stage and what is the reflectivity of the crystal structure in this orientation. The measured diffractogram can be compared to the reference data of the corresponding mineral phase in The International Centre for Diffraction Data ICDD, PDF-4 Mineral database.

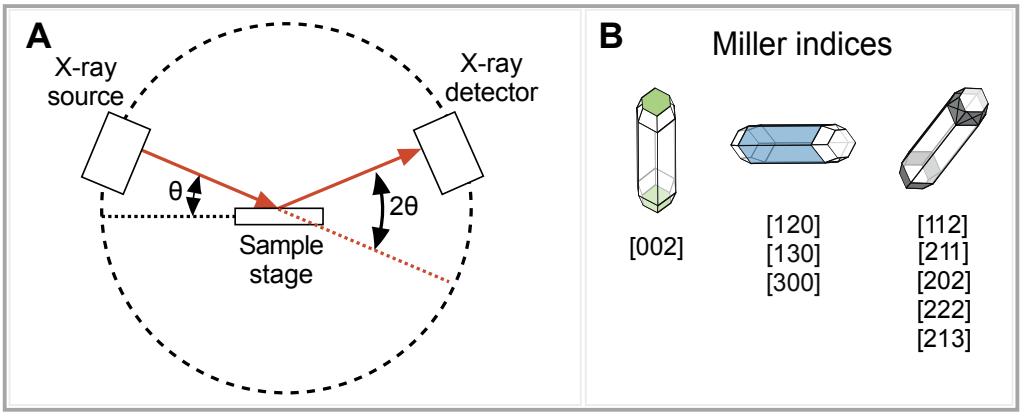

Fig. 39 A) Schematic presentation of a powder diffractometer showing the relative positions of the x-ray source, sample and the detector. Reflections occur only from the crystallographic planes that are parallel to the sample stage. The angle of the reflection (θ) is proportional to the d-spacing of the crystallographic plane from which the X-ray beam reflected. B) In a powder sample, the individual crystals can be oriented differently. The intensity of the diffracted reflection is dependent on the dominance of the particular crystallographic orientation at the plane of the sample stage. In this study, the following crystal planes of apatite are observed: plane {002} (green) is perpendicular to the c-axis, and the prism faces {120}, {130} and {300} (blue) are perpendicular to a-axes. Apatite crystals also have diagonal bipyramidal crystal planes (gray) of which the orientations {112}, {202} and {213} are closer to being parallel with the a-axes, and the orientations {211} and {222} are closer to being parallel with the c-axis.

When comparing the X-ray diffraction patterns of the samples of the enamel, the dentin of the M1 and the jawbone powder (Fig. 40), certain differences can be observed. The enamel sample reveals the most distinct peaks that correspond to planes {002}, {211}, {112}, {300} and {130}. The intensity of these reflections indicates relatively large apatite crystals. Most of the peaks are lower in the dentin sample and the lowest in the jawbone powder, where only the strongest peaks can be recognized from the background noise. The peaks {002}, {112}, {213} are slightly higher in the dentin sample than in the enamel sample.

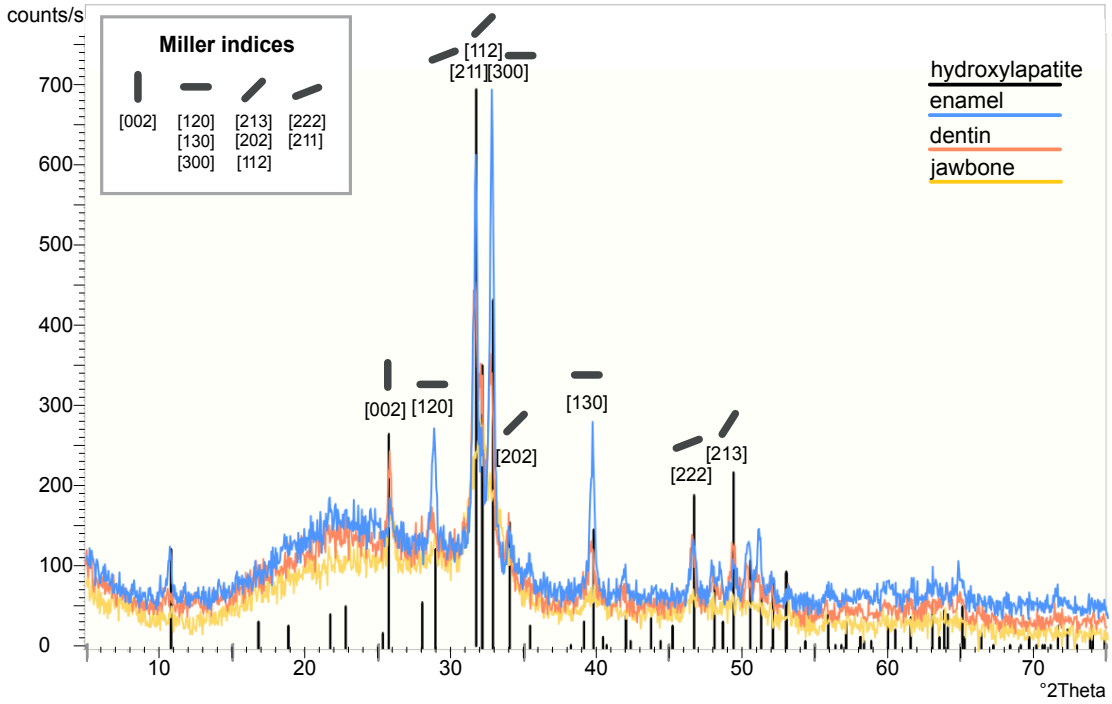

Fig. 40. X-ray diffraction patterns of powder samples of pig M1 enamel (blue), dentin (orange) and jawbone (yellow). The measured diffraction patterns are compared to the peak position and intensity data of pure hydroxylapatite (black). The enamel reveals distinct peaks that correspond to {002}, {211}, {112}, {300} and {130} Miller indices, which indicates relatively large apatite crystals. The dentin powder gives lower diffraction in general, except for the planes {002}, {112} and {213}. The jawbone material is characterized by the lowest and widest diffraction peaks, indicating lower amount and/or very small crystals.

In the powder diffraction pattern of enamel material, the peak that corresponds to the {002}-plane is relatively weak; approximately 11% of the tallest peak, whereas in the hydroxylapatite reference data, its height is 37,8% of the height of the tallest peak {211}. In a SEM-image of the same enamel powder sample, acicular shape of the particles can be observed (Fig. 41). As the apatite crystals are oriented c-axis approximately parallel to the enamel rods, the weakness of the {002} reflections, as well as the reflections {112} and {213}, can be explained by the preferred orientation of the needle-like particles that tend to coincide with the underlying glass plate surface. The peaks that correspond to the lattice planes {120}, {300} and {130} are elongate prism faces of apatite, and appear relatively high in the diffractogram of the enamel compared to non-oriented hydroxylapatite reference data. The peak of the plane {002} in dentin is almost as high as in the reference data.

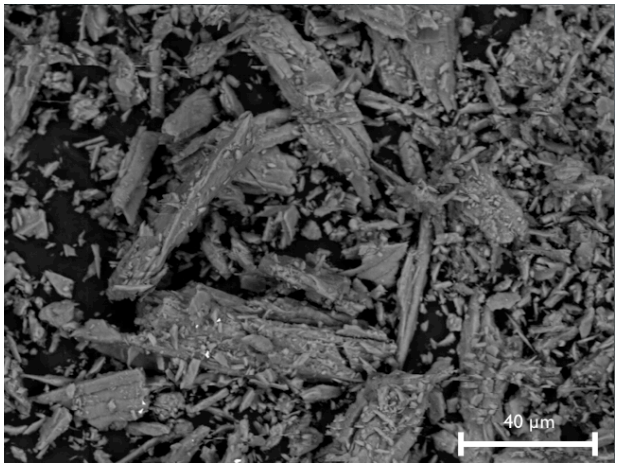

Fig. 41. SEM-image of enamel powder. The c-axis is the longest axis in hydroxyl-apatite, and the crystals in enamel are 3-4 nm thick. The needle-like structure of enamel rods is still visible in enamel powder and therefore the peak of plane {002} does not get higher even if the enamel is ground to a fine powder.

Next, two additional x-ray diffraction measurements were done directly from the thin sections of the M1. The purpose of this test was to compare the relative intensity of the peaks of the planes {002}, {211}, {112}, and {300}. One measurement was done from a frontal section of the trigonid cusps, and another from a tangential section of the enamel surface (Fig. 42). In the frontal section of the trigonid, the peak {002} remained again comparably low, which is consistent with the previous results: very few apatite crystals were cut perpendicular to the c-axis in the frontal section. In the diffractogram of the tangential cut, the only distinct peaks are for the planes {002} and {112}, which indicates that on tangential section the crystals are mostly ether upright or slightly tilted from that. These samples were glued on glass, and amorphous materials, such as glue, glass and organic matter increases the background noise in the x-ray diffraction patterns.

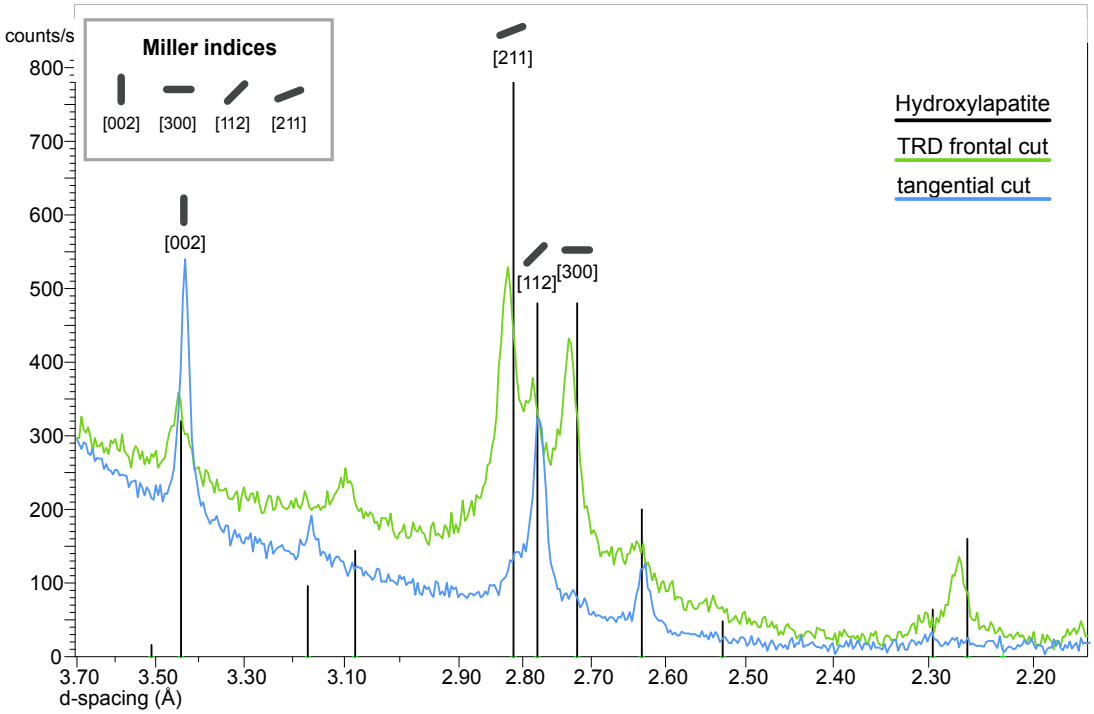

Fig. 42. X-ray diffraction patterns of pig (M1) enamel: A frontal section of the trigonid (green) and a tangential section of a cusp tip (blue). The frontal cut has higher peaks for planes that are parallel or nearly parallel to the elongate prism faces of apatite, whereas tangential cut has very high peaks for the planes {002} and {112} that represent pinakoidal and bipyramidalfaces that lie perpendicular or almost perpendicular to the c-axis of apatite. Thin section diffractograms have higher background noise, because there is glue and more organic matter on the samples compared to the powder samples.

4.5 SEM analyses

The structure of the dentin is visible already in the low magnifications electron microscope images (Fig. 43 A), whereas the enamel rod structure requires higher magnification to become visible (Fig 43 B). The inner structure of the enamel rods and the interrod enamel are visible at 10 000 x magnification and above (Fig. 43 C). The EDJ is a 20 µm zone that separates the dentin and the enamel. The enamel rods are composed of needle-like crystals that mostly coincide with the enamel rods, and the interrod enamel is composed of perpendicular crystals (Fig. 43 D). The interrod crystal orientation is clearer that the enamel rod crystal orientation as they are not as packed as the enamel rod crystals.

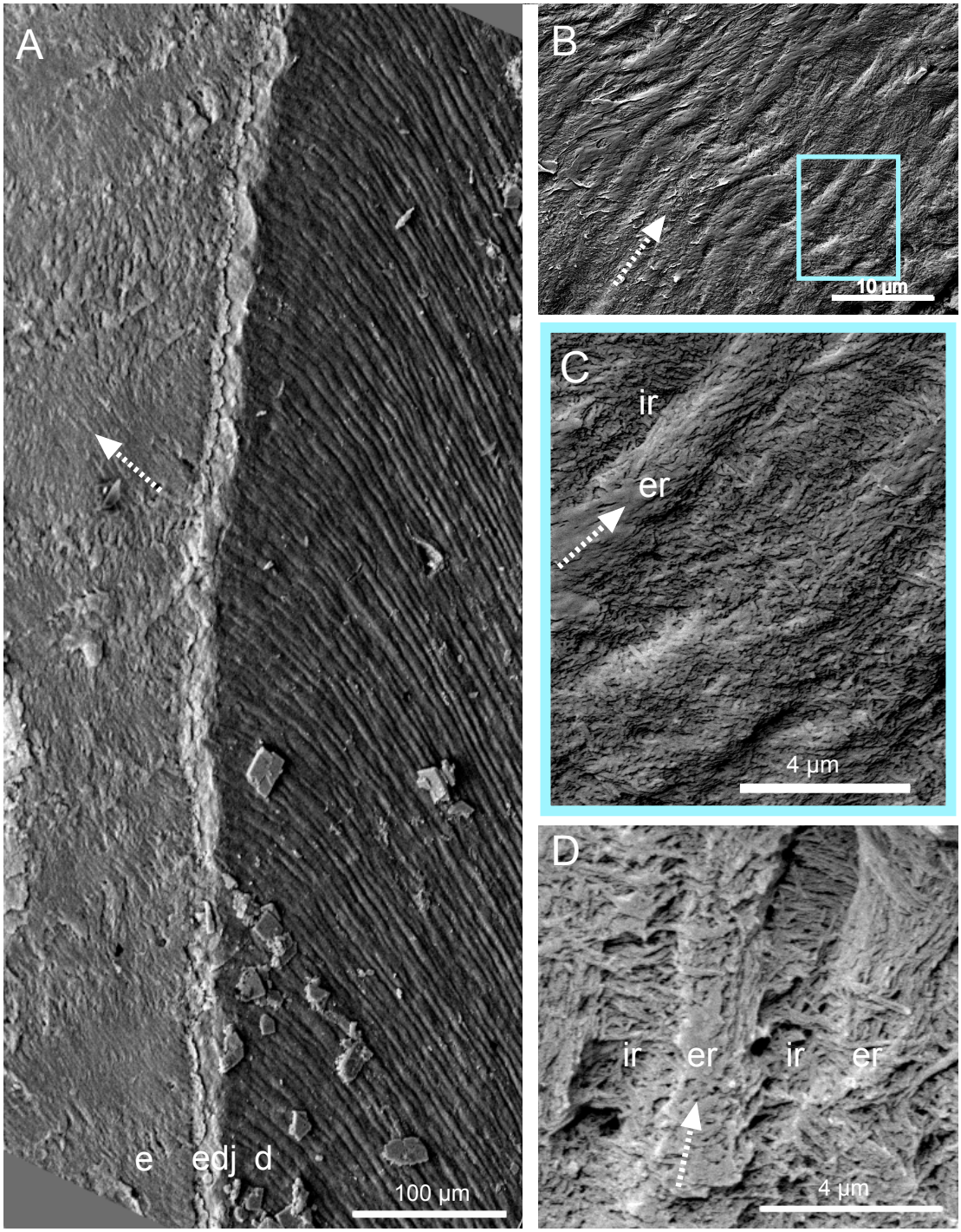

Fig. 44. SEM-images of the enamel and dentin near to cusp tip in the M2 of Pig C. A) The dentin tubules are visible already in smaller magnification, where the enamel structure needs greater magnification. The course of the enamel rods shown with an arrow that points to the direction of the tooth surface in every image. B) The enamel rods do not have completely straight course from the EDJ to the tooth surface. C) a close up from the figure B with enamel rods and interrod enamel. D) A detail of enamel: enamel rods (r) and interrod enamel (ir) that both constitute of needle-like crystals. Enamel rods seem to be more tightly packed, and individual crystals are more difficult to recognize than in interrod enamel. The interrod enamel crystals are more or less perpendicular to the enamel rod crystals.

The enamel rod thickness is approximately 1.5–2.5 µm at a distance of 60 µm from the EDJ (Fig. 44). There seem to be some difference in the thickness of the enamel rods on different levels of the tooth, and the rods tend to be thicker closer to the cusp tips where the maturation has progressed further. The measured thickness of enamel rods is also dependent on the section of the area examined.

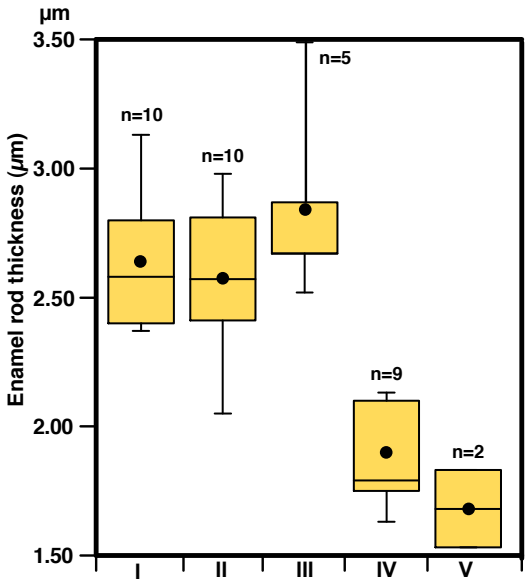

Fig. 44. In the M2 of Pig C, the measured enamel rods were thicker nearer to tooth cusp (I, II, III) where the maturation process is further and thinner in tooth neck (IV, V) where the mineralization is not so advanced yet. The thickness is measured approximately 60 µm from the EDJ.

5. DISCUSSION

5.1 MicroCT and RED-calibration

TX-ray microCT is becoming an increasingly widely used method in paleontological, biological and medical studies (eg. Ortiz et al. 2012, Schmitz et al. 2014, Tafforeau et al. 2012). The advantages of microCT are the relative rapidity, possibility of repetition and that it does not affect the sample besides the ionization.

A few challenges remain that slow down the success of the method: the machines are expensive, need for high computing power, knowledge and working hours are needed to realize the reconstruction process. Furthermore, different absorption models are difficult to compare as the absorption values are not absolute but differ between samples, and according to depth within and individual sample.

In many microCT-laboratories, so-called phantoms are used to calibrate the machine but when working with highly mineralized samples, the electron densities of the phantom samples stay below electron densities of the samples (e.g. Farah et al. 2010). One model of these phantoms is high-density hydroxylapatite powder standards that are technically challenging to fabricate and need special equipment to bond the powder crystals at high heat and/or high pressure to get equivalent densities to mineralized material. An additional challenge is to ensure that the electron density values are comparable between machines and laboratories.

5.1.1 Mineral standards

In this study, I tested calibration of individual absorption models using mineral grains, of which the chemical and physical properties are relatively well known. Three minerals were chosen from Division of Geology collections: fluorapatite, quartz and siderite. Apatite was an obvious choice as the biomineral in teeth is hydroxylapatite, the other two were chosen after testing several minerals in microCT. The idea was to have, in addition of apatite, one mineral that has higher, and other with lower electron density than the electron density of enamel and dentin. The mineral fragments for testing were chosen visually by the purity and tested in microCT. Of the other minerals that I tested after completing the imaging, and which might be suitable alternatives, were diamond (C) and corundum (Al_2O_3). The electron density of diamond is lower than that of quartz, and corundum has lower electron density than siderite but higher than apatite. Diamond, quartz and corundum are also comparatively easy to produce as synthetic minerals, which makes it even easier to obtain homogenous grains. As the electron density of hydroxylapatite is lower than that of fluorapatite, and the electron density of enamel is a bit lower than that of pure hydroxylapatite, diamond, quartz and fluorapatite would probably be a suitable set. During the study I also discovered that gluing the minerals together in a row makes the handling of the minerals easier and the calibration process faster.

5.1.2 Hardening effect

One of the problems with samples that have a high electron density is the artifacts caused by beam hardening. The beam hardening is an artifact of tomography, which makes the sample to appear artificially denser at or near its surface, and less dense in its central parts (Bruker 2014). The x-rays produced in laboratory x-ray sources have mixed x-ray photon energy. As this mixed beam of x-rays passes through the sample, the lower energy x-rays will be attenuated more rapidly than the higher energy x-rays. Due to this soft depletion the average photon energy increases along the beam path and the beam "hardens", causing absorption to decrease in the sample. Since absorption translates into density, the result in the reconstructed cross-section is an artifact where electron density of the sample is artificially increased near the surfaces, especially in sharp edges and, decreased deeper in the sample. The hardening effects can be corrected or reduced with specific algorithms that are used after the reconstruction.

This kind of artifact can be very difficult to recognize in tooth samples because of their structure: a tooth has a thin layer of enamel on the surface with higher electron density, and the base of the tooth is dentin with lower electron density. The hardening effect can be as thick as the enamel layer and then the result would be a tooth with slightly increased electron density in enamel and decreased electron density in dentin. The hardening effect can be detected using a gray scale profile of the known mineral grain (Fig. 45).

In my microCT data, the M3 of pig C showed high electron density values (Fig. 27 C). Comparison of the REDs shows that the values of dentin are higher in the M3 of Pig C than in any other molars of any pig (Fig. 28). The RED-curve of the M3 in Pig C looks otherwise similar to that of Pig A, but is higher and slightly deeper. Especially because in the M3 the mineralized tissues were thin, the generally elevated REDs are likely to be hardening artifacts. This tooth was scanned using higher resolution and later downsampled. A comparison of the RED-profiles of one calibration grain (apatite) shows the hardening effects: Sharp edges and deep bending in the middle (Fig. 45). The mean values calculated from Fig. 45, showing electron density sections through the fluorapatite standard used for M3 scans, are 3.18 gm/cc (pig A), 3.19 gm/cc (Pig B) and

3.23 gm/cc (pig C). The mean values of Pigs A and B are close to the reference value for fluorapatite (3.17 gm/cc) whereas the value of pig C is too high.

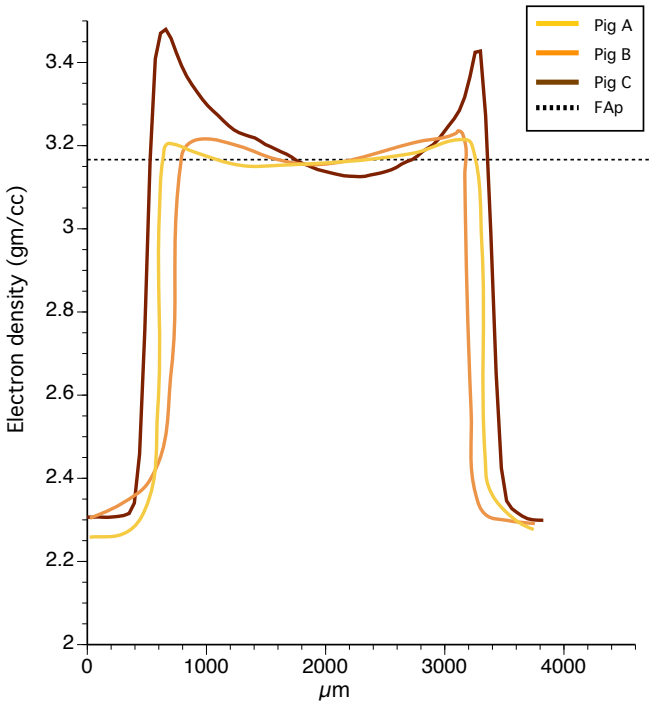

Fig 45. RED-value profiles for the fluorapatite grain in the absorption models of M3 of all three pigs. In the absorption model of Pigs A and B, the fluorapatite has constant values, with only a slight hardening effect on the edges. The absorption model of pig C has sharp edges and deep bending of values in the middle of the grain. The mean of the RED-values in Pig A absorption model is 3.18 gm/cc and 3.19 gm/cc for the pig B, whereas in the absorption model of pig C the mean RED is 3.23 gm/cc. The reference value for fluorapatite is 3.17 gm/cc (FAp). The calibration values were measured from the cores of the grains.

This result emphasizes the importance of the calibration minerals that allow an objective way to evaluate the data, and also the need to control for hardening effects during data acquisition. Below I concentrate my discussion on the REDs of Pigs A and B for the M3s, which did not show marked hardening effects.

5.1.3 Molar maturation schedule in pigs

In general, the microCT absorption models provided a good overall view of the developing teeth. The absorption models reveal the sequence of the tooth crown formation as described in the literature (e.g. Jordan & Kraus 1965, Jernvall 1995); the development starts from main cusps of the trigonid that are the highest of all the cusps, and development continues to the cusps of the talonid, and then to smaller cusps and cusplets. The differences in the REDs of the samples also matches with the sequence of the mineralization described in the literature (Berkovitz et al 2002); the electron density increases first on the EDJ of the cusp tips and continue to the direction of the tooth neck, but also from the EDJ to the direction of enamel surface. The microstructure of tooth enamel (e. g. enamel rods and their decussation) cannot be seen in absorption

models, as there are no differences in the state of mineralization or chemical composition among individual rods. The M2s show that the electron density of dentin increases faster than that of enamel, as is the situation in the M2 of Pig B, but eventually the electron density of enamel exceeds that of dentin, which is already the case in Pig A (and C) (Fig. 23 and 26). In M3s that are in the earliest stages of the development, only the highest cusp tips are visible in absorption models, and enamel and dentin still have equally low electron densities.

The absorption models show that dentin obtains its final electron density already before the tooth eruption (Fig. 28); Pig B is the only one where the difference between electron densities of M1 and M2 is visible. Compared to dentin, the enamel maturation continues longer and the difference of electron density in M1 and unerupted M2 enamel is still visible. Absorption models of M1s show that the electron density of mature enamel is clearly higher than that of dentin.

When comparing the microCT-reconstructions of the M2 in Pigs A and B (Fig. 23 and 24), and the mineralization diagram of human teeth in Fig. 12, Pig B M2 appears to be just before the point where the enamel maturation catches up with the dentin maturation, and in pig A that point is already passed, the enamel having electron density superior to the dentin. Kirkham et al. (1988) do not observe the mineral content of dentin or bone in pigs, but they report that the enamel mineral content does not reach 60% per volume before the tooth eruption. In humans, the same level is reached not that long after point A (Fig. 46) (Sicher 1966). In Pig B, the dentin of M2 has a lower electron density than dentin of the erupted M1, but in Pig A and C, the electron densities of dentin in the M1 and the M2 are equal (Fig. 28). This means that the electron density of dentin does not increase notably after the eruption, whereas the electron density of enamel does increase after the eruption.

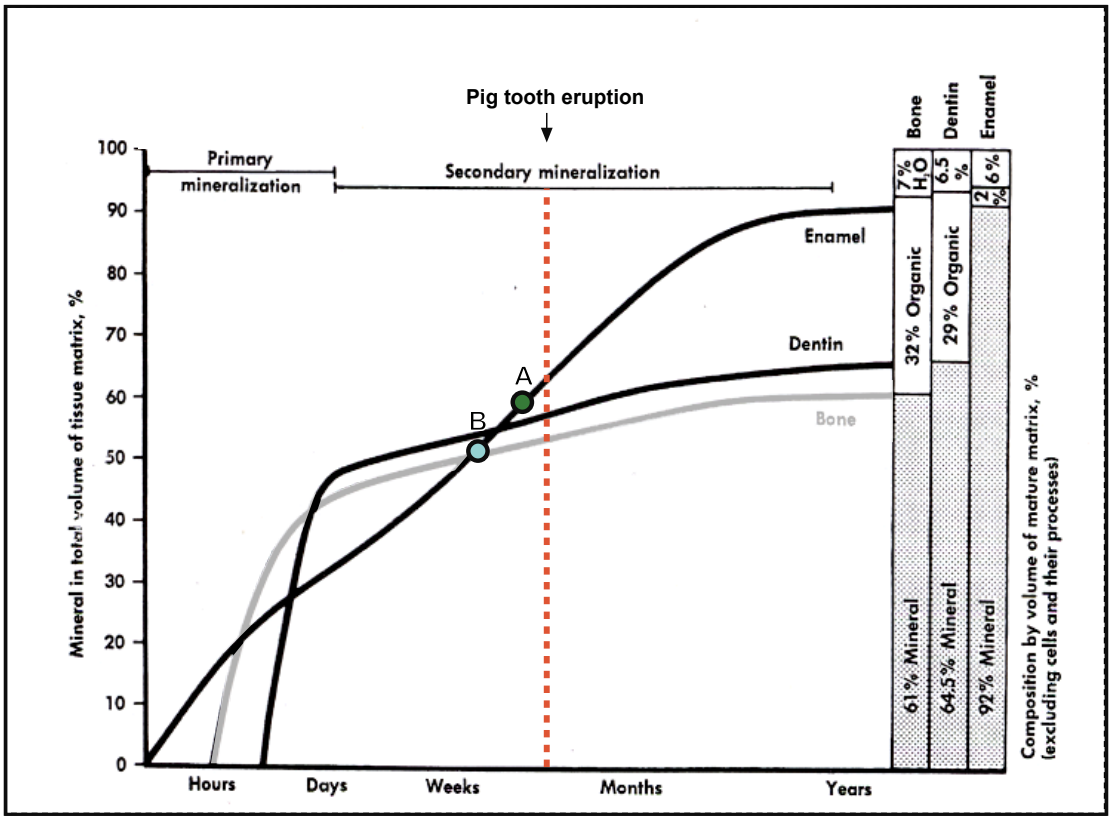

Fig 46. The mineral content of the pig enamel surpasses 60% per volume before eruption. The maturation of the M2s in Pigs A and C seem to be approximately in the point A, as the enamel has a higher electron density than the dentin. For the M2 of Pig B, the tooth maturation would be approximately in the point B, as the enamel still has a lower electron density than the dentin. The M3s are near the point where enamel and dentin maturation graphs cross (Edited from Sicher 1966).

The primary mineralization in the beginning of the maturation stage appears to be relatively fast, as already M3 shows mineralization. The fast onset of the initial mineralization determines the EDJ shape of the cusps and the whole tooth later on. In the M3 of Pig B, the EDJ cannot be seen yet, indicating that the mineral content of dentin and enamel are somewhat equal (Fig. 45). In Pig A (and C), the EDJ is already visible, the EDJ itself having a lower electron density than enamel or dentin.

In the M3s, the cusp maturation of the trigonid is well visible whereas the talonid maturation has only begun. Nevertheless, the longitudinal differences in electron densities of enamel disappear comparably fast, whereas the vertical differences stay until the end of the crown formation. In the erupted teeth, the electron density is comparable from the cusp tips to the tooth neck.

Kirkham et al. (1988) compared the mineral content of enamel in the pig, the dog and the rat. For the pig, their results showed that the final mineral content of enamel is 50–

60% per volume. As this is even lower than that of human dentin, (64.5% per volume (Fig. 12)), it is unfortunate that they did not study the mineralization of dentin. In the pigs that I studied, the electron density of enamel gets higher than that of dentin before the tooth eruption. In Kirkham et al. (1988), where they observed the calcium and mineral content of mature enamel and compared their results to the studies with other species (rat, bovine and coypu), they state, "*Why permanent porcine enamel should remain in this relatively immature condition is not clear*." One possible reason is the relatively rapid development of pig teeth. The time difference of tooth development in human and pig is notable; pig tooth development being considerably faster, even if the tooth size and enamel thickness are smaller in human teeth. Human tooth development is relatively slow and, for example, in M1, the period from the initiation of enamel mineralization to the end of crown formation is over 2 years, and mineralization still continues for 4 more years before tooth eruption (Fig. 47). In contrast, in pig M1 development, the period from the initial enamel mineralization to the tooth eruption is only 4 months. Based on the data from the M2, it is conceivable that it is developmentally easier to speed up the process of enamel matrix secretion than the enamel mineralization process. Another consideration is that in most ungulates, the secondary morphology of molars is functionally more important than the primary morphology, and semi-matured enamel may help to quickly acquire the functional morphology during tooth eruption. In *Sus scrofa domesticus* both, primary and secondary morphologies are functional.

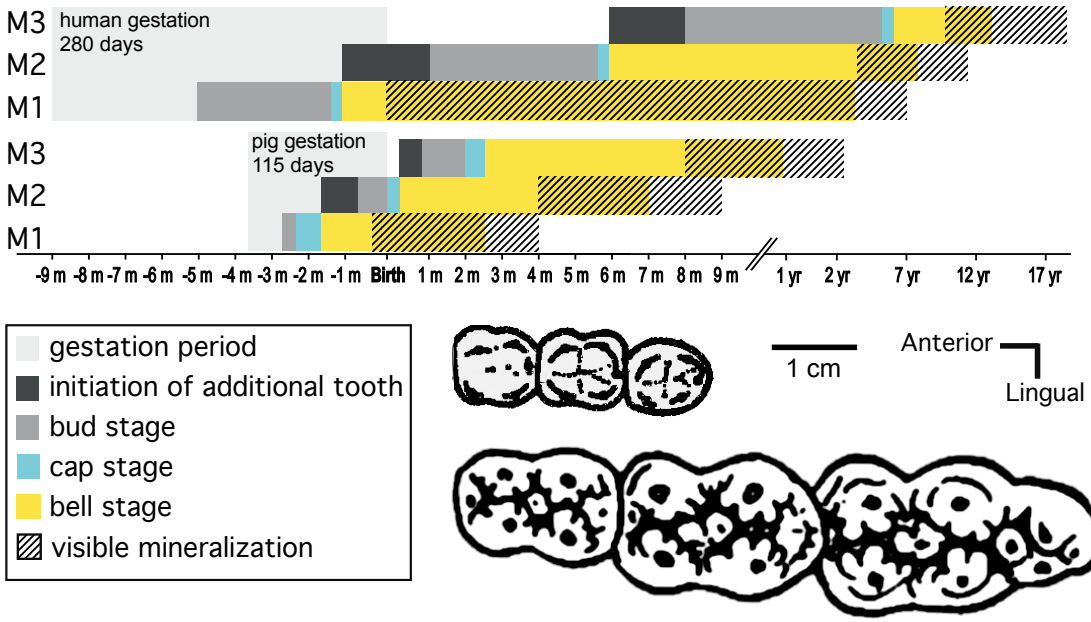

Fig. 47. Human tooth development is considerably slower than that of pigs. Human gestation period, when deciduous teeth develop and M1 development starts, is over twice as long as in pigs, and where M1 of pig takes months to develop, in human M1 development takes years. Bell stage ends when crown formation is complete. Visible mineralization here ends when tooth erupts. In real, the mineralization still continues for months in oral cavity. There is individual variation in times, so ages are approximate. NOTE: time scale changes after one year. (Kraus & Jordan 1965, Berkovitz et al. 2002, Wang et al. 2014)

Kirkham et al. (1988) mention that in pig teeth "*the levels of mineralization characteristic of mature enamel could be achieved but only at a considerable period after eruption, perhaps due to post-eruptive mineral uptake*". My data does not allow a direct evaluation of the post-eruption mineralization. In human teeth, the post-eruption mineralization takes 6 months, and if the process is similar in pig teeth, the M1s of pigs studied here would have had 4 more months to mineralize, as they had erupted approximately 2 months before their last meal. The development stage of pig teeth is more immature at the time of the tooth eruption than human teeth (Fig. 46). It would also be useful to revisit the analyses of Kirkham et al. (1988) and compare the results directly to microCT data.

Pig molar development, as described in the literature, is in Table 3. There is always some variation between individuals, and my data also shows some differences to the published data. In the studied pigs of 6 months, the M2 crown formation seems to be complete, or nearly complete (7 months in the literature) and the enamel mineralization of M3 has already started (8 months in the literature). In the molars of this study, the M2 of Pigs A and C have lower electron density in the neck region and between the cusps, whereas the M2 of Pig B has still low and equal electron density in the whole

enamel. The M2 of Pigs A and C will presumably reach the secondary mineralization at age of 7 months, Pig B seem to have some delay in the tooth development compared to other two pigs. Pig B also has larger M2 than the other two pigs studied. One likely reason for the faster mineralization in my data can be that the initiation of enamel mineralization in the literature is observed from x-ray pictures, which may be less sensitive in detecting the onset of mineralization. Similarly, the mineralization of the enamel in M3 can be seen earlier than reported (Tonge & McCance 1973). It is also possible that modern domestic pigs are developing faster, which is a common target for animal breeding programs.

5.2 Hardness, electron density and thin sections

S. Karlström (1931) studied enamel hardness of human teeth but he also compared the hardness of enamel in such species as the pig, the dog and the ox, and compared their hardness to human teeth. His result was that "*the surface hardness of the teeth of pigs is astonishingly low"*. The experiment was done with permanent teeth; unfortunately he did not mention the exact tooth or the age of the animals. Vickers hardness tester is used also in human enamel defect research e.g. Fagrell et al. 2010, Sunil et al. 2012.

In this study, I compared the hardness of developing teeth in pig. Hardness as measured here is not the functional hardness of the teeth, as the sections were done perpendicularly to the occlusal surface, and parallel to the c-axis of apatite crystals. However, these measurements provide comparable data of the differences in the level of mineralization of different teeth.

The Vickers measurements of the enamel reflect the results of the electron density values; M1 being the hardest, M2 the second hardest, and M3 being by far the least hard (Fig. 32). The hardness of dentin was comparable among all the teeth, and a roughly similar pattern was found in the electron density. However, compared to enamel hardness, dentin is harder than the electron density values would indicate. Whereas dentin has comparable hardness to M2 enamel hardness, the electron density of dentin is comparatively low by being closer to M3 electron density (Figs. 28 and 32). Dentin matures faster and organic matter has bigger role in its final structure. 29% of dentin is

organic, mostly collagen which is likely to provide structural strength while not having high electron density. In immature enamel, the organic matter is in solution and not part of the structure.

5.2.1 Optical and electronic thin sections compared to Vickers measurements

Thin sections are the most traditional way to observe the inner structure of teeth, but the technology has improved with digital imaging that is making the images even sharper and easier to storage. The different structures of enamel and dentin, the incremental lines, HSB and the enamel rod structure are clearly visible in thin sections, which is not the case in the microCT-images.

In the M1, the timing of the accentuated growth line match with the time of the birth, so most likely it is the neonatal line (Fig. 33) Furthermore the different appearance of the enamel on different sides of the line supports that, as in the womb the fetus receives its nutrition through placenta directly to blood circulation, whereas a newborn receives all the nutrition through digestive channel in milk, until the individual starts to eat by itself. These dietary shifts have effects on the chemistry of teeth and bones. One interesting detail was the hardness of the neonatal line that was slightly inferior to the hardness of surrounding enamel, even if in the thin sections, the neonatal was optically more coherent. The higher optical coherence could indicate lower degree organic matter compared to the surrounding enamel. One reason for the optical difference may be the dietary shift at time of the birth, which may disrupt the matrix secretion. The mineralization process may still continue as long as there are free ions around, and the circumstances stay favorable for the crystal formation. On the other hand, the organic matter, even if its quantity is small, acts as an adhesive in the enamel structure, and if it is lacking, the apatite crystals could perhaps slide away under the diamond pyramid of the hardness tester.

In the M2 enamel, there were several incremental lines of which two were more accentuated than the others. The mineralization of the M2 starts 4 month after the birth, so these lines would not be linked to the birth. In Finland the weaning of pigs is approximately in age of 3 or 4 weeks, when the pigs are also moved away from sows (Farmit Website). Life history events and stress are well documented to leave traces in

tooth enamel (Schwartz et al. 2006, Austin et al. 2013, Eli et al. 1989), and the lines documented here are likely to reflect life history events, such as weaning. If the weaning was the cause of these lines, it could be possible to show this with the barium distribution analyses that have been used by Austin et al. (2013). Under XPL, contrary to the neonatal line, the observed M2 stress lines were not optically coherent but remained opaque also when the microscope stage was rotated. Therefore, it seems that stressful life events, other than birth, may disrupt the overall process of mineralization.

The M2s and the M3s show that in a certain stage of maturation, enamel has a pigmented appearance in thin sections. Kirkham et al. (1988) split enamel development in four chemically distinct stages:
Stage 1 - secretion, deposition of soft, partially mineralized matrix;
Stage 2 - transition, loss of organic matrix becomes apparent;
Stage 3 - maturation, occlusion of porous tissue by mineral ions; and
Stage 4 - hard translucent enamel.

In the M2, the pigmented zone is in cusp tip region except the very first secreted layers next to the EDJ, which also had higher electron density. In the M3 all enamel is still pigmented through the thickness. Berkovitz et al. (2002) state that the content of organic matrix differs in different regions of enamel: where the crystal arrangement is straight and regular, the organic matter content may be only 0.05% by weight, whereas in the areas where the enamel rods and crystals are more irregular, the organic matter content may be 3%. It may be possible that where the enamel structure is simpler, for example on the sides of the tooth, the organic matrix is removed faster, and in tooth cusps, where the enamel structure is more complex, the organic matrix is removed more slowly. This still does not necessarily affect the rate of the crystal growth, and on the sides of the tooth, where the matrix is secreted the last, the enamel is still porous, and this is seen in the low electron density values.

Compared to the optical thin sections, the microCT-images give information of larger scale. The ultrastructure of the enamel cannot be seen, but the general view of the tooth structure, and the progression of the enamel maturation are well seen. When observing transvers slices of the developing tooth (M2), the electron density values seem to get

higher first near the EDJ, and finally on the surface. The values are the highest on the cusp surfaces only after the tooth eruption (M1) (Fig. 48).

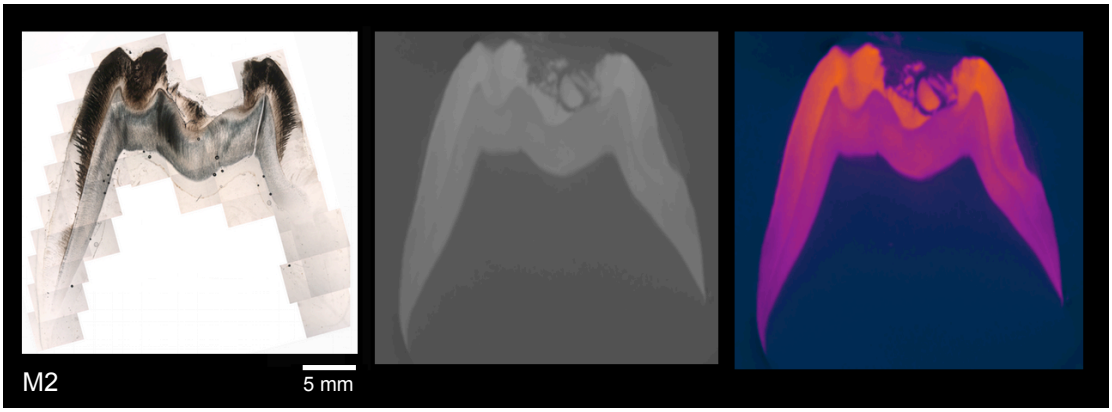

Fig 48. The optical thin section, microCT absorption model and its false color image of M2. The general picture of the enamel ultrastructure is still the best seen in the optical thin sections. The microCT-images give large-scale information of the electron density. The 3-dimensional image of the ultrastructure could be observed in synchrotron imaging that was not used in this work. Note: As the microCT measurements were done when the tooth was still in dental sac, the fractions of tooth that lack in the optical thin section are still in the electron density images.

In Fig. 48, the combined photomicrograph of M2 of Pig C shows two distinct phases in the enamel: a pigmented phase that is present in the tooth cusps and a transparent phase that is present near tooth neck and at the cusp tips next to the EDJ. On the sides of the tooth, the pigmented zone continues further down near to EDJ than on tooth surface. The interface of pigmented and transparent phases is ragged. Comparison of the combined photomicrograph and the microCT-image from the same tooth shows that the electron density of enamel follows the differences in thin section appearance, except close to the EDJ (Fig. 48). As it is reasonably easy to find the same section form the microCT-images and the thin sections, the microCT-absorption models can be used also as a guide to find the best plane for other, destructive methods.

5.3 The crystal orientation, thin sections and x-ray diffraction analyses

The X-ray diffraction patterns of the powder analyses and thin section both showed strong crystal orientations. The thin sections show that there are specific areas where the crystal orientation is more coherent than elsewhere. In the thin sections, the direction of the cut had a clear influence to the diffraction pattern (Fig. 42). So even if the optical coherence in the optical thin section was not entirely clear (with exceptions of the

surface, the EDJ and the neonatal line), the crystals have largely the same orientation as the enamel rods, although the angle differs on that plane.

The dentin, and especially the jawbone, reveal smaller, and slightly wider peaks in the X-ray diffractogram that indicate poorer crystallinity and smaller crystal size. These structures also had a slightly different emphasis on the peaks compared to enamel (Fig. 40).

6. CONCLUSIONS

6.1 Biological conclusion

For the modern domestic pigs of the study, the mineralization of the M3 seemed to start earlier than anticipated (Tonge & MacCance 1973). This may be the result of breeding that selects for fast growing and large individuals (the received pigs were also clearly heavier than mentioned in Tonge & MacCance 1973) or, it can be an effect of methodological improvements.

In the domestic pig, the enamel matrix secretion seems to be nearly completed before the secondary mineralization starts, contrary to what is reported in humans. The shift from the primary mineralization to secondary mineralization may be quite prompt, as my data on M2s indicate (Fig. 28).

In the M1, the enamel was slightly softer in the neonatal line, but the crystal orientation appeared optically more coherent than the surrounding enamel. The other stress lines in the M2 were pigmented and with no visible optical features. Birth, at least in the studied pig, appears to have affected the enamel formation differently than other stresses later in the pig's life.

The cusp development of the M3s is well advanced in the main cusps of the trigonid whereas talonid cusp tips are only appearing. Nevertheless, the difference in electron density of the trigonid and talonid disappears very quickly because two of the studied

M3s show comparable electron density values between trigonid and talonid. In contrast, the vertical difference in electron density stays until the end of the crown formation.

The crowns of M1s and M2s were fully formed at the age of 6 months in all the pigs studied. M3 was approximately half of its final size. Nevertheless, the trigonid and talonid cusp tips of the forming M3s had the same difference in their lateral dimensions than the fully formed M3s. This suggests that the growth rates of the valleys separating cusps are the same in the trigonid and the talonid, and the wider separation of trigonid cusps results from the earlier initiation of the trigonid development.

The X-ray diffraction and thin sections approved the orientation and degree of mineralization of a biomineral containing tissue. The mineralized and still developing zones were easily identified in the thin sections.

6.2 Methodological conclusion

The microCT proved to be a good starting point for the traditional destructive methods used in the study of biomineralization, but cannot substitute the other methods. It gives plenty of visual information and numerical values and in this study I explored some methods that can be combined with microCT data.

The relative mineral calibration turned out to be fairly straightforward and helpful method for the microCT-absorption models, and helped to compare different samples that required separate scanning due to size. Additionally, the mineral grains help to detect a common challenge in microCT imaging, namely the hardening effects. However, the mineral grains were not completely homogenous and pure, which would had given a more certain results, other changes suggested in discussion 5.1.

The thin sections were possible to prepare with the methods of petrographic thin sections, with some precautions: the final polishing is better to do by hand, as the machinery technic is too robust and breaks the enamel. In some thin sections, there occurred some blurriness, and it is possible that these were due to organic matter present in the samples.

The biggest challenges with methods were with Vickers hardness tester, SEM-imaging and XRD. The Vickers hardness tester is designed to measure the hardness of ore minerals that are opaque and reflect the light. With my tooth samples that are semi-transparent, it was difficult to distinguish the indentations with the relatively weak light of the tester. It helped somewhat to replace the light with a powerful torch. In SEM-imaging the acid treatment is challenging, but the SEM-images give good information about the enamel rod orientation that is not possible to obtain with the other methods. The X-ray diffraction analyses are a useful method for the relative level of mineralization and the orientation of crystals of biominerals and confirmed other results.

The results of this study highlight the importance and pitfalls of obtaining data from different tissues. First, electron density and hardness data from enamel and dentin appeared quite comparable within each tissue, but one must be careful when comparing results obtained using different methods across different tissues. Second, if I had measured only the enamel, it would have been relatively easy to overlook spurious electron density measurements caused by the hardening effect. Therefore, I feel that studying the structural differences of both the enamel and dentin have helped me to obtain better understanding of the whole process of tooth maturation and the role of different tissues during the development.

7. ACKNOWLEDGEMENTS

I would like to thank Pasi Heikkilä for supervising, thorough advices and corrections in writing, and the courageous jump out from his comfort zone: he really enabled this project to be as interdisciplinary as it is. I would like to thank Mikael Fortelius who was the main instigator of this project. I would also like to thank HK Ruokatalo, Chef Wotkin's and Finnish Museum of Natural History for the research material, Juha Laakkonen who enabled the tooth pulling operation, Helena Korkka for the help with the sample preparation, Elina, Tobias, Henrik, Radek and Electron Microscopy unit at BI for the help with microscopy-imaging, and Aki Kallonen for the MicroCT- scanning.

My grateful thanks to Jackie and Jussi for reading and corrections, and other Helsinki EvoDevo -people, such as Ian, Al, Scott, Carin, Pekka, Jussi, Teemu, Johann and Outi, it is marvelous to work with people that possess such a vast knowledge. Many thanks to my friends Gudrun, Mona, Kaisa, Elodie, Tuija, Catherine and specially Jossu for your support and friendship.

I would especially like to thank Jukka for the advices in writing, technical tutoring, making this all possible.

8. REFERENCES

Ash, M. M. and Nelson, S. J. 2009. Wheeler's Human Dental Anatomy, Physiology, and Occlusion. Ten Cate's Oral Histology: Development, Structure, and Function. 9th edition, 335 pp.

Austin C., Smith T.M., Bradman A., Hinde K., Joannes-Boyau R., Bishop D., Hare D. J., Doble, P. and Eskenazi B., Arora M. 2013. Barium distributions in teeth reveal early-life dietary transitions in primates. Nature 498, 216–219

Bei, M. 2009. Molecular genetics of tooth development. Current Opinion in Genetics & Development 19, 504–510.

Berkovitz, B. K. B., Holland, G. R. and Moxham, B. J. 2002. Oral anatomy, Histology and Embryology 3rd Edition. Harcourt Publisher Limited. 378 pp.

Bruker. 2014. AN overview of NRecon: reconstructing the best images from your microCT scan. Bruker-microCT Method note 62. 48 pp.

Boyde A. and Fortelius M. 1986. Development, structure and function of rhinoceros enamel. Zoological Journal of the Linnean Society 87, 181–214.

Boyde, A. 1989. Enamel. Handbook of Microscopic Anatomy (Teeth) 6, 310–473.

Cuif, J-P. Dauphin, Y. and Sorauf, J. E. Biominerals and Fossils Trough Time. 2011. Cambridge University Press. 490 pp.

Enax, J., Prymak, J., Raabe, D. and Epple, M. 2012. Structure, composition, and mechanical properties of shark teeth. Journal of Structural Biology 178, 290–299.

Evans A.R., Wilson G.P., Fortelius M. and Jernvall J. 2007. High-level similarity of dentitions in carnivorans and rodents Nature 445, 78–81.

Fagrell, T. G., Dietz, W., Jälevik B. and Norén J. G. 2010. Chemical, mechanical and morphological properties of hypomineralized enamel of permanent first molars. Acta Odontologica Scandinavica 68, 215–222.

Farah R.A., Swain M.V., Drummond B.K., Cook R. and Atieh M. 2010. Mineral density of hypomineralized enamel. Journal of Dentistry 38, 50–58.

Farmit Website Oy. Visited 10.9. 2014 http://www.farmit.net/kotielain/porsas/porsaan-vieroitus

Ferguson V. L., Boyde A. and Bushby A. J. 2005. Elastic modulus of dental enamel: effect of enamel prism orientation and mineral content. Mechanical Properties of Bioinspired and Biological Materials. In: (Eds) Viney, C., Katti, K., Ulm, F. J., Hellmich, C. MRS Proceedings 844, 75–80.

Fortelius. M. 1985. Ungulate cheek teeth: developmental, functional, and evolutionary interrelations. Acta Zoologica Fennica 180, 1–76.

Fortelius, M., Eronen, J. T., Jernvall, J., Liu, L., Pushkina, D., Rinne, J., Tesakov, A., Vislobokova, I. A., Zhang, Z. and Zhou. L. 2002. Fossil Mammals Resolve Regional Patterns of Eurasian Climate Change During 20 Million Years. Evolutionary Ecology Research 4, 1005-1016.

Gilbert S. F. 2000. Developmental biology 6th edition. Sinauer Associates Inc. pp. 695

Gilbert S. F. 2013. Developmental biology 10th edition. Sinauer Associates Inc. pp. 719

Godefroit, P., Cau, A., Dong-Yu, H., Escuillié, F., Wenhao, W. and Dyke G. 2013. A Jurassic avialan dinosaur from China resolves the early phylogenetic history of birds. Nature 498, 359–362.

Haaramo, M. 2015 Mikko's Phylogeny Archive (WWW database). Visited 11.6. 2015 http://www.helsinki.fi/~mhaaramo/

Harjunmaa, E., Seidel, K, Häkkinen, T., Renvoisé, E., Corfe, I. J., Kallonen, A., Zhang, Z-Q., Evans, A. R., Mikkola, M. L., Salazar-Ciudad, I. Klein, O. D. and Jernvall, J. 2014. Replaying evolutionary transitions from the dental fossil record. Nature 51, 44–48

Hillson, S. 2005. Teeth 2nd Edition. Cambridge University Press. 388 pp.

The New IMA List of Minerals – A Work in Progress – Updated: September 2014. Visited 6.11.2014. http://pubsites.uws.edu.au/ima-cnmnc/IMA_Master_List_%282014-03%29.pdf

Jernvall, J. 1995. Mammalian molar cusp patterns: Developmental mechanisms of diversity. Acta Zoologica Fennica 198, 1–61

Jernvall, J. 2000. Linking development with generation of novelty in mammalian teeth. Proceedings of the National Academy of Sciences. 97, 2641–2645

Jernvall, J. and Jung, H-S. 2000. Genotype, Phenotype, and Developmental Biology of Molar Tooth Characters. Yearbook of Physical Anthropology 43, 171–190.

Jernvall, J. and Thesleff, I. 2012. Tooth shape formation and tooth renewal: evolving with the same signals. Development 139: 3487–3497.

Jones. D, Evans, A. R., Siu, K. K. W., Rayfield, E. J. and Donoghue, P. C. J. 2012. The sharpest tools in the box? Quantitative analysis of conodont element functional morphology. Proceedings of the Royal Society 279, 2849–2854.

Kallonen, A. 2011. X-Ray Microtomography Studies od Developing Mouse Teeth. Master thesis. Department of Physics. University of Helsinki. pp. 63.

Karlström S. 1931. Physical, physiological and pathological studies of dental enamelwith special references to the question of its vitality. A. B. Fahlcrantz' Boktryckeri.

Kawasaki K. Weiss K. M. 2006. Evolutionary Genetics of Vertebrate Tissue Mineralization: The Origin and Evolution of the Secretory Calcium-Binding Phosphoprotein Family. Journal of Experimental Zoology 306, 295–316.

Kierdorf, U., Kierdorf, H. and Fejerskov, O. 1993: Fluoride induced developmental changes in enamel and dentin of European roe deer (Capreolus capreolus L.) as a result of environmental pollution. Archives of Oral Biology 38, 1071–1081.

Kierdorf, U., Kierdorf, H., Sedlacek, F. and Fejerskov, O. 1996: Structural changes in fluorosed dental enamel of red deer (Cervus elaphus L.) from a region with severe environmental pollution by fluorides. Journal of Anatomy 188, 183–195.

Kierdorf, H., Kierdorf, U., Richards, A., Josephsen, K. and Sedlacek, F. 2000: Disturbed enamel formation in wild boars (*Sus scrofa L.*) from fluoride polluted areas in Central Europe. The Anatomical Record 259, 12–24.

Kierdorf, U., Bahelková, P., Sedláček, F. and Kierdorf, H. 2012. Pronounced reduction of fluoride exposure in free-ranging deer in North Bohemia (Czech Republic) as indicated by the biomarkers skeletal fluoride content and dental fluorosis. Science of the Total Environment 414, 686–695

Kirschvink J. L. and Gould J. L. 1981. Biogenic magnetite as a basis for magnetic field detection in animals. Biosystems 13,181–201.

J. Kirkham, J., Robinson, C., Weatherell, J.A., Richards, A., Fejerskov, O. and Josephsen, K. 1988. Maturation in Developing Permanent Porcine Enamel. Journal of Dental Research 67, 1156–1160

Koenigswald, v. W., Rensberger, J. M. and Pretzschner, H. U. 1987. Changes in the tooth structure of early Paleocene mammals allowing increased diet diversity. Nature 328, 150–152.

Koenigswald, v. W. 1999. Glossary of Enamel Microstructure. Visited 26.10.2014 http://faculty.baruch.cuny.edu/jwahlert/enamel/schmelz.html.

Koenigswald, v. W., Holbrook, L. T., and Rose, K. D,. 2011. Diversity and Evolution of Hunter-Schreger Band Configuration in Tooth Enamel of Perissodactyl Mammals. Acta Palaeontologica Polonica 56, 11–32.

Kraus, B. S., Jordan, R. E., 1965. The Human Dentition Before Birth. Philadelphia, Pa. Lea and Febiger. 218 pp.

Line R. S. P. and Novaes P. D. 2005. The Development And Evolution Of Mammalian Enamel: Structural And Functional Aspects. Brazilian Journal of Morphological Science 22, 67–72

Lowenstam, H. A. and Weiner, S. 1989. On Biomineralization. Oxford University Press. New York. 324 pp.

Lucas P. W. 2004. Dental Functional Morphology. Cambridge University Press. 355 pp.

Luo, Z-X. 2014. Evolution: Tooth structure re-engineered. Nature 512, 36–37

Mathur, A. K. and Polly, P. D. 2000. The Evolution of Enamel Microstructure: How Important Is Amelogenin? Journal of Mammalian Evolution 7, 23–37.

Nanci A. Ten Cate's Oral Histology: Development, Structure, and Function. Elsevier Health Sciences 2014. 400 pp.

Nickel E. H. 1995. The definition of a mineral. The Canadian Mineralogist 33, 689–690

Nieminen, P. 2007. Bite-It, Gene expression in tooth (WWW database). Visited 6.11.2014 http://bite-it.helsinki.fi

Ortiz, A. Skinner, M. M., Baileya, S. E. and Hublin, J-J. 2012. Carabelli's trait revisited: An examination of mesiolingual features at the enamel-dentin junction and enamel surface of Pan and Homo sapiens upper molars. Journal of Human Evolution 63, 586–596.

Pilson, M. E. Q. 2013 An Introduction to the Chemistry of the Sea. 2nd Edition Cambridge University Press. 533 pp.

Qu, Q., Haitina, T., Min Zhu M. and Ahlberg P. E. 2015. New genomic and fossil data illuminate the origin of enamel. Nature 526: 108–111.

Riding, R. 2007. The term stromatolite: towards an essential definition. Lethaia 1215, 321–330.

Riding, R. E., Awramik, S. M. 2000. Microbial Sediments. Springer Science & Business Media, pp. 331

Robinson, C., Kirkham, J., Brookes S. J. and Shore, R. C. 1995. Chemistry of Mature Enamel. In: Structure of Mature Enamel. (eds) Robinson, C., Kirkham, J., Shore, R. C., Boca Raton CRC Press.

Robinson, C., Kirkham, J., Brookes S. J., Bonass, W. A., Shore, R. C. 1995. The chemistry of enamel development. International Journal of Developmental Biology 39, 45–152.

Sahni, A. and Lester, K. S. 1988. The nature and significance of enamel tubules in therapsids and mammals. In: Russell, D. E., Santoro, J.-P. and Sigogneau-Russell, D. (eds) Teeth Revisited, Proceedings of the VII International Symposium on Dental Morphology, Paris 1986. Memoires du Museum National d'Histoire naturelle 53, 85–99.

Schour, I. and Hoffman, M. M. 1939. Studies in tooth development. The 16 microns calcification rhythm in the enamel and dentin from fish to man. Journal of Dental Research 18, 91–102.

Schwartz, G. T., Reid, D. J., Dean, M. C. and Zihlman, A. L. 2006. A Faithful Record of Stressful Life Events Preserved in the Dental Developmental Record of a Juvenile Gorilla. International Journal of Primatology, 27, 1201–1219.

Sicher, H. (ed.). 1966. Orban's oral histology and embryology. Mosby, 6th. edition. pp. 417.

Sunil, CH R., Sujana, V., Manisha Choudary, T. and Nagesh, B. 2012. In vitro action of various carbamide peroxide gel bleaching agents on the micro hardness of human enamel. Contemporary Clinical Dentistry 3: 193–196.

Suga S. Taki Y. Wada K. and Ogawa M. 1983. Evolution of Fluoride and Iron concentration on the Enameloid of Fish Teeth In: Suga, S. and Nakahara, H. (eds.) Mechanisms and Phylogeny of Mineralization in Biological Systems. Springer Japan. 517 pp.

Smith, M. M. and Sanson I. J. 2000. Evolutionary origins of dentin in the fossil record of early vertebrates: diversity, development and function. In: Teaford, M. F., Smith, M. M., Ferguson, M. W. J. (Eds) Development, Function and Evolution of Teeth. University of Manchester. Cambridge University Press. 314 pp.

Ungar, P. S. 2010. Mammal Teeth: Origin, Evolution, and Diversity. The Johns Hopkins University Press. 312 pp.

Tafforeau, P., Zermeno, J., and Smith, T. 2012. Tracking cellular-level enamel growth and structure in 4D with synchrotron imaging. Journal of Human Evolution 62, 424–428.

Tonge C. H. and McCance R. A. 1973. Normal development of the jaws and teeth in pigs, and the delay and malocclusion produced by calorie defiencies. Journal of Anatomy 155, 1–22.

Tseng, Z. J. 2012. Connecting Hunter-Schreger Band microstructure to enamel microwear features: New insights from durophagous carnivores. Acta Palaeontologia Polonica 57, 473–484

Wang, F., Xiao, J., Cong, W., Li, A., Song, T., Wei, F., Xu, J., Zhang, C., Fan, Z. and Wang, S. 2014. Morphology and chronology of diphyodont dentition in miniature pigs, Sus Scrofa. Oral Disease 20, 367–79.

Willmott, N. S, Bryan, R. A. and Duggal, M. S. Molar-Incisor- Hypomineralisation: A literature review. European Archives of Paediatric Dentistry 2008;9:172–179.

Wilson G.P., Evans A.R., Corfe I.J., Smiths P.D., Fortelius M. and Jernvall J. 2012. Adaptive radiation of multituberculate mammals before the extinction of dinosaurs. Nature 483, 457–460.

Ziscovici, C., Lucas, P. W., Constantino P. J., Bromage T. G. and van Casteren A. 2014. Sea otter dental enamel is highly resistant to chipping due to its microstructure. Biology letters 10, 20140484.